WTAP is Transcriptionally Regulated by p65 and Promotes Inflammation through m^{6}A Modification and Phase Separation

Yong Ge[1, 2,] †, Rong Chen[1, 2,] †, Tao Ling [1, 2], Biaodi Liu[1], Jingrong Huang[1, 2], Youxiang Cheng[1, 2], Yi Lin[1, 2], Hongxuan Chen[1], Xiongmei Xie[1], Guomeng Xia[1], Guanzheng Luo[1], Shaochun Yuan[1, 2, 4,] ✉ & Anlong Xu[1, 3,] ✉

[1]Guangdong Province Key Laboratory of Pharmaceutical Functional Genes, MOE Key Laboratory of Gene Function and Regulation, State Key Laboratory of Biocontrol, School of Life Sciences, Sun Yat-Sen University, Guangzhou, China.

[2]Southern Marine Science and Engineering Guangdong Laboratory (Zhuhai), Zhuhai, China.

[3]School of Life Sciences, Beijing University of Chinese Medicine, Beijing, China.

[4]Laboratory for Marine Biology and Biotechnology, Pilot National Laboratory for Marine Science and Technology, Qingdao, China.

†These authors contributed equally.

✉Correspondence: lssxal@mail.sysu.edu.cn (A.X.); yuanshch@mail.sysu.edu.cn (S.Y.)

Abstract

Emerging evidence has linked dysregulation of N^6-methyladenosine (m^6A) to inflammation and inflammatory diseases, but the underlying mechanism remains lacking. Here, we found that high m^6A modification in a variety of hyperinflammatory states is p65-dependent, because WTAP, a key component of the writer complex, is transcriptionally regulated by p65 and its overexpression can lead to higher m^6A modification. Mechanistically, upregulated WTAP is more prone to phase separation to facilitate the aggregation of "writer" complex to nuclear speckles and the deposition of m^6A marks onto transcriptionally active inflammatory transcripts, thereby accelerating proinflammatory response. Furthermore, myeloid deficiency of WTAP attenuates the severity of LPS-induced sepsis and DSS-induced IBD. Thus, the proinflammatory effect of WTAP is a general risk-increasing mechanism, and interrupting the assembly of m^6A writer complex by targeting the phase separation of WTAP to reduce the global m^6A level may be a potential and promising therapeutic strategy for alleviating hyperinflammation.

Introduction

Inflammation is usually a physiological healing response that is triggered by noxious stimuli and conditions, such as infection and tissue injury (Cao, 2016). Moderate inflammation is essential for the pathogen clearance, tissue repair and regeneration. However, dysregulated inflammation disrupts immune homeostasis, which may lead to the development of a variety of inflammatory diseases, such as chronic inflammation, metabolic disorders, autoimmune diseases (ADs) and cancer (Gong *et al*, 2020; Greten & Grivennikov, 2019). To maintain immune homeostasis and prevent harmful outcomes, the activation or induction of proinflammatory regulators and effectors must be precisely controlled at multiple levels, including the transcriptional (Medzhitov & Horng, 2009), posttranscriptional (Carpenter *et al*, 2014) and posttranslational (Liu *et al*, 2016) levels, and these are thus potential targets for the treatment of inflammatory diseases (Banerjee *et al*, 2017; Yeung *et al*, 2018). The therapeutic strategies for inflammatory diseases have been established and even become invaluable by developing antagonists or inhibitors against principal inflammatory effectors (NF-κB, STAT3 and JAK) and multifunctional proinflammatory cytokines (IL-6, TNF-α, IL-17A and IL-23) (Bradley, 2008; Hunter & Jones, 2015), such as specific antibodies against IL-6(R) (e.g., tocilizumab and siltuximab) and TNF-α (e.g., infliximab, etanercept and adalimumab), which have been used in the treatment of many autoimmune diseases (Kang *et al*, 2019). However, due to pleiotropy, the therapeutic effects of targeting specific cytokines such as IL-6 or IL-17A greatly vary among different inflammatory diseases (Stone *et al*, 2017). In contrast, small-molecule inhibitors targeting the NF-κB and STAT3 signalling pathways lead to significant side effects that alter the homeostasis of the immune system as well as the nonimmune cells (Siegel *et al*, 2011; Zhang *et al*, 2017). Therefore, in-depth research into how inflammation is precisely regulated remains particularly important for the development of new treatments against excessive inflammatory responses.

In the past two decades, studies on immune regulation have mainly focused on posttranslational modifications of proteins, such as phosphorylation and ubiquitination. Recently, emerging evidence has strongly indicated that immune signalling can trigger dynamic alterations to the epitranscriptome, which orchestrates the regulation of immune response (Li & Rana, 2022; O'Connell *et al*, 2015). Among those dynamic epitranscriptomics alterations, m^6A modification is the most abundant and reversible RNA modification and can influence pre-mRNA splicing,

stability, translation, location and transport (Fu *et al*, 2014). The m^6A modification is mediated by a methyltransferase complex called "writer" and removed by demethylase, namely "eraser". In addition to playing roles in distinct biological processes such as embryonic development, hematopoiesis and cancer, the roles of m^6A modification in inflammatory regulation have recently attracted intense attention (Luo *et al*, 2021; Shulman & Stern-Ginossar, 2020). For example, depleting METTL3, the key methyltransferase in the "writer" complex, reduces the m^6A abundance on *TRAF6* mRNA and decreases the expression of TRAF6 by entrapping the transcripts in the nucleus, which inhibits the activation of the NF-κB and mitogen-activated protein kinase (MAPK) signalling pathways (Zong *et al*, 2019). In contrast, another study revealed that METTL3 is significantly elevated in patients with rheumatoid arthritis (RA) and that high expression of METTL3 attenuates the inflammatory response in macrophages which are stimulated with LPS (Wang *et al*, 2019). Not only METTL3, but also inconsistent results have been obtained in functional studies of demethylases. For instance, knocking-down the demethylase FTO leads to an increased overall m^6A abundance, STAT3 phosphorylation and secretion of proinflammatory cytokines (Tang *et al*, 2022), whereas the knockdown of ALKBH5 inhibits cell viability and production of inflammatory cytokines (Zhu & Lu, 2020). In addition to the m^6A writers and erasers, m^6A readers, such as YTHDF2, play different or even opposite roles in regulating different inflammatory events. For example, a previous study showed that YTHDF2 limits the decay of *KDM6B* mRNA in a m^6A-dependent manner and promotes the demethylation of histone 3 lysine 27 trimethylation (H3K27me3), which is required for the transcription of certain proinflammatory cytokines (Wu *et al*, 2020). However, another study indicated that YTHDF2 is an inflammatory suppressor that downregulates m^6A-modified transcripts in inflammatory response and thereby protects hematopoietic stem cells from excessive proinflammatory signals (Mapperley *et al*, 2021). Thus, although notable evidence clearly points to m^6A modification in modulating inflammatory responses, its effects appear to depend greatly on the disease status or specific target genes.

Recently, due to the finding of aberrant RNA methylation in inflammatory diseases (Luo *et al.*, 2021) and cancers (Jiang *et al*, 2021), small-molecule inhibitors, which target specific "writer" or "eraser" to reprogram the m^6A epitranscriptome, have attracted considerable attention and have been proven to be feasible (Barbieri & Kouzarides, 2020). Notably, a research group identified a

selective METTL3 catalytic inhibitor STM2457, that can suppress the growth of acute myeloid leukemia (AML) (Yankova *et al*, 2021). Moreover, two FTO inhibitors (FB23 and FB23-2) have been designed to bind FTO directly and inhibit FTO demethylase activity, and exert a selective inhibitory effect on the proliferation of AML cells (Huang *et al*, 2019). In addition to the aforementioned inhibitors used to treat AML, potential inhibitors of m^6A methylase and demethylase remain in the research stage for the treatment of other inflammatory diseases. Because m^6A methylation contributes to pluripotency, identification of the intrinsic principles underlying the mechanism through which m^6A regulates inflammation and inflammatory diseases is extremely important before a therapeutic approach can be developed to target the m^6A mark. The investigation of other general regulators, in addition to m^6A methylase and demethylase inhibitors, may provide another method for developing effective and even safer treatments for inflammatory diseases.

By revealing the basic principle of m^6A modification in inflammatory regulation, we report a new function of the m^6A "writer" protein Wilms' tumour 1-associating protein (WTAP) in controlling inflammatory responses and associated diseases. We found that WTAP is an NF-κB p65-stimulated gene and that its expression is significantly upregulated in response to a variety of inflammatory stimuli and in many inflammatory diseases. Mechanistically, after an increase in its concentration, WTAP spontaneously undergoes phase separation, which facilitates the aggregation of the "writer" complex to nuclear speckles and the deposition of m^6A onto transcriptionally active proinflammatory genes. Hence, WTAP enhances the protein synthesis of many m^6A-modified proinflammatory transcripts, including IL6ST, IL18R1, IL15RA, IL-1A, IL12B and CXCL11, in response to inflammatory stimuli, which accelerates the process of inflammatory responses and aggravates the severity of many inflammatory diseases, such as LPS-induced sepsis, IBD and psoriasis. Thus, our study here identified WTAP as a risk factor in inflammatory responses and thereby provides mechanistic insights into WTAP as a novel and potential therapeutic target for preventing excessive inflammation.

Results

Hyperinflammation is accompanied by elevated WTAP levels in many inflammatory diseases

Although some evidence has indicated that m^6A modification plays an essential role in inflammation and inflammatory diseases (Cui *et al*, 2022; Xu *et al*, 2022), the intrinsic principles remain unclear. By analyzing data obtained from the Gene Expression Omnibus (GEO) dataset (GSE13887/137268/69063/97779/166388/208303, Appendix Table S1), we found that the expression of WTAP is commonly upregulated in patients with SLE, asthma, sepsis, rheumatoid arthritis, psoriasis, or Crohn's disease (Fig EV1A-F). To verify this phenomenon, we then performed statistical analyses of previously published microarray datasets (GSE19315/198326/2411/2638/227851/189847, Appendix Table S1) and further identified that only the mRNA abundance of WTAP was significantly increased after LPS stimulation in THP-1 cells (Fig EV1G) and human macrophages (Fig EV1H). Similar results were obtained from the lung tissue of mice with LPS-induced lung injury (Fig EV1I). In addition, we found that the mRNA abundance of WTAP also increased in TNF-α stimulated human microvascular endothelial cells (HMECs) (Fig EV1J), *Mycobacterium tuberculosis* (H37Rv)-infected THP-1 cells (Fig EV1K) and *Salmonella typhimurium* (SL1344)-infected macrophages (Fig EV1L). These observations suggest that the overexpression of WTAP is a common phenomenon in hyperinflammation states.

To verify the abovementioned observations, THP-1 cells were treated with the Toll-like receptor 4 (TLR4) agonist LPS, an ideal reagent to activate the inflammatory signalling cascade *in vivo* (Triantafilou & Triantafilou, 2002). RNA-sequencing (RNA-seq) analysis was then performed and the results confirmed that only the mRNA abundance of *WTAP* was significantly upregulated in the LPS-stimulated THP-1 cells (Fig 1A). Further qRT–PCR (Fig 1B-D) or immunoblotting (Fig 1E-G) analyses conducted with THP-1 cells, peripheral blood mononuclear cells (PBMCs) and mouse bone marrow-derived macrophages (BMDMs) after LPS stimulation confirmed that the expression of WTAP was upregulated. To determine whether the upregulated expression of WTAP is ubiquitous upon specific inflammatory stress, we treated THP-1 cells and BMDMs with different TLR agonists or heat-killed bacteria, such as CL097 (a TLR7/8 ligand), Pam3CSK4 (a TLR1/2 ligand), heat-killed *Salmonella typhimurium* (HKST) and heat-killed *Listeria monocytogenes* (HKLM), and found that the mRNA and protein abundance of WTAP were both

147 significantly increased (Fig 1H-M). Thus, high WTAP expression is positively correlated with
148 hyperinflammation states, implying a potential role of WTAP in the regulation of inflammation.
149
150 **WTAP is an NF-κB p65-stimulated gene**
151 Protein abundance can be regulated at the transcriptional, translational, or posttranslational level.
152 To reveal the specific mechanism underlying the upregulation of WTAP at both the mRNA and
153 protein levels upon inflammatory stimulation, bioinformatics analyses using the Promoter 2.0
154 prediction server (http://www.cbs.dtu.dk/services/promoter/), CpG plot
155 (http://www.ebi.ac.uk/Tools/seqstats/emboss_cpgplot/) and JASPAR (http://jaspar.genereg.net/)
156 were performed to identify the region between −800 and +250 in the genomic sequence of human
157 *WTAP* containing the TATA box, CAAT box and GC box, which are characteristic of promoters.
158 Further analyses of transcription factor-binding sites revealed that the *WTAP* promoter contains
159 NF-κB p65-, C/EBPβ- and IRF3-binding motifs, and among these, the p65-binding motifs exhibit
160 the highest prevalence and are distributed in a relatively concentrated and overlapping region (Fig
161 2A). Similar results were obtained from an analysis of the mouse *Wtap* promoter region (Fig 2B).
162 As shown in Fig 2A and B, we constructed a series of reporter plasmids containing the wide-type
163 (WT) WTAP promoter with NF-κB p65-, C/EBPβ-, IRF3-binding motifs or mutated or deleted
164 p65-binding motifs based on the pGL3 basic construct. These reporter plasmids were then
165 cotransfected with increasing amounts of NF-κB p65-, C/EBPβ- or IRF3-expressing plasmids into
166 293T cells. The results revealed that that NF-κB p65 but not IRF3, increased the expression of the
167 respective *WTAP* promoter reporter in a dose-dependent manner (Figs 2C and EV2A and B).
168 However, deletion or mutation of the core p65-binding sites in the *WTAP* promoter inhibited the
169 expression of the reporter gene (Fig 2D). Similar results were obtained using reporter plasmids
170 that contained the mouse *Wtap* promoter (Fig EV2C). Furthermore, the treatment of THP-1 cells
171 or PBMCs with the p65 inhibitor PG490 (triptolide) inhibited the induction of WTAP by LPS or
172 Pam3CSK4 (Figs 2E-H and EV2D and E). Using *RELA*$^{-/-}$ (encoding p65) THP-1 cells generated
173 using the CRISPR-mediated genome editing approach (Fig EV2F), we found that the upregulation
174 of WTAP was inhibited in *RELA*$^{-/-}$ THP-1 cells after LPS, Pam3CSK4, HKST or HKLM
175 stimulation (Figs 2I-L and EV2G and H). DNA pull-down assays confirmed the direct binding of
176 Flag-tagged p65 to biotin-labelled p65-binding probes of the *WTAP* promoter *in vitro* (Fig 2M and

177 N). In addition, C/EBPβ can also slightly activate the expression of WTAP (Fig EV2A), and DNA
178 pull-down assays confirmed the direct binding of C/EBPβ to the *WTAP* promoter (Fig EV2I).
179 Because p65 can further activate some inducible transcription factors such as ATF3, C/EBPδ and
180 C/EBPβ, to enhance the LPS-induced transcriptional response (Medzhitov & Horng, 2009), we
181 hypothesized that although C/EBPβ may play some role in the transcription of *WTAP*, the
182 upregulation of *WTAP* predominantly depends on the activation of NF-κB p65.
183
184 **WTAP positively regulates the expression of proinflammatory cytokines**
185 To determine the significance of WTAP in inflammatory responses, we first generated *WTAP*-
186 knockout THP-1 cells using the CRISPR/Cas9 approach. Two sgRNAs were designed to target the
187 second and third exons (E2 and E3) of *WTAP*. sgRNA1 caused two bases insertion, whereas
188 sgRNA2 caused one base deletion in the *WTAP* genome locus (Fig EV3A and B), leading to the
189 introduction of a new stop codon upstream of the CDS and resulting in an early termination of
190 WTAP translation. However, with open reading frame (ORF) prediction, it was found that the cells
191 may skip these mutations by alternative translation initiation to produce alternative WTAP
192 isoforms with 376 and 319 aa, respectively (Fig EV3C). A subsequent immunoblotting assay
193 using a monoclonal antibody (mAb) purchased from Abcam confirmed the extremely low
194 expression of these two isoforms (Fig EV3D). Thus, the cell lines were designated as "$WTAP^{\Delta 1\text{-}20}$
195 THP-1 cells" and "$WTAP^{\Delta 1\text{-}77}$ THP-1 cells". In addition to generating KO THP-1 cells, we also
196 generated the *Wtap* conditional KO (CKO) mice by crossing $Wtap^{flox/flox}$ mice with mice
197 expressing Cre recombinase under the control of the lysozyme 2 promoter (*LyzM*-Cre) (Fig
198 EV3E). Genomic sequencing confirmed that the third exon was fully removed after crossing,
199 which also resulted in early termination of WTAP translation (Fig EV3F and G). Similarly, ORF
200 prediction showed that gene-edited BMDMs may also produce alternative WTAP isoforms with
201 319 aa (Fig EV3G). Because the WTAP mAb purchased from Abcam did not recognize mouse
202 WTAP, we used a polyclonal antibody (pAb) purchased from Proteintech to detect the WTAP
203 isoforms in mice, and the results showed that only WT WTAP could be identified (Fig EV3H and
204 I).
205 It has been demonstrated that WTAP possesses a nuclear localization signal (NLS) at its N
206 terminus (Fig EV3C), and mutation of this signal can affect the entry of the protein into the

207 nucleus and its function (Scholler *et al*, 2018). Since the NLS is missing in both alternative
208 isoforms, their entry to the nucleus may be affected. The nuclear-cytoplasmic extraction assays
209 confirmed the extremely low concentrations of $WTAP^{\Delta 1\text{-}20}$ and $WTAP^{\Delta 1\text{-}77}$ both in the cytoplasm
210 and nucleus (Fig EV3J). Moreover, LC–MS/MS assays indicated that ectopic expression of WT
211 WTAP but not the two alternative isoforms in *WTAP* KO 293T cells could increase the global m^6A
212 modification level (Fig EV3K). Similarly, the m^6A modification levels of $WTAP^{\Delta 1\text{-}20}$ and $WTAP^{\Delta 1\text{-}}$
213 ^{77} THP-1 cells were significantly lower than those of wild-type cells (Fig EV3L). Although we
214 could not conclude that the $WTAP^{\Delta 1\text{-}20}$ and $WTAP^{\Delta 1\text{-}77}$ isoforms are not functional at all, we found
215 that their expression is extremely low and that their function is likely severely impaired due to the
216 lack of NLS, therefore, the status of $WTAP^{\Delta 1\text{-}20}$ and $WTAP^{\Delta 1\text{-}77}$ THP-1 cells should be very close to
217 that of cells in which the protein is completely knocked out. Moreover, the m^6A abundance in
218 BMDMs from *LyzM*-Cre^+ $Wtap^{\Delta 1\text{-}77}$ mice was decreased significantly, consistent with the results
219 observed in THP-1 cells (Fig EV3M). Thus, although we do not have another antibody to further
220 confirm whether the $WTAP^{\Delta 1\text{-}77}$ is present in *Wtap* KO BMDMs, we can assume that even if
221 $WTAP^{\Delta 1\text{-}77}$ exists, its expression should be extremely low and that its function is impaired in CKO
222 mice. Additionally, no differences in the proportion of major immune cell populations were
223 observed between $Wtap^{fl/fl}$ and *LyzM*-Cre^+ $Wtap^{\Delta 1\text{-}77}$ mice in steady state (Fig EV4A-C), indicating
224 that the depletion of *Wtap* in myeloid cells did not affect macrophage development and
225 maturation.
226 After verifying the status of WTAP KO THP-1 cells and CKO BMDMs, we next performed RNA-
227 seq analyses with WT and $WTAP^{\Delta 1\text{-}77}$ THP-1 cells before and after LPS treatment. KEGG
228 enrichment analyses showed that the transcripts downregulated in $WTAP^{\Delta 1\text{-}77}$ THP-1 cells were
229 mainly enriched in the cytokine production and inflammatory signalling pathways (Fig 3A and B).
230 In contrast, KEGG analyses of the genes upregulated in $WTAP^{\Delta 1\text{-}77}$ THP-1 cells showed that there
231 were enriched in a few pathways that are not associated with inflammatory responses (Fig EV5A).
232 To confirm the results obtained by RNA-seq, qRT–PCR analyses were performed and revealed
233 marked reductions in *IL6*, *CCL2*, *CCL8* and *CXCL8* expression in $WTAP^{\Delta 1\text{-}77}$ THP-1 cells after
234 stimulation with LPS (Fig 3C). Similar results were obtained with $WTAP^{\Delta 1\text{-}77}$ THP-1 cells treated
235 with Pam3CSK4, HKST or HKLM (Fig EV5B). Consistently, $WTAP^{\Delta 1\text{-}77}$ THP-1 cells exhibited a
236 significant reduction in IL-6 secretion in response to the aforementioned stimuli compared with

237 the WT cells (Fig 3D). Furthermore, ectopic expression of WTAP (Fig EV5C) substantially
238 facilitated the expression of IL-6 under inflammatory stimulation (Fig EV5D). These results
239 confirmed that WTAP accelerates inflammatory responses by promoting the expression of many
240 proinflammatory cytokines during multiple inflammatory stimuli.
241
242 **WTAP aggravates LPS-induced sepsis in mice**
243 Because WTAP was upregulated after LPS stimulation and because its deficiency can reduce
244 inflammatory responses in macrophages in THP-1 cells, we next examined the biological effects
245 of WTAP on the progression of inflammatory diseases in *LyzM*-Cre^{+} *Wtap*$^{\Delta 1\text{-}77}$ mice. BMDMs first
246 isolated from *Wtap*$^{fl/fl}$ and *LyzM*-Cre^{+} *Wtap*$^{\Delta 1\text{-}77}$ mice were treated with LPS and then used for
247 RNA-seq analyses. The results showed that WTAP depletion in BMDMs exhibited a significant
248 reduction in the expression of proinflammatory cytokines upon LPS stimulation (Fig 3E), which is
249 consistent with the trend observed in THP-1 cells. As mentioned above, the *WTAP* mRNA
250 abundance was significantly higher in the PBMCs of sepsis patients than in those of healthy ones
251 (Fig EV1C). A retrospective study of publicly available data also revealed that WTAP is a risk
252 gene for sepsis. Specifically, its expression was significantly correlated with 28-day cumulative
253 mortality (Zhang *et al*, 2020). Thus, we further investigated the biological effects of WTAP using
254 *LyzM*-Cre^{+} *Wtap*$^{\Delta 1\text{-}77}$ and *Wtap*$^{fl/fl}$ mouse models of LPS-induced sepsis. Consistent with the
255 results obtained from LPS-induced macrophages, the LPS-triggered expression of *Il6*, *Ccl2* and
256 *Ccl8* in lung and colon tissues was decreased in *LyzM*-Cre^{+} *Wtap*$^{\Delta 1\text{-}77}$ mice compared with *Wtap*$^{fl/fl}$
257 mice (Fig 3F-H), whereas the expression of *Il1a*, *Il1b* and *Tnfa* showed no significant differences
258 (Fig EV6A and B). The same trend was obtained with RNA-seq data from colon samples (Fig 3I).
259 Notably, *LyzM*-Cre^{+} *Wtap*$^{\Delta 1\text{-}77}$ mice showed less lung inflammation and fewer pathological
260 characteristics of lung injury (Fig 3J) and were therefore more tolerant to LPS-induced fatal sepsis
261 (Fig 3K) than their WT counterparts. Moreover, the serum concentration of IL-6 was significantly
262 reduced in *LyzM*-Cre^{+} *Wtap*$^{\Delta 1\text{-}77}$ mice compared with their *Wtap*$^{fl/fl}$ littermates (Fig 3L). Similarly,
263 after intraperitoneal injection of *Pseudomonas aeruginosa* (*P. aeruginosa*) or *Listeria*
264 *monocytogenes* (*L. monocytogenes*), the induced expression of *Il6*, *Ccl2* and *Ccl8* in lung (Figs
265 3M and EV6C and D) and colon (Fig EV6E-G) tissues, as well as the secretion of IL-6 into serum
266 (Fig 3N), were decreased in *LyzM*-Cre^{+} *Wtap*$^{\Delta 1\text{-}77}$ mice. Collectively, these data suggested that the

267 increased expression of WTAP aggravates LPS- or bacteria-induced inflammatory responses *in*
268 *vivo*.
269
270 **WTAP promotes activation of the STAT3 signalling axis through the m^{6}A modification to**
271 **accelerate inflammatory responses**
272 As a key m^{6}A "writer", WTAP is required for anchoring METTL3 and other cofactors to nuclear
273 speckles to modulate m^{6}A modification of RNA (Ping *et al*, 2014). To determine whether WTAP
274 affects the inflammatory responses through m^{6}A modification, we first quantified m^{6}A abundance
275 in cells by LC–MS/MS assays. The results showed that the total m^{6}A level was observably
276 increased in WTAP-overexpressing 293T cells and reduced in *WTAP* KO 293T cells (Fig EV7A
277 and B). In particular, the overall m^{6}A modification level increased in WT cells but not WTAP-
278 deficient cells after LPS stimulation (Fig EV7A and B). These data suggested that upregulation of
279 WTAP can significantly improve the overall m^{6}A modification level during inflammatory stimuli,
280 which is consistent with the previous conclusion that WTAP is responsible for the observed
281 increase in m^{6}A modification upon bacterial infection (Wu *et al.*, 2020).
282 We then performed methylated RNA immunoprecipitation sequencing (MeRIP-Seq) analyses to
283 map mRNA transcripts with different m^{6}A peaks accompanied by different mRNA levels in WT
284 and *WTAP*$^{\Delta 1\text{-}77}$ THP-1 cells or *Wtap*$^{\Delta 1\text{-}77}$ BMDMs after LPS stimulation. According to the MeRIP-
285 Seq data, the consensus m^{6}A core motifs were enriched in the m^{6}A peaks in all the samples (Fig
286 EV7C). A peak distribution analysis showed that the m^{6}A sites were enriched in both exons and
287 3'UTRs (Fig EV7D), with the highest enrichment near the stop codon (Fig EV7E and F).
288 Moreover, the MeRIP-Seq analysis revealed that the m^{6}A peaks of nearly 5,000 or more than
289 1,500 transcripts were lower in *WTAP*$^{\Delta 1\text{-}77}$ THP-1 cells or in *Wtap*$^{\Delta 1\text{-}77}$ BMDMs compared with
290 those in WT cells upon LPS treatment, respectively (Fig 4C). These identified transcripts were
291 enriched in many inflammatory signalling pathways, including the NF-κB (TNF-
292 α/TLR/NLR/CLR-mediated), JAK-STAT and MAPK pathways (Fig EV7G and H). We further
293 compared the transcripts with reduced m^{6}A marks after WTAP deletion between THP-1 cells and
294 BMDMs treated with LPS and identified 989 overlapping transcripts (Fig 4C). KEGG enrichment
295 analyses revealed that these overlapping transcripts were closely related to bacterial infection and
296 inflammatory signalling pathways (Fig 4D), such as *IL6ST*, *IL15RA*, *IL18R1*, *TYK2*, *JAK2*,

297 *RIPK2*, *IL1A*, *IL12B* and *CXCL11* (Fig 4C).

298 Both RNA-seq and MeRIP-seq indicated that WTAP is closely related to inflammatory pathways,
299 such as the NF-κB, JAK-STAT and MAPK pathways. We then explored the effect of WTAP on the
300 activation of these pathways. As shown in Fig 4E and F, the phosphorylation level of STAT3, but
301 not that of p65 or p38, was significantly decreased in *WTAP*$^{\Delta 1\text{-}77}$ THP-1 cells in response to LPS or
302 HKST treatment. To further confirm this effect, the same treatments were performed with
303 BMDMs from *Wtap*$^{fl/fl}$ or *LyzM*-Cre^{+} *Wtap*$^{\Delta 1\text{-}77}$ mice, and similar results were obtained (Fig 4G
304 and H). Consistently, i.p. injection of LPS upregulated the phosphorylation level of STAT3 (Fig 4I
305 and J). However, such induction was significantly reduced in the lung (Fig 4I) and colon (Fig 4J)
306 tissues from *LyzM*-Cre^{+} *Wtap*$^{\Delta 1\text{-}77}$ mice. We further found that the LPS-induced mRNA expression
307 of *IL6*, *CCL2*, *CCL8* and *CXCL8* (Fig 4K), but not that of *TNFA*, *IL1B* and *LTA* (Fig EV7I), was
308 markedly reduced after pretreatment with SC144 (Xu *et al*, 2013), a gp130 (IL6ST) inhibitor that
309 abrogates the IL-6/STAT3 signalling axis. Interestingly, although the expression of many
310 proinflammatory cytokines was reduced in *WTAP*$^{\Delta 1\text{-}77}$ THP-1 cells, the expression and secretion of
311 IL-1β, TNF-α or LTA (TNF-β) showed no significant change compared with those of WT THP-1
312 cells in response to the indicated stimuli (Figs 4L and EV7J-L), which is consistent with the fact
313 that p65 activation is not affected by WTAP. Together, these data suggested that WTAP-mediated
314 m^{6}A modification is deeply involved in the regulation of bacterial infection and inflammatory
315 response in both human and mice and may accelerate inflammatory responses by enhancing the
316 STAT3 signalling axis.

317

318 **WTAP promotes the protein output of proinflammatory genes through m^{6}A modification**

319 Consistent with our experimental results, many m^{6}A-modified genes that were found to be
320 regulated by WTAP based on the sequencing data are involved in the activation and regulation of
321 the STAT3 signalling axis, such as IL6ST, TYK2, JAK2, IL15RA and IL18R1 (Figs 4C and
322 EV8A-I). Since the transcription and secretion of IL-6 is significantly reduced in our analyses and
323 its contribution to the activation of STAT3 may be predominant in acute inflammatory response,
324 we then further measured the protein abundance of the identified key components involved in the
325 IL-6/STAT3 signalling axis, including IL6ST, IL6R, TYK2, JAK1, JAK2 and STAT3 (Hirano,
326 2021). The results showed that the protein abundance of IL6ST but not the other tested

327 components was reduced in *WTAP*$^{\Delta 1\text{-}77}$ THP-1 cells and *Wtap*$^{\Delta 1\text{-}77}$ BMDMs compared with control
328 cells (Figs 5A and EV9A). Moreover, the upregulation of IL6ST induced by LPS was inhibited in
329 the *WTAP*$^{\Delta 1\text{-}77}$ THP-1 cells (Fig 5B). Consistently, the expression of IL6ST was significantly
330 reduced on the cell surface of *Wtap*$^{\Delta 1\text{-}77}$ macrophages (Fig 5C). Notably, the analysis of mouse
331 models of LPS-induced sepsis showed that the increased protein expression of IL6ST and WTAP
332 (Fig EV9B and C) was reduced in the lung and colon tissues (Fig 5D) from *LyzM*-Cre^{+} *Wtap*$^{\Delta 1\text{-}77}$
333 mice. We next generated *IL6ST*$^{-/-}$ THP-1 cells using the CRISPR/Cas9 approach, and as shown in
334 *WTAP*$^{\Delta 1\text{-}77}$ THP-1 cells, the phosphorylated STAT3 level was significantly decreased in *IL6ST*$^{-/-}$
335 THP-1 cells after stimulation with LPS (Fig 5E). The expression of IL-6 was also reduced in
336 *IL6ST*$^{-/-}$ THP-1 cells in response to different inflammatory stimuli (Fig 5F).
337 MeRIP-Seq revealed that the m^{6}A peaks obtained with high confidence were distributed in regions
338 near the stop codon in *IL6ST* transcripts (Fig EV8A). We then designed two gene-specific primer
339 pairs, F1/R1 and F2/R2 (Appendix Table S2), to measure the change in m^{6}A abundance at sites 1
340 and 2 of *IL6ST* transcripts via MeRIP-qPCR assay (Fig 5G). The results showed that the m^{6}A
341 marks enriched at both site 1 and site 2 in the *IL6ST* transcripts were markedly decreased in
342 *WTAP*$^{\Delta 1\text{-}77}$ THP-1 cells compared with control cells (Fig 5H). For verification, we mutated the
343 putative m^{6}A-modified adenosine by replacing it with a thymine in the *IL6ST* mRNA and inserted
344 the wild-type (WT) or mutated (Mut) UTRs into a reporter gene plasmid (psiCHECKTM-2) (Fig
345 5I). Luciferase reporter assay data showed that the luciferase activities of the Mut reporter were
346 significantly weaker than those of the WT reporter (Fig 5J). Moreover, the luciferase activities of
347 the WT reporter were weakened in *WTAP* KO 293T cells (Fig 5K). Ectopic expression of Flag-
348 tagged WTAP in *WTAP* KO 293T cells the enhanced luciferase activities of the WT reporter (Fig
349 EV9D). All these data indicated that the detected m^{6}A mark sites in *IL6ST* transcripts are direct
350 substrates of WTAP and crucial for maintaining the output of the IL6ST protein.
351 Because m^{6}A modification can affect many aspects of gene expression, including nuclear export,
352 splicing, 3'-end processing, decay and translation (Zaccara *et al*, 2019), we evaluated the mRNA
353 expression of *IL6ST* and found that deleting WTAP did not affect the *IL6ST* mRNA abundance or
354 stability (Fig EV9E and F). Due to the decay of *IL6ST* mRNA may not be affected by WTAP, we
355 next measured the translation efficiency of IL6ST through polysome profiling (Fig EV9G). We
356 calculated the proportion of mRNAs in polysome fractions via qRT–PCR and found that the

357 distribution of *IL6ST* mRNA shifted to the lighter fraction in *WTAP*$^{\Delta 1\text{-}77}$ THP-1 cells after
358 stimulation with LPS for 4 h (Fig 5L). However, this difference was not observed in *GAPDH*
359 mRNA (Fig EV9H). Taken together, WTAP can facilitate the expression of IL6ST by enhancing
360 the translation efficiency via m^{6}A modification. Functional interpretation of m^{6}A modification is
361 realized by RNA-binding proteins called "readers", mainly YTHDF1/2/3 and YTHDC1/2, which
362 can influence the degradation or translation of m^{6}A-modified RNA (Shi *et al*, 2017; Zhao *et al*,
363 2020). Because YTHDF1 and YTHDF3 are the major m^{6}A readers that promote the translation of
364 m^{6}A-modified mRNA, we sought to determine whether YTHDF1 or YTHDF3 targets cellular
365 *IL6ST* transcripts to regulate their translation. Immunoblot analyses showed that the deletion of
366 YTHDF1 or YTHDF3 in THP-1 cells using a CRISPR-mediated genome editing approach
367 reduced the protein expression of IL6ST (Fig EV9I). To verify the direct binding of YTHDF1 and
368 YTHDF3 to m^{6}A-methylated *IL6ST* mRNA, we synthesized biotin-labelled RNA probes based on
369 the distribution of the m^{6}A peak on *IL6ST* transcripts (Fig EV9J) and performed an RNA pull-
370 down assay followed by immunoblotting of the isolated proteins. The results revealed that
371 methylated *IL6ST* transcripts strongly interacted with YTHDF1 and YTHDF3 (Fig EV9K).
372 Furthermore, RNA immunoprecipitation (RIP) analyses with antibodies against YTHDF1 or
373 YTHDF3 followed by qRT–PCR revealed that the amount of *IL6ST* mRNA bound to YTHDF1 or
374 YTHDF3 was significantly increased after stimulation with LPS but reduced after WTAP
375 depletion (Fig EV9L). These results suggested that the m^{6}A marks on *IL6ST* mRNA mediated by
376 WTAP obviously promoted the binding of YTHDF1 and YTHDF3 to *IL6ST* mRNA. Polysome
377 profiling assays showed that deletion of YTHDF1 or YTHDF3 in THP-1 cells efficiently
378 decreased the protein expression of IL6ST by hindering its translation (Fig EV9M and N).
379 Overall, these results demonstrated that the increased efficiency of IL6ST translation induced by
380 the m^{6}A modification is mediated by YTHDF1 and YTHDF3.
381 In addition to IL-6/IL6ST/STAT3 signalling, the IL-15/IL15R and IL18/IL18R signalling which
382 dictate T cell response, regulate B cell homing, and activate NK cells (Wawrocki *et al*, 2016), may
383 also mediate the regulation of inflammatory responses by activating STAT3 (Mishra *et al*, 2014;
384 Yasuda *et al*, 2019). In our data, the m^{6}A peaks distributed in the 3'-UTR regions of *IL15RA* and
385 *IL18R1*, the crucial receptor molecules for IL-15/IL15R and IL18/IL18R signaling, also almost
386 disappeared when WTAP was depleted (Fig EV8B and C). The mRNA and protein abundance of

387 IL15Rα and IL18Rα was significantly reduced in *WTAP*$^{\Delta 1\text{-}77}$ THP-1 cells and BMDMs compared
388 with the control cells (Figs 5M and N and EV9O), which suggested that WTAP-mediated m^{6}A
389 modification can regulate the expression of IL15Rα and IL18Rα proteins. Although WTAP only
390 affects the mRNA decay of *IL18R1* but not *IL15RA* (Figs 5O and EV9P), further reporter assays
391 performed by replacing the putative m^{6}A-modified adenosine with a thymine in the 3' UTR of
392 *IL15RA* and *IL18R1* mRNA confirmed that the protein abundances of *IL15RA* and *IL18R1* were
393 promoted by WTAP-mediated m^{6}A (Fig 5P-R). Furthermore, the m^{6}A methylation of many
394 proinflammatory factors, such as *RIPK2*, *IL1A*, *IL12B* and *CXCL11*, was significantly reduced in
395 *WTAP*$^{\Delta 1\text{-}77}$ THP-1 cells (Fig EV8F-I), and reporter assays confirmed that WTAP promoted the
396 protein output of these proinflammatory genes via m^{6}A modification (Fig EV9Q-S). Hence, our
397 work in macrophages not only revealed the significance of WTAP for finetuning the activation of
398 IL6/STAT3 signalling axis, but also implied that the protein synthesis of many proinflammatory
399 genes can be regulated by WTAP via m^{6}A modification in immune homeostasis and disease
400 occurrence, which is unique to WTAP compared to other m^{6}A regulators.
401
402 **The phase separation of WTAP promotes METTL3 recruitment to efficiently modify**
403 **inflammatory transcripts**
404 By verifying the MeRIP-seq data, we found that the genes affected by WTAP in THP-1 cells did
405 not completely overlap before and after LPS treatment (Fig EV10A). Transcripts with low m^{6}A
406 abundance in *WTAP*$^{\Delta 1\text{-}77}$ THP-1 cells were involved in very few metabolic pathways in the resting
407 state (Fig EV10B) but were mainly enriched in cytokine production and inflammatory signalling
408 pathways after LPS treatment (Fig EV10C). Additionally, metagene profiles of the m^{6}A peak
409 distribution showed that inflammatory stimulation increased the abundance of m^{6}A marks but
410 decreased the number of m^{6}A peaks (Fig EV7E and F). These observations implied that the
411 expression of WTAP activated by p65 may lead to more concentrated deposition of m^{6}A marks on
412 inflammatory genes.
413 Recently, liquid-liquid phase separation (LLPS) has emerged as a widespread mechanism through
414 which cells dynamically recruit and organize key signalling molecules. LLPS has also been
415 revealed to play an important role in the formation of the m^{6}A "writer" complex and the regulation
416 of the fate of m^{6}A-modified mRNAs (Chong & Forman-Kay, 2016; Han *et al*, 2022; Ries *et al*,

2019; Zhang *et al*, 2021a). An analysis of the disordered regions in the WTAP protein using the IUPred2A (https://iupred2a.elte.hu/) and PLAAC (http://plaac.wi.mit.edu/) tools revealed a low-complexity region of 16.5 kDa in the C-terminus of the WTAP coding sequence (CDS) (Fig 6A and B), which may form liquid droplets as a result of phase separation (Nott *et al*, 2015). We then further explored whether WTAP has an ability to undergo LLPS upon inflammatory stress and how it plays its roles in the progress of m^6A modification of those inflammatory transcripts. To this end, recombinantly expressed green fluorescent protein (GFP)-WTAP fusion proteins were bacterially expressed and purified (Fig EV11A). The GFP-WTAP formed spherical droplets with an aspect ratio close to 1, and an increase in the protein concentration and salt concentration increased the abundance of GFP droplets from barely detectable small foci to regular and large droplets (Figs 6C and EV11B). Through time-lapse microscopy, we found that the droplet size of GFP-WTAP increased over time (Fig EV11C), and captured the fusion between droplets within 40 s (Fig EV11D), implying the high dynamics and fluidity of the GFP-WTAP droplets. Conversely, droplet formation was substantially inhibited by 10% 1,6-hexanediol (Hex), a compound that putatively dissolves liquid-liquid phase-separated condensates (Fig EV11E).

To further test the ability of WTAP to undergo LLPS in intact cells, we constructed a C-terminal enhanced GFP (EGFP)-tagged WTAP vector and ectopically expressed it in 293T cells (Fig EV11F). We found that GFP-tagged WTAP formed discrete puncta in the nucleus (Fig 6D). In line with those *in vitro* results, fluorescence recovery after photobleaching (FRAP) assays in 293T cells showed that the fluorescence of GFP-tagged WTAP was efficiently and gradually recovered after bleaching (Fig 6E and F), indicating the potential phase separation capability of WTAP *in vivo*. Notably, endogenous WTAP condensates formed in HeLa cells, and the number of these droplets increased significantly after cell stimulation with TNF-α due to upregulated expression of WTAP (Figs 6G and H and EV11G), suggesting that upregulated WTAP induced by inflammatory stimuli is more prone to phase separation. In consistent with other study, the WTAP droplets colocalized with the nuclear speckle marker SC35 (Ping *et al.*, 2014) (Fig 6G and I). However, no difference in the number of SC35 droplets was found before and after inflammatory stimulation (Fig 6J), suggesting that endogenous WTAP droplets formed by self-occurring LLPS rather than the dynamics of the nuclear speckles, and the LLPS of WTAP may facilitate its colocalization with nuclear speckles.

447 To further identify the regions in WTAP that are needed for phase separation, we used the PONDR
448 tool (http://www.pondr.com) to predict 5 unfolded intrinsically disordered regions (IDRs) with
449 scores greater than 0.7 in the WTAP protein sequence (Fig EV11H). A series of truncated WTAP
450 mutants labelled with GFP were then constructed (Fig EV11H) and expressed in 293T cells (Fig
451 EV11I). Through confocal imaging, we found that WTAP failed to form droplets only when amino
452 acid residues 225-287 were deleted (Figs 6K and EV11J), suggesting that this sequence is
453 essential for the LLPS of WTAP. Biomolecular condensates formed through LLPS can maintain
454 locally elevated concentrations of resident proteins and/or RNAs (Banani *et al*, 2017). Hence, we
455 subsequently explored the biological function of the phase separation of WTAP. Previous studies
456 revealed that WTAP recruits METTL3 and other cofactors to nuclear speckles and that the RNA-
457 binding capacity of METTL3 is profoundly reduced in the absence of WTAP (Ping *et al.*, 2014).
458 Here, we found that mCherry-METTL3 (Fig EV11K) readily fused with phase-separated GFP-
459 WTAP and colocalized to all GFP-WTAP droplets (Fig EV11L), demonstrating that fusion with
460 WTAP enhanced the METTL3 LLPS *in vitro*. *In vivo*, METTL3 also formed liquid droplets with
461 the help of WTAP (Fig 6L-N), but deleting the LLPS sequence on WTAP significantly reduced the
462 ability of WTAP to recruit METTL3 through LLPS (Fig 6L) without affecting the direct binding
463 of METTL3 and WTAP (Fig EV11M), suggesting that WTAP LLPS might prime METTL3
464 condensation in cells. To confirm that the LLPS of WTAP promotes METTL3 to methylate
465 inflammatory mRNAs, RIP with antibodies against METTL3 followed by qRT–PCR was
466 performed and the results revealed that the amount of *IL6ST*, *IL15RA* and *IL18R1* mRNAs bound
467 by METTL3 was significantly increased after stimulation with LPS and was reduced by WTAP
468 depletion (Figs 6O and EV11N and O). These data further indicated that the LLPS of WTAP
469 facilitates the aggregation of METTL3 and the methylation of inflammatory mRNAs.
470 Consistently, the absence of phase transition capability observably inhibited WTAP-dependent
471 m^6A modification (Figs 6P and EV11P). Taken together, these data suggested that upregulated
472 WTAP undergoes phase separation to facilitate the assembly of the writer complex and the
473 localization of the writer complex to nuclear speckles. Since the nuclear speckles are active
474 regions for gene transcription and RNA processing and are rich in transcriptionally active
475 proinflammatory transcripts during inflammatory stress, WTAP-medicated LLPS may improve the
476 accessibility between the m^6A writer complex and inflammatory transcripts in nuclear speckles,

477 promoting the deposition of m^6A onto transcriptionally active inflammatory transcripts and the
478 activation of proinflammatory responses (Fig 6Q).
479
480 **WTAP deficiency alleviates the disease progression of DSS-induced IBD in mice**
481 All the aforementioned data suggest that WTAP is a true proinflammatory risk factor. To further
482 investigate the potential role and clinical relevance of upregulated WTAP in the progression of
483 inflammatory diseases, we first revealed that both WTAP and IL6ST were upregulated in SLE,
484 asthma, sepsis, RA, psoriasis and IBD patients (Figs EV1A-E and EV12A). Moreover, high
485 expression of WTAP was significantly positively correlated with the level of inflammation in
486 patients. For example, the upregulation of WTAP was significantly inhibited in psoriasis patients
487 treated with anti-IL17A therapy and Crohn's disease (CD) patients treated with anti-TNF therapy
488 (GSE137218/16879, Appendix Table S1), correspondingly, proinflammatory cytokine expression
489 was also significantly decreased in these patients after treatment (Fig 7A and B). We further
490 evaluated the expression of WTAP in the progression of IBD. An analysis of a single-cell dataset
491 of IBD patients (GSE125527, Fig 7C and Appendix Table S1) showed that the expression of
492 WTAP rather than METTL3 was significantly increased in some immune cell subsets in IBD
493 patients, particularly in monocytes (Fig 7D). The prevalence of WTAP upregulation in IBD patient
494 samples was then verified using more public datasets (GSE119600/10616, Fig EV12B and C and
495 Appendix Table S1). Moreover, using data from the IBDMDB database, an analysis of the
496 correlation between genes involved in m^6A methylation and genes that have been identified as
497 IBD risk genes or biomarkers showed that WTAP exhibited the highest correlation with the
498 expression of IBD genes among all the m^6A regulators (Fig EV12D). Observably, increased
499 expression of WTAP was accompanied by an increase in the global m^6A abundance in various
500 inflammatory diseases (Fig EV12E and F), which is consistent with our results in LPS-induced
501 macrophages. Consistent with this finding, similar tendencies were observed in mouse models of
502 imiquimod (IMQ)-induced psoriasis (Figs 7E and EV12G) and 3% dextran sodium sulfate (DSS)-
503 induced colitis (Figs 7F and EV12H). Thus, the high expression of WTAP accompanied by a high
504 level of m^6A modification and high expression levels of proinflammatory cytokines should be a
505 common characteristic of distinct inflammatory diseases, such as IBD.
506 To verify the biological correlation between WTAP and IBD signatures, we subjected *LyzM*-Cre^+

507 *Wtap*$^{\Delta 1\text{-}77}$ mice and their *Wtap*$^{fl/fl}$ control littermates to DSS to induce acute colitis. The
508 administration of DSS in drinking water can cause the death of intestinal epithelial cells and thus
509 compromise gut barrier function and cause inflammation (Wirtz *et al*, 2017). We found that
510 compared with their *Wtap*$^{fl/fl}$ control littermates, the *LyzM*-Cre^{+} *Wtap*$^{\Delta 1\text{-}77}$ mice treated with DSS
511 displayed attenuated colitis, accompanied by less weight loss (Fig 7G) and a lower disease activity
512 index (Fig 7H). Moreover, WTAP deficiency substantially attenuated the shortening of the colon
513 length in the DSS-challenged mice (Fig 7I and J). The low expression of *Il6*, *Il1a*, *Ccl2* and *Ccl8*
514 in DSS-challenged *LyzM*-Cre^{+} *Wtap*$^{\Delta 1\text{-}77}$ mice indicated attenuated colonic inflammation (Fig 7K).
515 A histopathological assessment revealed that the colonic mucosa of *LyzM*-Cre^{+} *Wtap*$^{\Delta 1\text{-}77}$ mice was
516 relatively intact, with less inflammatory cell infiltration after DSS treatment (Fig 7L).
517 Furthermore, *LyzM*-Cre^{+} *Wtap*$^{\Delta 1\text{-}77}$ mice exhibited later death onset and a lower death rate (Fig
518 7M). Taken together, these results suggested that WTAP deficiency attenuates the severity of DSS-
519 induced IBD, revealing a clinically relevant correlation between the WTAP levels and IBD
520 progression. Because the increased expression of WTAP is ubiquitous in many inflammatory
521 diseases, we hypothesize that WTAP is a novel and important risk factor that exerts a broad
522 spectrum of effects on inflammatory diseases and may serve as a novel potential therapeutic target
523 in the treatment of inflammatory diseases.
524

Discussion

WTAP is a smart adapter in the assembly of the m^6A writer complex

Inflammation is vital for protecting the host against invading pathogens and for repairing tissue damage, which requires tight and concise control of pro- and anti-inflammatory gene expression. m^6A, the most prevalent internal mRNA modification, has emerged as an abundant modification throughout the transcriptome and has been recently linked to various inflammatory states, including autoimmunity, infection, metabolic diseases, and cancers. Although the roles played by m^6A in virus replication, host defense, immune cell activation and disease occurrence have been extensively investigated, basic knowledge of the relationship between the m^6A modification and inflammatory diseases has been largely unattained. Here, we found that WTAP, as a p65-controlled gene, is universally upregulated after distinct inflammatory stimuli. Increased WTAP protein is related to higher levels of m^6A modification and excessive inflammatory responses. Noteworthy, the transcription and expression of WTAP have been shown to be regulated in various biological processes. For example, at the transcriptional and posttranscriptional levels, HIF1α (Shao *et al*, 2023) and STAT3 (Liu *et al*, 2023) can transactivate WTAP gene expression by directly binding to its promoter region, and WTAP can also be upregulated by the epigenetic alteration of H3K4me3, resulting in the senescence of nucleus pulposus cells (NPCs) (Li *et al*, 2022a). At the translational and posttranslational levels, a recent study revealed that through epigenetic modifications, the pseudogene WTAPP1 can bind to WTAP mRNA to promote its translation by recruiting the EIF3 translation initiation complex, accelerating the progression of pancreatic ductal adenocarcinoma (PDAC) (Deng *et al*, 2021). And our previous study showed that WTAP undergoes degradation via the ubiquitination-proteasome pathway in virus-infected cells, leading to reductions in the abundance of m^6A marks and the subsequent protein output of *IRF3* and *IFNAR1* and providing the negative feedback to attenuate the intensity of IFN-I signalling (Ge *et al*, 2021). Using smart adapters without methyltransferase activity, such as WTAP, may provide more precise adjustment of m^6A "writer" complex activity, which is evolutionarily and physiologically beneficial to the dynamic regulation of phenotypic diversity and homeostasis in higher organisms, may be realized.

In addition to showing that WTAP is a p65-controlled gene, the basic mechanism by which WTAP coordinates the assembly dynamics of the writer complex to promote the m^6A modification of

555 many inflammatory genes was further revealed in this study. Although WTAP has been shown to
556 be critical for the localization of the m^6A "writer" complex to nuclear speckles, the dynamic
557 assembly of the "writer" complex is not fully unexplored. A previous study reported that METTL3
558 can also undergo LLPS (Han *et al.*, 2022), and METTL3 interacts with m^6A-METTL-associated
559 complex (MACOM) mainly through WTAP (Su *et al*, 2022). Here, we further found that when
560 WTAP is absent or cannot undergo LLPS, METTL3 is dispersedly distributed in the nucleus,
561 which indicates that the LLPS of WTAP is essential for the assembly of the writer complex,
562 providing dynamic m^6A regulation in distinct biological or physiological conditions. In this study,
563 we found that highly expressed WTAP spontaneously forms condensates through LLPS under
564 inflammatory stress, which may be important for the recruitment of more "writer" proteins to
565 nuclear speckles. Because nuclear speckles are sites with many transcriptionally active genes
566 (Faber *et al*, 2022), WTAP-mediated LLPS may increase the local "writer" concentrations and
567 improve the accessibility between the m^6A "writer" complex and inflammatory transcripts in
568 nuclear speckles, thereby promoting the m^6A modification of inflammatory genes and accelerating
569 of inflammatory response. In the past decade, biomolecular condensates formed by LLPS have
570 been widely reported to modulate many cellular functions by compartmentalizing specific proteins
571 and nucleic acids in subcellular environments with distinct properties (Shin & Brangwynne, 2017;
572 Vendruscolo & Fuxreiter, 2022). Our finding further expands the regulatory roles of phase
573 separation to the dynamic assembly of writer complex and the methylation of specific transcripts,
574 describing how cells utilize the composition and compartmentation of multivalent condensates to
575 affect the m^6A epitranscriptome.
576
577 **The finetuning of the STAT3 signalling axis by targeting of WTAP LLPS may be an effective**
578 **therapeutic strategy for excessive inflammation**
579 m^6A modification has been reported to regulate inflammatory responses and related diseases. For
580 example, KDM6B (Wu *et al.*, 2020), SOCS1 (Du *et al*, 2020), TRAF3 and TRAF6 (Zheng *et al*,
581 2017; Zong *et al.*, 2019) are dynamically regulated by m^6A modification in controlling
582 inflammatory responses. Through analyses of clinical data and mouse disease models, we clearly
583 found that increased expression of WTAP is associated with inflammatory diseases, such as sepsis,

584 SLE, asthma (Mo *et al*, 2022), RA, psoriasis (Mande *et al*, 2018) and IBD (Nie *et al*, 2022) (Fig
585 EV1). A recent study also suggested the relationship of WTAP to the anti-inflammatory effect of
586 *Astragalus mongholicus polysaccharide* (APS) (Long *et al*, 2022). In addition to showing the
587 relationship between increased WTAP and higher m^6A modification in inflammation, we
588 specifically showed that an increase in WTAP protein was accompanied by increases in the m^6A
589 abundances on *IL6ST*, *IL15RA*, *IL18R1*, and many other transcriptionally active proinflammatory
590 cytokines. High IL6ST, IL15RA and IL18R1 protein abundance promotes activation of the STAT3
591 signalling axis, which in turn contributes to the production of proinflammatory cytokines, such as
592 IL-6, CCL2 and CCL8 (Fig 6Q). Consistently, two recent studies individually noted that the
593 knockdown of FTO can significantly increase the overall m^6A abundance, STAT3 phosphorylation
594 and the secretion of proinflammatory cytokines and thereby positively regulates the inflammation
595 and IFN-I response (McFadden *et al*, 2022; Tang *et al.*, 2022). Moreover, the IL-6/STAT3
596 pathway is aberrantly hyperactivated in many cancers, and such hyperactivation is generally
597 associated with a poor clinical prognosis (Johnson *et al*, 2018). Recent studies have also shown
598 that high levels of m^6A modification enhance JAK1 translation in high-metastatic hepatocellular
599 carcinoma (HCC) cells, thereby promoting the activation of STAT3 (Liu *et al.*, 2023).
600 Interestingly, the expression of WTAP is also significantly elevated in many cancers, such as
601 pancreatic carcinoma (Deng *et al.*, 2021), osteosarcoma (Ren *et al*, 2022), HCC (Chen *et al*, 2019)
602 and nasopharyngeal carcinoma (Li *et al*, 2022b). This implies that the strategy of finetuning the
603 STAT3 signalling axis by WTAP may also play an important role in the progression of multiple
604 cancers. Because the STAT3 axis has been well characterized as a mechanism to accelerate the
605 production of a variety of cytokines and chemokines (Tanaka *et al*, 2014) and is highly associated
606 with inflammatory diseases, including cytokine storm syndromes, autoimmune diseases and
607 cancers (Gharibi *et al*, 2020; Matsuyama *et al*, 2020) , the novel NF-κB/WTAP/STAT3 axis
608 identified in this study indicated that WTAP is an ideal therapeutic target in the treatment of many
609 inflammatory diseases and cancers.
610 To date, effective therapeutic interventions for excessive inflammation by inhibiting STAT3
611 activity in the clinic remain to be further developed, largely due to the challenge of directly
612 targeting STAT3 (STAT3 is a transcription factor that lacks enzymatic activity), and in part due to
613 the complexity and diversity of the biological functions of STAT3 (Yu *et al*, 2014). Small-

molecule inhibitors targeting the NF-κB and STAT3 signalling pathways cause side effects because the long-term suppression of the NF-κB or STAT3 affects the homeostasis of the immune system as well as normal cell growth, differentiation, and survival (Siegel *et al.*, 2011; Zhang *et al.*, 2017). Here, we found that hyperinflammatory states in the body are often accompanied by high levels of m^6A methylation. Reducing the abundance of m^6A marks by STM2457 (Fig EV13A), a METTL3 inhibitor, significantly inhibited HKST-induced expression of proinflammatory genes (Fig EV13B). We also verified this effect in a mouse model of LPS-induced sepsis by showing that the m^6A modification levels of colon and lung tissues from mice were significantly reduced by STM2457 (Fig EV13C and D). A decrease in the m^6A modification level blocked the expression of inflammatory cytokines and activation of inflammatory signals induced by LPS (Fig EV13E and F). Similarly, STM2457 effectively alleviated lung inflammation and the pathological characteristics of lung injury (Fig EV13G). Based on these data combined with one study showing that STM2457 can effectively reduce the severity of DSS-induced IBD in mice (Yang *et al*, 2022), we believe that reversing the high abundance of m^6A modifications in disease states has broad prospects in the treatment of inflammatory diseases in the future. Because WTAP is more concentrated in the inflammatory context to affect the m^6A modification of nascent inflammatory genes, epigenetic therapies targeting WTAP to reprogram the m^6A landscape in cells may achieve more effective and safer therapeutic outcomes.

Elvitegravir (EVG), which was originally developed to treat HIV infection (Sato *et al*, 2006), was recently found to efficiently inhibit YAP oncogenic transcription by specifically disrupting SRC-1 LLPS (Zhu *et al*, 2021), demonstrating the feasibility of targeting LLPS to treat diseases. For the purpose of reducing hyperinflammation, one possible strategy is the development or identification of small-molecule drugs that can block WTAP LLPS to reduce the overall m^6A abundance, which might reverse the hyperinflammatory state of diseases. Moreover, interfering with WTAP LLPS during inflammatory state may reduce the damage to constitutively expressed genes and normal cells to successfully combat autoimmunity, infection, metabolic diseases, and cancers. In addition, given the critical role played by the NF-κB signalling pathway in cancer and various chronic diseases, NF-κB has become a potential target for pharmacological intervention, and numerous inhibitors of NF-κB may play important roles in the treatment of various inflammatory diseases in the future (Freitas & Fraga, 2018). Here, we found that the NF-κB p65 inhibitor PG490

644 significantly reduced the overall m^6A abundance by inhibiting the expression of WTAP (Fig
645 EV13H). Thus, for the development of novel small anti-inflammatory molecules, researchers may
646 need to consider the effects of these inhibitors on epitranscriptome.
647 In summary, we provide the first demonstration that high m^6A modification in a variety of
648 hyperinflammatory states is p65-dependent, due to the key component of the writer complex
649 WTAP is transcriptionally regulated by p65 and its overexpression can lead to higher m^6A
650 modification. We also discovered that upregulated WTAP undergoes phase separation, which
651 facilitates the aggregation of the writer complex and its localization to nuclear speckles and the
652 deposition of m^6A onto transcriptionally active transcripts, which results in the promotion of
653 proinflammatory responses. Based on the mouse model of inflammatory diseases generated in this
654 study and many online clinical data, we hypothesize that higher expression of WTAP should be a
655 risk factor in many hyperinflammatory states and inflammatory diseases. Interrupting the
656 assembly of the m^6A writer complex by targeting the phase separation of WTAP to reduce the
657 global m^6A level may be a potential therapeutic strategy for preventing excessive inflammation.

Material and Methods

Mice.

C57BL/6 *LyzM*-Cre^{+} *Wtap*$^{fl/fl}$ mice were generated by Gempharmatech Co., Ltd. using the CRISPR/Cas9 approach. All mouse lines were maintained at Sun Yat-sen University under specific pathogen-free (SPF) conditions in ventilated microisolator cages. The Institutional Animal Care and Use Committee (IACUC) of Sun Yat-sen University (Guangzhou, China) approved all the experimental protocols concerning the handling of mice. The study is compliant with all relevant ethical regulations regarding animals.

Cells.

The 293T, HeLa and THP-1 cell lines were purchased from ATCC. All these cells were cultured in endotoxin-free DMEM or RPMI-1640, supplemented with 10% FBS and 1% penicillin–streptomycin. PBMCs and BMDMs were isolated and cultured as described previously(Ge *et al.*, 2021).

In vitro recombinant protein expression and purification.

The expressing plasmids (pET-32a) encoding WTAP conjugated eGFP and METTL3 conjugated mCherry were transformed into BL21 *E.coli*. *E.coli* were cultured in LB with Ampicillin (50 μg/mL) at 37 °C for about 12 hr till OD600 = 0.6. After induction with 1 mM IPTG at 37 °C for 8 hr, the cultured *E.coli* was harvested by centrifugation at 4000 rpm, 4 °C, 10 min and resuspended in lysis buffer. Cells were lysed by sonication on ice and centrifuged (12,000 rpm, 30 min, 4 °C) to remove debris and collected the supernatant. The supernatant was purified by incubation with Ni-NTA agarose beads (QIAGEN) overnight at 4 °C. Then, Ni-NTA beads were washed with wash buffer (50 mM NaH2PO4, 300 mM NaCl, 20 mM imidazole, pH 7.8), and proteins were eluted with elution buffer (50 mM NaH2PO4, 300 mM NaCl, 300 mM imidazole, pH 7.8). The purified proteins were further dialyzed by using PD10 column (GE Healthcare), and concentrated using Amicon Ultra 30 K (Millipore) concentrators at 4 °C. Concentrated proteins were quantified by the BCA method (Thermo Fisher) and stored at -80 °C.

687 **Generation of knockout THP-1 cells**.

688 Knockout (KO) cells were constructed using the CRISPR/Cas9 system. Small guide RNAs
689 (gRNAs) targeting the genome sequence of target genes were designed using an online gRNA
690 design tool (by Zhang Feng laboratory, http://crispr.mit.edu/), and subcloned into the lentiCRISPR
691 v2 vector. This vector was transfected into the HEK293T cells along with the following two
692 lentiviral packing plasmids: psPAX2 and pVSV-G. The culture supernatants were collected at 48
693 and 60 hours after transfection and concentrated by ultracentrifugation before use for infection.
694 The infection-positive (GFP^+) cells were selected by flow cytometry, monoclonal cells were
695 confirmed by genomic sequencing and immunoblotting analysis with the corresponding antibody.
696 The gRNA sequences used for generating the KO cells are listed in Table S2.

697

698 ***In vivo* LPS challenge.**

699 For endotoxicity studies, age-matched female *Wtap*$^{fl/fl}$ and *LyzM-cre*$^+$ *Wtap*$^{fl/fl}$ mice (8 weeks old)
700 were intraperitoneally injected with LPS (40 mg kg^{-1}). Mouse survival was monitored every 4 hr.
701 Female *Wtap*$^{fl/fl}$ and *LyzM-cre*$^+$ *Wtap*$^{\Delta 1\text{-}77}$ mice (8 weeks old) were intraperitoneally injected with
702 LPS (10 mg kg^{-1}) or isodose PBS. After 12 hr, the mice were killed, blood was collected, and
703 serum levels of IL-6 were measured by ELISA. Lung and colon tissues were collected, and RNA
704 samples were extracted for qRT-PCR to determine the mRNA levels of inflammatory cytokines.
705 Female *Wtap*$^{fl/fl}$ and *LyzM-cre*$^+$ *Wtap*$^{\Delta 1\text{-}77}$ mice (8 weeks old) were intraperitoneally injected with
706 LPS (10 mg kg^{-1}) or PBS. After 6 hr, the mice were killed, and lungs from control or LPS-
707 stimulated mice were dissected, fixed in 4% paraformaldehyde (PFA) embedded in paraffin,
708 sectioned, stained with hematoxylin and eosin (H&E) solution, and examined by light microscopy
709 to detect histological changes.
710 Female *Wtap*$^{fl/fl}$ and *LyzM-cre*$^+$ *Wtap*$^{\Delta 1\text{-}77}$ mice (8 weeks old) were intraperitoneally injected with
711 *P. aeruginosa* (ATCC27853, 2×10^8 CFU) or *L. monocytogenes* (ATCC19116, 1×10^8 CFU) or
712 PBS. After 16 hr, the mice were killed, and the related phenotypes were measured as described
713 above.

714

715 **ELISA assays and quantitative RT–PCR (qRT–PCR)**.

716 The concentrations of IL-6, IL-1β and TNF-α in culture supernatants were measured using kits

717 from R&D Systems or Proteintech, according to the manufacturer's instructions.
718 Total RNA was extracted using TRIzol reagent (Invitrogen) and reversed-transcribed with a
719 PrimeScript™ RT reagent kit with gDNA Eraser (TaKaRa) according to the manufacturer's
720 instructions. And 2×Polarsignal® qPCR mix (MIKX) was used for quantitative real-time PCR
721 analysis. The data were normalized by the level of *GAPDH* or *ACTB* expression in each individual
722 sample, and primer sequences used are listed in Table S2.
723
724 **Luciferase reporter gene assay**.
725 For a promoter reporter gene assay, 293T cells were plated in 48-well plates and transiently
726 transfected with WTAP promoter reporter (pGL3 basic plasmid), with increasing doses of Flag-
727 tagged NF-κB p65, IRF3 or C/EBPβ and 7.5 ng of the Renilla luciferase reporter vector using
728 Lipofectamine 2000. 24 hrs post-transfection, luciferase activities were measured with a dual-
729 luciferase reporter assay system (Promega) according to the manufacturer's instructions. Reporter
730 gene activity was determined by normalization of Firefly luciferase activity to Renilla luciferase
731 activity.
732 For other reporter gene assays, wild-type or *WTAP* KO 293T cells were plated in 48-well plates
733 and transiently transfected with the indicated reporter vectors (psiCHECK™-2) expressing wild-
734 type or mutated UTRs of *IL6ST* using Lipofectamine 2000. 24 hrs post-transfection, the luciferase
735 activities were measured as above. Reporter gene activity was determined by normalization of the
736 Renilla luciferase activity to Firefly luciferase activity.
737
738 **Small interfering RNAs (siRNAs) and RNA interference**.
739 The control nontargeting and WTAP-, YTHDF1-, YTHDF3-specific siRNAs were designed and
740 synthesized by RiboBio. THP-1 cells (8×10^5 cells/mL) were transiently transfected with siRNA
741 (final concentration of 20 μM) using Lipofectamine RNAiMAX following the manufacturer's
742 instructions. The sequences of siRNAs are listed in Table S2.
743
744 **RNA decay assay.**
745 $WTAP^{\Delta 1\text{-}77}$ and WT THP-1 cells were seeded at a density of 8×10^5 cells/mL in 12-well plates.
746 After treatment with PMA (50 ng/mL, Sigma), the cells were treated with transcription inhibitor

747 Act D (5 μg/mL, Sigma) to block *de novo* RNA synthesis, and collected at different times. RNA
748 samples were extracted for qRT–PCR to determine the mRNA levels of the indicated genes.
749
750 **Laser scanning confocal microscopy (LSCM).**
751 Cells for fluorescence experiments were cultured in glass bottom culture dishes (Nest Scientific).
752 After treated with indicated stimulation, cells were fixed by 4% paraformaldehyde for 10 min,
753 followed with 3 times wash with PBS. Then, cells were permeabilized with methyl alcohol for
754 30 min at −20 °C and rinsed with PBS for 3 times. After blocking in 5% goat serum for 1 h at
755 room temperature, cells were incubated with primary antibodies at 4 °C, overnight. 1 × PBST
756 (PBS with 0.1% Tween20) was used to wash the cells for 3 times and subsequently incubated with
757 fluorescently labeled secondary antibodies at room temperature for 1 h. Confocal images were
758 obtained by Leica TCS SP8 STED 3X confocal microscope. The number of condensates were
759 counted and analyzed by ImageJ software.
760
761 **Live-cell imaging.**
762 At 24 hrs posttransfection incubation, cells were loaded into temperature- and CO2-controlled
763 live-cell imaging chamber of Leica TCS SP8 STED 3X confocal microscope. Cells were imaged
764 typically by use of 2 laser wavelengths (488 nm for eGFP imaging and 560 nm for mCherry
765 imaging).
766
767 **In vitro phase separation assay.**
768 The purified recombinant proteins were mixed at indicated concentration with LLPS buffer and
769 5% PEG8000 at 37 °C. The mixture was pipetted onto glass bottom dish and imaged by Leica
770 TCS SP8 STED 3X confocal microscope equipped with 100 × 1.40 NA oil objectives.
771
772 **Fluorescence recovery after photobleaching (FRAP) assay.**
773 FRAP assay was conducted by Leica TCS SP8 STED 3X confocal microscopy. 488- or 568-nm
774 laser beam was used to bleach the fluorescent protein at a region of interest (ROI), followed with
775 collecting time-lapse images. Fluorescence intensity of indicated ROI was measured and

776 normalized to the fluorescence intensity of pre-bleaching image by Leica AS Lite.

777

778 **m^6A dot blots.**

779 Total RNA was extracted with TRIzol reagent. Equal amounts of RNA (300 ng) were denatured at
780 95 °C for 3 min. The samples were immediately chilled on ice, added to a positively charged nylon
781 membrane (PALL), and then cross-linked with a UV crosslinker. After blocking and incubating
782 with the m^6A antibody (CST) overnight, the membrane was incubated with the secondary antibody
783 at room temperature for 1 hr. Signals were detected using a chemiluminescence imaging system.
784 Methylene blue in 0.3 M sodium acetate (pH 5.2) was used to indicate the amount of total RNA.

785

786 **RNA immunoprecipitation assay**.

787 RIP was conducted using a RIP assay Kit (MBL) following the manufacturer's instructions. In
788 brief, Protein A/G magnetic beads coated with 5 μg of specific antibody or normal IgG were
789 incubated with cell lysates at 4 °C overnight. Proteins were then extracted for immunoblot
790 analysis, and the co-precipitated RNAs were isolated by elution buffer and purified by TRIzol
791 reagent, and subsequently subjected to qRT–PCR analysis.

792

793 **DNA/RNA pull-down assay**.

794 Biotin-labeled DNA and RNA probes were synthesized by RiboBio. For DNA pull-down assay,
795 Flag-tagged NF-κB p65 expression constructs were transfected into 293T cells. 24 hrs post-
796 transfection, whole cell lysates were extracted from 293T cells using IP lysis buffer. Biotin-
797 coupled DNA-protein complex was pulled down by incubating whole cell lysates with high-
798 capacity streptavidin agarose beads (Thermo Fisher) according to the manufacturer's instructions.
799 The bound proteins were eluted and used for immunoblot analysis.

800 For RNA pull-down assay, biotin-coupled RNA complex was pulled down by incubating cell
801 lysates with high-capacity streptavidin agarose beads, bound proteins were then extracted for
802 immunoblot analysis.

803

804 **m^6A RNA-IP-qRT–PCR (MeRIP–qPCR)**.

805 An MeRIP assay was performed following a previously described procedure with minor

806 modifications (Ge *et al.*, 2021). Briefly, 200 μg of total RNA was fragmentated to approximately
807 150-200 nt in length, purified by magnetic beads, and then incubated with anti-m^6A antibody- or
808 IgG-conjugated protein A/G magnetic beads in 1 × IP buffer at 4 °C overnight.
809 Immunoprecipitated methylated RNAs were competitive eluted by free m^6A, and recovered with a
810 RNeasy kit (QIAGEN). One-tenth of the fragmented RNA was saved for use as the input control
811 and further analyzed by qRT–PCR with the MeRIP RNAs using primers for the targeted gene. The
812 related enrichment of m^6A in each sample was calculated by normalizing the number of
813 amplification cycles (Cq) of the m^6A-IP portion to the Cq of the corresponding input portion.
814
815 **Quantification of the m^6A modification by LC-MS/MS.**
816 200 ng extracted mRNA was digested into nucleosides by Nuclease P1 (1 U, NEB, M0660S) and
817 shrimp alkaline phosphatase (rSAP, 1 U, NEB, M0371S) in 50 μL RNase-free water at 37 °C
818 overnight. The mixture was diluted to 100 μL, 10 μL of which was injected into an LC–MS/MS
819 system consisting of a high-performance liquid chromatographer (Shimadzu) equipped with a
820 C18-T column (Weltech) and a Triple Quad 4500 (AB SCIEX) mass spectrometer in positive ion
821 mode by multiple-reaction monitoring. Mass transitions of m/z 268.0–136.0 (A), m/z 245.0–113.1
822 (U), m/z 244.0–112.1 (C), m/z 284.0–152.0 (G) and m/z 282.0–150.1 (m^6A) were monitored. A
823 concentration series of pure commercial nucleosides (MCE) was employed to generate standard
824 curves. The concentration of nucleosides in samples were obtained by fitting signal intensity to a
825 standard curve with certain ratios calculated subsequently.
826
827 **RNA-seq and data analysis**.
828 Whole-cell total RNA was isolated using TRIzol reagent and quantified using a NanoDrop 2000
829 spectrophotometer (Thermo). The cDNA library was constructed by Biomarker Technologies.
830 Sequencing was performed on an Illumina HiSeq 2500 platform. High-quality reads were mapped
831 to the human reference genome (hg19) using HISAT2. DESeq, an R package, was applied for
832 differential gene expression analysis. We filtered the differentially expressed genes based on a
833 false discovery rate (FDR) <0.05.
834
835 **Methylated RNA immunoprecipitation sequencing (MeRIP-seq) and data analysis**.

836 Total RNA was extracted by TRIzol reagent and mRNA was isolated using a Dynabeads mRNA
837 purification kit (Thermo Fisher). Then, cellar mRNA was fragmented using a fragmentation kit
838 (Thermo Fisher), and subsequent m^6A immunoprecipitation, MeRIP-seq and data analysis was
839 carried out as previously described with minor modifications (Zhang *et al*, 2021b).
840
841 **Statistical analysis.**
842 The data are represented as the mean ± s.d. unless otherwise indicated, and two-tailed Student's *t*-
843 test or Mann–Whitney U test with a confidence interval of 95% were performed for all statistical
844 analyses (survival curves were compared by the log-rank test) with GraphPad Prism 6 software.
845 Differences between two groups were considered statistically significant when the *P* value was
846 less than 0.05.
847
848 **Data and code availability**
849 Publicly available datasets, which were analyzed in this study including GSE19315, GSE198326,
850 GSE2411, GSE2638, GSE69063, GSE13887, GSE137268, GSE97779, GSE166388, GSE208303,
851 GSE125527, GSE16879, GSE193193, GSE179874, GSE119600, GSE10616, GSE137218,
852 GSE227851 and GSE189847 are available at the GEO database
853 (https://www.ncbi.nlm.nih.gov/geo/).
854 The validated IBDMDB data and relevant participants' information are available at the IBDMDB
855 database (http://ibdmdb.org).
856 All data generated for this paper have been deposited at the SRA under access number:
857 PRJNA943438.
858
859 ## Acknowledgments
860 This work was supported by projects from National Natural Science Foundation of China
861 (91942301, 31970852, 32200712), Guangdong Science and Technology Department
862 (2020B1212060031, 2023A1515010541), Ministry of Science and Technology of the People's
863 Republic of China (2018YFD0900502), "Decoding TCM" collaborative research project of
864 BUCM (90010060920009), Innovation Group Project of Southern Marine Science and
865 Engineering Guangdong Laboratory (Zhuhai) (311021006), National Key Research and

Development Project (2019YFC1710104) and Fundamental Research Funds for the Central Universities (23yxqntd001).

Author Contributions

Y.G., S.Y. and A.X. designed the study, analyzed the data, and prepared the manuscript with input from the other authors. Y.G., R.C., T.L., Y.C., J.H., Y.L., X.X. and G.X. performed the experiments collaboratively. B.L., H.C. and G.L. performed the data analysis of MeRIP-seq. S.Y. and A.X. conceived the study, supervised experiments, and wrote the paper. A.X. and S.Y. led the project and finally approved the manuscript.

Declaration of Interests

The authors declare that they have no competing interests.

References

Banani SF, Lee HO, Hyman AA, Rosen MK (2017) Biomolecular condensates: organizers of cellular biochemistry. ***Nat Rev Mol Cell Biol*** 18: 285-298

Banerjee S, Biehl A, Gadina M, Hasni S, Schwartz DM (2017) JAK-STAT signaling as a target for inflammatory and autoimmune diseases: current and future prospects. ***Drugs*** 77: 521-546

Barbieri I, Kouzarides T (2020) Role of RNA modifications in cancer. ***Nat Rev Cancer*** 20: 303-322

Bradley JR (2008) TNF-mediated inflammatory disease. ***J Pathol*** 214: 149-160

Cao XT (2016) Self-regulation and cross-regulation of pattern-recognition receptor signalling in health and disease. ***Nat Rev Immunol*** 16: 35-50

Carpenter S, Ricci EP, Mercier BC, Moore MJ, Fitzgerald KA (2014) Post-transcriptional regulation of gene expression in innate immunity. ***Nat Rev Immunol*** 14: 361-376

Chen YH, Peng CH, Chen JR, Chen DY, Yang B, He B, Hu WD, Zhang YP, Liu H, Dai LF *et al* (2019) WTAP facilitates progression of hepatocellular carcinoma via m^6A-HuR-dependent epigenetic silencing of ETS1. ***Mol Cancer*** 18: 127

Chong PA, Forman-Kay JD (2016) Liquid-liquid phase separation in cellular signaling systems. ***Curr Opin Struct Biol*** 41: 180-186

Cui L, Ma R, Cai JLY, Guo CY, Chen ZY, Yao LL, Wang YY, Fan R, Wang X, Shi YL (2022) RNA modifications: importance in immune cell biology and related diseases. ***Signal Transduct Target Ther*** 7: 334

Deng JG, Zhang JL, Ye Y, Liu KJ, Zeng LX, Huang JY, Pan L, Li M, Bai RH, Zhuang LS *et al* (2021) N^6-methyladenosine-mediated upregulation of WTAPP1 promotes WTAP translation and Wnt signaling to facilitate pancreatic cancer progression. ***Cancer Res*** 81: 5268-5283

Du J, Liao W, Liu WC, Deb DK, He L, Hsu PJ, Nguyen T, Zhang LD, Bissonnette M, He C *et al* (2020) N^6-adenosine methylation of Socs1 mRNA is required to sustain the negative feedback control of macrophage activation. ***Dev Cell*** 55: 737-753.e737

Faber GP, Nadav-Eliyahu S, Shav-Tal Y (2022) Nuclear speckles - a driving force in gene expression. ***J Cell Sci*** 135: jcs259594

Freitas RHCN, Fraga CAM (2018) NF-kappa B-IKK beta pathway as a target for drug development: realities, challenges and perspectives. ***Curr Drug Targets*** 19: 1933-1942

Fu Y, Dominissini D, Rechavi G, He C (2014) Gene expression regulation mediated through reversible m^6A RNA methylation. ***Nat Rev Genet*** 15: 293-306

Ge Y, Ling T, Wang Y, Jia X, Xie XM, Chen R, Chen SW, Yuan SC, Xu AL (2021) Degradation of WTAP blocks antiviral responses by reducing the m^6A levels of IRF3 and IFNAR1 mRNA. ***EMBO Rep*** 22: e52101

Gharibi T, Babaloo Z, Hosseini A, Abdollahpour-alitappeh M, Hashemi V, Marofi F, Nejati K, Baradaran B (2020) Targeting STAT3 in cancer and autoimmune diseases. *Eur J Pharmacol* 878: 173107

Gong T, Liu L, Jiang W, Zhou RB (2020) DAMP-sensing receptors in sterile inflammation and inflammatory diseases. ***Nat Rev Immunol*** 20: 95-112

Greten FR, Grivennikov SI (2019) Inflammation and cancer: triggers, mechanisms, and consequences. ***Immunity*** 51: 27-41

Han D, Longhini AP, Zhang X, Hoang V, Wilson MZ, Kosik KS (2022) Dynamic assembly of the mRNA m^6A methyltransferase complex is regulated by METTL3 phase separation. ***PLoS biol*** 20: e3001535

923 Hirano T (2021) IL-6 in inflammation, autoimmunity and cancer. ***Int Immunol*** 33: 127-148
924 Huang Y, Su R, Sheng Y, Dong L, Dong Z, Xu HJ, Ni TF, Zhang ZS, Zhang T, Li CY *et al* (2019)
925 Small-molecule targeting of oncogenic FTO demethylase in acute myeloid leukemia. ***Cancer Cell*** 35:
926 677-691
927 Hunter CA, Jones SA (2015) IL-6 as a keystone cytokine in health and disease. ***Nat Immunol*** 16: 448-
928 457
929 Jiang XL, Liu BY, Nie Z, Duan LC, Xiong QX, Jin ZX, Yang CP, Chen YB (2021) The role of m^6A
930 modification in the biological functions and diseases. ***Signal Transduct Target Ther*** 6: 74
931 Johnson DE, O'Keefe RA, Grandis JR (2018) Targeting the IL-6/JAK/STAT3 signalling axis in cancer.
932 ***Nat Rev Clin Oncol*** 15: 234-248
933 Kang SJ, Tanaka T, Narazaki M, Kishimoto T (2019) Targeting interleukin-6 signaling in clinic.
934 ***Immunity*** 50: 1007-1023
935 Li GC, Ma L, He SJ, Luo RJ, Wang BJ, Zhang WF, Song Y, Liao ZW, Ke WC, Xiang Q *et al* (2022a)
936 WTAP-mediated m^6A modification of lncRNA NORAD promotes intervertebral disc degeneration. ***Nat***
937 ***Commun*** 13: 1469
938 Li N, Rana TM (2022) Regulation of antiviral innate immunity by chemical modification of viral RNA.
939 ***Wiley Interdiscip Rev RNA*** 13: e1720
940 Li ZX, Zheng ZQ, Yang PY, Lin L, Zhou GQ, Lv JW, Zhang LL, Chen FP, Li YQ, Wu CF *et al* (2022b)
941 WTAP-mediated m^6A modification of lncRNA DIAPH1-AS1 enhances its stability to facilitate
942 nasopharyngeal carcinoma growth and metastasis. ***Cell Death Differ*** 29: 1137-1151
943 Liu BW, Cao JL, Wu BT, Hao KX, Wang XY, Chen X, Shen ZF (2023) METTL3 and STAT3 form a
944 positive feedback loop to promote cell metastasis in hepatocellular carcinoma. ***Cell Commun Signal***
945 21: 121
946 Liu J, Qian C, Cao XT (2016) Post-translational modification control of innate immunity. ***Immunity***
947 45: 15-30
948 Long HJ, Lin HY, Zheng P, Hou LJ, Zhang M, Lin SY, Yin K, Zhao GJ (2022) WTAP mediates the
949 anti-inflammatory effect of Astragalus mongholicus polysaccharide on THP-1 macrophages. ***Front***
950 ***Pharmacol*** 13: 1023878
951 Luo JH, Xu T, Sun K (2021) N^6-methyladenosine RNA modification in inflammation: roles,
952 mechanisms, and applications. ***Front Cell Dev Biol*** 9: 670711
953 Mande P, Zirak B, Ko WC, Taravati K, Bride KL, Brodeur TY, Deng A, Dresser K, Jiang ZZ, Ettinger
954 R *et al* (2018) Fas ligand promotes an inducible TLR-dependent model of cutaneous lupus-like
955 inflammation. ***J Clin Invest*** 128: 2966-2978
956 Mapperley C, van de Lagemaat LN, Lawson H, Tavosanis A, Paris J, Campos J, Wotherspoon D,
957 Durko J, Sarapuu A, Choe J *et al* (2021) The mRNA m^6A reader YTHDF2 suppresses proinflammatory
958 pathways and sustains hematopoietic stem cell function. ***J Exp Med*** 218: e20200829
959 Matsuyama T, Kubli SP, Yoshinaga SK, Pfeffer K, Mak TW (2020) An aberrant STAT pathway is
960 central to COVID-19. ***Cell Death Differ*** 27: 3209-3225
961 McFadden MJT, Sacco MTA, Murphy KA, Park MS, Gokhale NSY, Somfleth KYM, Horner SM
962 (2022) FTO suppresses STAT3 activation and modulates proinflammatory interferon-stimulated gene
963 expression. ***J Mol Biol*** 434: 167247
964 Medzhitov R, Horng T (2009) Transcriptional control of the inflammatory response. ***Nat Rev Immunol***
965 9: 692-703
966 Mishra A, Sullivan L, Caligiuri MA (2014) Molecular pathways: interleukin-15 signaling in health and

967 in cancer. ***Clin Cancer Res*** 20: 2044-2050
968 Mo BW, Li XM, Li SM, Xiao B, Yang J, Li HM (2022) m^{6}A echoes with DNA methylation:
969 Coordinated DNA methylation and gene expression data analysis identified critical m^{6}A genes
970 associated with asthma. ***Gene*** 828: 146457
971 Nie K, Yi J, Yang YY, Deng MZ, Yang Y, Wang TY, Chen XJ, Zhang ZY, Wang XY (2022) A broad
972 m^{6}A modification landscape in inflammatory bowel disease. ***Front Cell Dev Biol*** 9: 782636
973 Nott TJ, Petsalaki E, Farber P, Jervis D, Fussner E, Plochowietz A, Craggs TD, Bazett-Jones DP,
974 Pawson T, Forman-Kay JD *et al* (2015) Phase transition of a disordered nuage protein generates
975 environmentally responsive membraneless organelles. ***Mol Cell*** 57: 936-947
976 O'Connell MA, Mannion NM, Keegan LP (2015) The epitranscriptome and innate immunity. ***PLoS***
977 ***Genet*** 11: e1005687
978 Ping XL, Sun BF, Wang L, Xiao W, Yang X, Wang WJ, Adhikari S, Shi Y, Lv Y, Chen YS *et al* (2014)
979 Mammalian WTAP is a regulatory subunit of the RNA *N*^{6}-methyladenosine methyltransferase. ***Cell Res***
980 24: 177-189
981 Ren ZP, Hu YC, Sun J, Kang YX, Li GS, Zhao HJ (2022) *N*^{6}-methyladenosine methyltransferase
982 WTAP-stabilized FOXD2-AS1 promotes the osteosarcoma progression through m^{6}A/FOXM1 axis.
983 ***Bioengineered*** 13: 7963-7973
984 Ries RJ, Zaccara S, Klein P, Olarerin-George A, Namkoong S, Pickering BF, Patil DP, Kwak H, Lee
985 JH, Jaffrey SR (2019) m^{6}A enhances the phase separation potential of mRNA. ***Nature*** 571: 424-428
986 Sato M, Motomura T, Aramaki H, Matsuda T, Yamashita M, Ito Y, Kawakami H, Matsuzaki Y,
987 Watanabe W, Yamataka K *et al* (2006) Novel HIV-1 integrase inhibitors derived from quinolone
988 antibiotics. ***J Med Chem*** 49: 1506-1508
989 Scholler E, Weichmann F, Treiber T, Ringle S, Treiber N, Flatley A, Feederle R, Bruckmann A, Meister
990 G (2018) Interactions, localization, and phosphorylation of the m^{6}A generating METTL3-METTL14-
991 WTAP complex. ***RNA*** 24: 499-512
992 Shao YL, Li YQ, Li MY, Wang LL, Zhou HS, Liu DH, Yu L, Lin J, Gao XN (2023) HIF1 alpha-
993 mediated transactivation of WTAP promotes AML cell proliferation via m^{6}A-dependent stabilization of
994 KDM4B mRNA. ***Leukemia*** 37: 1254-1267
995 Shi HL, Wang X, Lu ZK, Zhao BXS, Ma HH, Hsu PJ, Liu C, He C (2017) YTHDF3 facilitates
996 translation and decay of *N*^{6}-methyladenosine-modified RNA. ***Cell Res*** 27: 315-328
997 Shin Y, Brangwynne CP (2017) Liquid phase condensation in cell physiology and disease. ***Science*** 357:
998 eaaf4382
999 Shulman Z, Stern-Ginossar N (2020) The RNA modification *N*^{6}-methyladenosine as a novel regulator
1000 of the immune system. ***Nat Immunol*** 21: 501-512
1001 Siegel AM, Heimall J, Freeman AF, Hsu AP, Brittain E, Brenchley JM, Douek DC, Fahle GH, Cohen
1002 JI, Holland SM *et al* (2011) A critical role for STAT3 transcription factor signaling in the development
1003 and maintenance of human t cell memory. ***Immunity*** 35: 806-818
1004 Stone JH, Tuckwell K, Dimonaco S, Klearman M, Aringer M, Blockmans D, Brouwer E, Cid MC,
1005 Dasgupta B, Rech J *et al* (2017) Trial of tocilizumab in giant-cell arteritis. ***N Engl J Med*** 377: 317-328
1006 Su SC, Li SS, Deng T, Gao MS, Yin Y, Wu BX, Peng C, Liu JZ, Ma JB, Zhang KM (2022) Cryo-EM
1007 structures of human m^{6}A writer complexes. ***Cell Res*** 32: 982-994
1008 Tanaka T, Narazaki M, Kishimoto T (2014) IL-6 in Inflammation, Immunity, and Disease. ***Cold Spring***
1009 ***Harb Perspect Biol*** 6: a016295
1010 Tang SY, Meng JY, Tan J, Liu XY, Zhou HX, Li N, Hou SP (2022) *N*^{6}-methyladenosine demethylase

FTO regulates inflammatory cytokine secretion and tight junctions in retinal pigment epithelium cells. ***Clin Immunol*** 241: 109080

Triantafilou M, Triantafilou K (2002) Lipopolysaccharide recognition: CD14, TLRs and the LPS-activation cluster. ***Trends Immunol*** 23: 301-304

Vendruscolo M, Fuxreiter M (2022) Protein condensation diseases: therapeutic opportunities. ***Nat Commun*** 13: 5550

Wang JH, Yan SS, Lu HY, Wang SF, Xu DH (2019) METTL3 attenuates LPS-induced inflammatory response in macrophages via NF-kappa B signaling pathway. ***Mediators Inflamm*** 2019: 3120391

Wawrocki S, Druszczynska M, Kowalewicz-Kulbat M, Rudnicka W (2016) Interleukin 18 (IL-18) as a target for immune intervention. ***Acta Biochim Pol*** 63: 59-63

Wirtz S, Popp V, Kindermann M, Gerlach K, Weigmann B, Fichtner-Feigl S, Neurath MF (2017) Chemically induced mouse models of acute and chronic intestinal inflammation. ***Nat Protoc*** 12: 1295-1309

Wu CL, Chen WX, He JC, Jin SH, Liu YK, Yi Y, Gao ZX, Yang JY, Yang JH, Cui J *et al* (2020) Interplay of m^6A and H3K27 trimethylation restrains inflammation during bacterial infection. ***Sci Adv*** 6: aba0647

Xu HJ, Lin CJ, Yang JH, Chen X, Chen YY, Chen JG, Guo AZ, Hu CM (2022) The role of N^6-methyladenosine in inflammatory diseases. ***Oxid Med Cell Longev*** 2022: 9744771

Xu SL, Grande F, Garofalo A, Neamati N (2013) Discovery of a novel orally active small-molecule gp130 inhibitor for the treatment of ovarian cancer. ***Mol Cancer Ther*** 12: 937-949

Yang LC, Wu GT, Wu Q, Peng LX, Yuan LW (2022) METTL3 overexpression aggravates LPS-induced cellular inflammation in mouse intestinal epithelial cells and DSS-induced IBD in mice. ***Cell Death Discov*** 8: 62

Yankova E, Blackaby W, Albertella M, Rak J, De Braekeleer E, Tsagkogeorga G, Pilka ES, Aspris D, Leggate D, Hendrick AG *et al* (2021) Small-molecule inhibition of METTL3 as a strategy against myeloid leukaemia. ***Nature*** 593: 597-601

Yasuda K, Nakanishi K, Tsutsui H (2019) Interleukin-18 in health and disease. ***Int J Mol Sci*** 20: 649

Yeung YT, Aziz F, Guerrero-Castilla A, Arguelles S (2018) Signaling pathways in inflammation and anti-inflammatory therapies. *Curr Pharm Des* 24: 1449-1484

Yu H, Lee H, Herrmann A, Buettner R, Jove R (2014) Revisiting STAT3 signalling in cancer: new and unexpected biological functions. ***Nat Rev Cancer*** 14: 736-746

Zaccara S, Ries RJ, Jaffrey SR (2019) Reading, writing and erasing mRNA methylation. ***Nat Rev Mol Cell Biol*** 20: 608-624

Zhang JZ, Mehta S, Zhang J (2021a) Liquid-liquid phase separation: a principal organizer of the cell's biochemical activity architecture. ***Trends Pharmacol Sci*** 42: 845-856

Zhang Q, Lenardo MJ, Baltimore D (2017) 30 years of NF-kappa B: A blossoming of relevance to human pathobiology. ***Cell*** 168: 37-57

Zhang S, Liu F, Wu ZS, Xie JF, Yang Y, Qiu HB (2020) Contribution of m^6A subtype classification on heterogeneity of sepsis. ***Ann Transl Med*** 8: 306

Zhang Z, Chen T, Chen HX, Xie YY, Chen LQ, Zhao YL, Liu BD, Jin LM, Zhang WT, Liu C *et al* (2021b) Systematic calibration of epitranscriptomic maps using a synthetic modification-free RNA library. ***Nat Methods*** 18: 1213-1222

Zhao YC, Shi YF, Shen HF, Xie WZ (2020) m^6A-binding proteins: the emerging crucial performers in epigenetics. ***J Hematol Oncol*** 13: 35

1055 Zheng QL, Hou J, Zhou Y, Li ZY, Cao XT (2017) The RNA helicase DDX46 inhibits innate immunity
1056 by entrapping m^6A-demethylated antiviral transcripts in the nucleus. ***Nat Immunol*** 18: 1361-1361
1057 Zhu GY, Xie JJ, Fu ZZ, Wang ML, Zhang QC, He H, Chen ZJ, Guo X, Zhu JD (2021) Pharmacological
1058 inhibition of SRC-1 phase separation suppresses YAP oncogenic transcription activity. ***Cell Res*** 31:
1059 1028-1031
1060 Zhu SM, Lu Y (2020) Dexmedetomidine suppressed the biological behavior of HK-2 cells treated with
1061 LPS by down-regulating ALKBH5. ***Inflammation*** 43: 2256-2263
1062 Zong X, Zhao J, Wang H, Lu ZQ, Wang FQ, Du HH, Wang YZ (2019) Mettl3 deficiency sustains long-
1063 chain fatty acid absorption through suppressing Traf6-dependent inflammation response. ***J Immunol***
1064 202: 567-578
1065

Figure legends

Figure 1. Multiple inflammatory stimuli markedly increased the expression of WTAP in macrophages.

A Heatmap showing a change in the mRNA abundance of m^6A-related genes in THP-1 cells stimulated with lipopolysaccharide (LPS) at the indicated time points.

B-D qRT-PCR showing the mRNA abundance of the METTL3/METTL14/WTAP heterotrimer in THP-1 cells (**B**), peripheral blood mononuclear cells (PBMCs) (**C**) and bone marrow-derived macrophages (BMDMs) (**D**) stimulated with LPS at the indicated time points.

E-G Immunoblots showing the protein abundance of the METTL3/METTL14/WTAP heterotrimer in THP-1 cells (**E**), PBMCs (**F**) and BMDMs (**G**) stimulated with LPS at the indicated time points.

H qRT-PCR showing the mRNA abundance of WTAP in THP-1 cells stimulated with CL097, Pam3CSK4, heat-killed *Salmonella typhimurium* (HKST) or heat-killed *Listeria monocytogenes* (HKLM) at the indicated time points.

I-K Immunoblots showing the protein abundance of the METTL3/METTL14/WTAP heterotrimer in THP-1 cells stimulated with Pam3CSK4 (**I**), HKST (**J**) or HKLM (**K**) at the indicated time points.

L qRT-PCR showing the mRNA abundance of WTAP in BMDMs stimulated with CL097, Pam3CSK4, HKST or HKLM at the indicated time points.

M Immunoblots showing the protein abundance of the METTL3/METTL14/WTAP heterotrimer in BMDMs stimulated with Pam3CSK4 at the indicated time points.

Data information: Data are presented as the mean ± s.d. in **B-D**, **H** and **L**, with individual measurements overlaid as dots, statistical analysis was performed using a two-tailed Student's *t*-test. Data are representative of three independent biological experiments in **E-G**, **I-K** and **M**.

Figure 2. WTAP is an NF-κB p65-stimulated gene.

A Schematic of the full-length, mutant and truncated human *WTAP* promoter.

B Schematic of the mouse *Wtap* promoter.

C, D Luciferase activity analyses in 293T cells transfected with a luciferase reporter for the *WTAP* promoter with WT (**C**), mutant or truncated (**D**) p65-binding motif, together with increasing doses of Flag-tagged NF-κB p65.

1096 **E-H** qRT-PCR or immunoblots showing the expression of WTAP in THP-1 cells (**E**, **F**) or PBMCs
1097 (**G**, **H**) treated with PG490, followed by stimulation with LPS at the indicated time points.
1098 **I-L** qRT-PCR or immunoblots showing the expression of WTAP in WT and *RELA*$^{-/-}$ THP-1 cells
1099 stimulated with LPS (**I**, **J**) or Pam3CSK4 (**K**, **L**) at different time points. m Schematic showing
1100 the biotin-labeled *WTAP* promoter probes. n DNA pull-down assays showing the effect of NF-κB
1101 p65 binding with *WTAP* promoter probes.
1102 Data information: Data are presented as the mean ± s.d. in **C-E**, **G**, **L** and **K**, with individual
1103 measurements overlaid as dots, statistical analysis was performed using a two-tailed Student's *t*-
1104 test. Data are representative of three independent biological experiments in **F**, **H**, **J**, **L** and **N**.
1105
1106 **Figure 3. WTAP positively regulates the expression of proinflammatory cytokines.**
1107 **A** KEGG analyses of down-regulated genes in *WTAP*$^{\Delta 1\text{-}77}$ THP-1 cells during LPS-induced
1108 inflammatory stress compared with WT cells.
1109 **B** Heatmap showing a change in the mRNA abundance of pro-inflammatory cytokines in WT and
1110 *WTAP*$^{\Delta 1\text{-}77}$ THP-1 cells stimulated with LPS at the indicated time points.
1111 **C** qRT–PCR showing the mRNA abundance of *IL6*, *CCL2*, *CCL8* and *CXCL8* in WT and *WTAP*$^{\Delta 1\text{-}}$
1112 ^{77} THP-1 cells stimulated with LPS at the indicated time points.
1113 **D** ELISAs were performed to detect IL-6 secretion in supernatants of WT and *WTAP*$^{\Delta 1\text{-}77}$ THP-1
1114 cells stimulated with LPS, Pam3CSK4, HKST or HKLM at 3 and 6 hr.
1115 **E** Heatmap showing a change of mRNA abundance of pro-inflammatory cytokines in WT and
1116 *Wtap*$^{\Delta 1\text{-}77}$ BMDMs stimulated with LPS at the indicated time points.
1117 **F-H** qRT–PCR showing the mRNA abundance of *Il6* (**F**), *Ccl2* (**G**) and *Ccl8* (**H**) in the lung or
1118 colon tissues from *Wtap*$^{fl/fl}$ and *LyzM-cre*$^{+}$ *Wtap*$^{\Delta 1\text{-}77}$ mice that were intraperitoneally injected with
1119 LPS (10 mg kg^{-1}) for 12 hr. n = 10 mice per group.
1120 **I** Heatmap showing a change of mRNA abundance of pro-inflammatory cytokines in the colon
1121 tissues from *Wtap*$^{fl/fl}$ and *LyzM-cre*$^{+}$ *Wtap*$^{\Delta 1\text{-}77}$ mice that were intraperitoneally injected with LPS
1122 for 12 hr.
1123 **J** Hematoxylin & eosin staining (H&E) assays showing the lung injury of the *Wtap*$^{fl/fl}$ and *LyzM-*
1124 *cre*$^{+}$ *Wtap*$^{\Delta 1\text{-}77}$ mice that were intraperitoneally injected with LPS (10 mg kg^{-1}) for 6 hr. Scale bars,
1125 50 μm. n = 4 mice per group.

1126 **K** The survival of *Wtap*$^{fl/fl}$ and *LyzM-cre*$^{+}$ *Wtap*$^{\Delta 1-77}$ mice was monitored for 32 hr following the
1127 intraperitoneal injection of LPS (40 mg kg^{-1}). n = 10 mice per group.
1128 **L** ELISAs were performed to detect IL-6 secretion in serum from *Wtap*$^{fl/fl}$ and *LyzM-cre*$^{+}$ *Wtap*$^{\Delta 1-}$
1129 ^{77} mice that were intraperitoneally injected with LPS (10 mg kg^{-1}) for 12 hr. n = 8 mice per group.
1130 **M** qRT–PCR showing the mRNA abundance of *Il6* in the lung tissues from *Wtap*$^{fl/fl}$ and *LyzM-cre*$^{+}$
1131 *Wtap*$^{\Delta 1-77}$ mice that were intraperitoneally injected with *P. aeruginosa* or *L. monocytogenes* for 16
1132 hr. n = 8 mice per group.
1133 **N** ELISAs were performed to detect IL-6 secretion in serum from *Wtap*$^{fl/fl}$ and *LyzM-cre*$^{+}$ *Wtap*$^{\Delta 1-}$
1134 ^{77} mice as in that were intraperitoneally injected with *P. aeruginosa* or *L. monocytogenes* for 16 hr.
1135 n = 3 mice per group.
1136 Data information: Data are presented as the mean ± s.d. in **C**, **D**, **F-H**, and **L-N**, with individual
1137 measurements overlaid as dots, statistical analysis was performed using a two-tailed Student's *t*-
1138 test. Data are representative of three independent biological experiments in **J**.
1139
1140 **Figure 4. WTAP promotes the activation of STAT3 signaling through the m^{6}A modification**
1141 **to accelerate inflammatory responses.**
1142 **A, B** LC–MS/MS quantification of m^{6}A abundance in mRNA extracted from WT and *WTAP*$^{\Delta 1-77}$
1143 THP-1 cells (**A**) or *Wtap*$^{\Delta 1-77}$ BMDMs (**B**) with or without LPS treatment.
1144 **C** Venn diagrams showing transcripts with decreased m^{6}A abundance in *WTAP*$^{\Delta 1-77}$ THP-1 cells
1145 and *Wtap*$^{\Delta 1-77}$ BMDMs compared with WT cells stimulated with LPS for 4 hr.
1146 **D** KEGG enrichment analysis of the overlapping transcripts presented in (**C**).
1147 **E-H** Immunoblots showing total and phosphorylated (p-) STAT3, p65 and p38 levels in WT and
1148 *WTAP*$^{\Delta 1-77}$ THP-1 cells (**E, F**) or BMDMs (**G, H**) stimulated with LPS or HKST at the indicated
1149 time points.
1150 **I, J** Immunoblots showing the total and phosphorylated (p-) STAT3 level in the lung (**I**) or colon
1151 (**J**) tissues from *Wtap*$^{fl/fl}$ and *LyzM-cre*$^{+}$ *Wtap*$^{\Delta 1-77}$ mice that had been intraperitoneally injected
1152 with LPS (10 mg kg^{-1}) for 6 hr.
1153 **K** qRT–PCR showing the expression of *IL6*, *CCL2*, *CCL8* and *CXCL8* in THP-1 cells treated with
1154 SC144, followed by stimulation with LPS at the indicated time points.
1155 **L** ELISAs were performed to measure IL-1β and TNF-α secretion in supernatants of WT and

1156 *WTAP*$^{\Delta 1\text{-}77}$ THP-1 cells that were stimulated with LPS at 3 and 6 hr.

1157 Data information: Data are presented as the mean ± s.d. in **A**, **B**, **K** and **L**, with individual
1158 measurements overlaid as dots, statistical analysis was performed using a two-tailed Student's *t*-
1159 test. Data are representative of three independent biological experiments in **E-J**.

1160

1161 **Figure 5. WTAP promotes the protein output of proinflammatory genes through m^{6}A**
1162 **modification**.

1163 **A** Immunoblots showing the expression of critical adapters in the IL-6/ STAT3 signaling pathway
1164 in WT and *WTAP*$^{\Delta 1\text{-}77}$ THP-1 cells.

1165 **B** Immunoblots showing the expression of IL6ST in WT and *WTAP*$^{\Delta 1\text{-}77}$ THP-1 cells stimulated
1166 with LPS at the indicated time points.

1167 **C** Representative flow cytometry data showing IL6ST-FITC fluorescence in cell surface of
1168 peritoneal macrophages and BMDMs.

1169 **D** Immunoblots showing the expression of WTAP and IL6ST in the lung or colon tissues from
1170 *Wtap*$^{fl/fl}$ and *LyzM-cre*$^{+}$ *Wtap*$^{\Delta 1\text{-}77}$ mice that had been intraperitoneally injected with LPS (10 mg
1171 kg^{-1}) for 12 hr.

1172 **E** Immunoblots showing the total and phosphorylated (p-) STAT3, p65 and p38 levels in WT and
1173 *IL6ST*$^{-/-}$ THP-1 cells stimulated with LPS at the indicated time points.

1174 **F** ELISAs were performed to measure IL-6 secretion in the supernatants of WT and *IL6ST*$^{-/-}$ THP-
1175 1 cells stimulated with LPS, Pam3CSK4, HKST or HKLM for 6 hr.

1176 **G** Schematic representation showing the position of m^{6}A motifs within the IL6ST transcripts.
1177 F1/R1 represents detection site 1, which includes four "DRACH" elements, and F2/R2 represents
1178 detection site 2, which includes three "DRACH" elements.

1179 **H** The abundance of *IL6ST* transcripts (with detection sites 1 and 2) among mRNAs
1180 immunoprecipitated with an anti-m^{6}A antibody in WT and *WTAP*$^{\Delta 1\text{-}77}$ THP-1 cells stimulated with
1181 LPS for 6 hr.

1182 **I** WT or mutant (Mut) m^{6}A consensus sequences (A-to-T mutation) on the *IL6ST*-3' UTR were
1183 fused with the Renilla luciferase reporter in the psiCHECK^{TM}-2 vector.

1184 **J** Relative luciferase activities in 293T cells after transfection with reporter vectors bearing *IL6ST*-
1185 3' UTR with WT or Mut m^{6}A sites. Renilla luciferase activity was measured and normalized to

1186 firefly luciferase activity.

1187 **K** Relative luciferase activities in WT and *WTAP* KO 293T cells after transfection with reporter
1188 vectors bearing the *IL6ST*-3' UTR with WT m^6A sites. Renilla luciferase activity was measured
1189 and normalized to firefly luciferase activity.

1190 **L** qRT–PCR showing the proportion of *IL6ST* mRNA in polysome fractions from WT and
1191 $WTAP^{\Delta 1\text{-}77}$ THP-1 cells stimulated with LPS for 6 hr.

1192 **M, N** Immunoblots (**M**) and qRT–PCR (**N**) analyses showing the mRNA and protein abundance of
1193 IL18Rα or IL15Rα in WT and $WTAP^{\Delta 1\text{-}77}$ THP-1 cells stimulated with LPS at the indicated time
1194 points.

1195 **O** qRT–PCR showing the mRNA abundance of *IL18R1* in WT and $WTAP^{\Delta 1\text{-}77}$ THP-1 cells treated
1196 with Act D at the indicated time points.

1197 **P** Relative luciferase activities in 293T cells after transfection with reporter vectors bearing
1198 *IL15RA*- or *IL18R1*-3' UTR with WT or Mut m^6A sites. Renilla luciferase activity was measured
1199 and normalized to firefly luciferase activity.

1200 **Q** Relative luciferase activities in WT and *WTAP* KO 293T cells after transfection with reporter
1201 vectors bearing the *IL15RA*- or *IL18R1*-3' UTR with WT m^6A sites.

1202 **R** Relative luciferase activities of reporter vectors bearing *IL15RA*- or *IL18R1*-3' UTR with wild-
1203 type m^6A sites after co-transfection with empty vector (EV) or Flag-tagged WTAP into *WTAP* KO
1204 293T cells.

1205 Data information: Data are representative of three independent biological experiments in **A-E** and
1206 **M.** Data are presented as the mean ± s.d. in **F**, **H**, **J-L** and **N-R**, with individual measurements
1207 overlaid as dots, statistical analysis was performed using a two-tailed Student's *t*-test.

1208

1209 **Figure 6. The phase separation of WTAP leads to METTL3 recruitment to modify**
1210 **inflammatory transcripts efficiently.**

1211 **A, B** Prediction of the disordered regions and prion-like domains (PrD) of WTAP using the
1212 IUPred2A (**A**) or PLAAC (**B**) tool.

1213 **C** Images of GFP-WTAP droplets formation at room temperature with indicated GFP-WTAP
1214 concentrations (350 mM NaCl).

1215 **D** LSCM images of 293T cells expressing PEGFP-N1 or GFP-tagged WTAP constructs.

1216 **E** FRAP assays of the GFP-tagged WTAP droplets before and after photobleaching.

1217 **F** FRAP quantification of GFP-WTAP droplets over a period of 65 s.

1218 **G** LSCM images of HeLa cells treated with TNF-α for 2 hr.

1219 **H** Statistics of the number of WTAP droplets in (**g**).

1220 **I** Quantitative line profile of colocalization along a white arrow of the image of (**g**).

1221 **J** Statistics of the number of SC35 droplets in (**g**).

1222 **K** LSCM images of 293T cells expressing full-length or truncated WTAP labeled with GFP.

1223 **L** LSCM images of the mCherry-tagged METTL3 droplets (red) in 293T cells before and after co-

1224 transfection with GFP-tagged full-length or truncated WTAP.

1225 **M** FRAP assays of the mCherry-tagged METTL3 droplets before and after photobleaching from

1226 (**l**).

1227 **N** FRAP quantification of mCherry-METTL3 droplets over a period of 100 s.

1228 **O** METTL3 was immunoprecipitated and RIP-qPCR was performed to assess the association of

1229 *IL6ST* transcripts with METTL3.

1230 **P** LC–MS/MS quantification of m^6A abundance in mRNA extracted from 293T cells transfected

1231 with indicated plasmids.

1232 **Q** Working model for WTAP facilitating inflammatory responses through m^6A modification and

1233 phase separation.

1234 Data information: Data are representative of three independent biological experiments in **C-E**, **G**,

1235 and **K-M**. Data are presented as the mean ± s.d. in **H**, **I**, **O-P**, with individual measurements

1236 overlaid as dots, statistical analysis was performed using a two-tailed Student's *t*-test. Indicated

1237 scale bars are shown in **C-E**, **G**, and **K-M**.

1238

1239 **Figure 7. WTAP deficiency alleviates the disease progression of DSS-induced IBD in mice.**

1240 **A** Heatmap showing the expression of WTAP and proinflammatory genes in samples from

1241 psoriasis patients before and after anti-IL-17A therapy.

1242 **B** Heatmap showing the expression of WTAP and proinflammatory genes in samples from CD

1243 patients before and after anti-TNF therapy.

1244 **C** Uniform manifold approximation and projection (UMAP) plots showing rectal tissue-derived

1245 CD45^{+} immune cells from all participants. The meaning of the cluster colors is indicated.

1246 **D** Dot plots showing the expression of METTL14, METTL3, WTAP and IL6ST in major immune

1247 cell groups.

1248 **E, F** LC-MS/MS quantification of m^{6}A abundance in mRNA extracted from skin tissues in IMQ-

1249 induced psoriasis (**E**) or colon tissues in DSS-induced colitis (**F**) of mice.

1250 **G** Body weight changes of mice given 3% DSS in their drinking water were monitored daily. n =

1251 7 mice per group.

1252 **H** The disease activity index of *Wtap*$^{fl/fl}$ and *LyzM-cre*$^{+}$ *Wtap*$^{\Delta 1-77}$ mice was scored daily. n = 7

1253 mice per group.

1254 **I, J** Macroscopic appearances (**I**) and colon lengths (**J**) of *Wtap*$^{fl/fl}$ and *LyzM-cre*$^{+}$ *Wtap*$^{\Delta 1-77}$ mice

1255 were recorded on day 6. n = 4 mice per group.

1256 **K** qRT–PCR showing the mRNA abundance of *Il6*, *Il1α*, *Ccl2* and *Ccl8* in the colon tissues from

1257 *Wtap*$^{fl/fl}$ and *LyzM-cre*$^{+}$ *Wtap*$^{\Delta 1-77}$ mice that had been given 3% DSS in their drinking water for 6

1258 days. n = 10 mice per group.

1259 **L** Histopathological changes in colon tissue were determined by H&E staining. n = 4 mice per

1260 group.

1261 **M** The survival of the *Wtap*$^{fl/fl}$ and *LyzM-cre*$^{+}$ *Wtap*$^{\Delta 1-77}$ mice after continuous feeding with 3%

1262 DSS was monitored for 15 days. n = 10 mice per group.

1263 Data information: Data are representative of three independent biological experiments in **I** and **L**.

1264 Data are presented as the mean ± s.d. in **E, F**, **G**, **K,** with individual measurements overlaid as

1265 dots, statistical analysis was performed using a two-tailed Student's *t*-test. Indicated scale bars are

1266 shown in **I** and **L**.

1267

1268 ## Expanded View Figure legends

1269 **Figure EV1. Hyperinflammation is accompanied by elevated WTAP level in many**
1270 **inflammatory diseases.**

1271 A-F Heatmap showing the mRNA abundance of m^6A-related genes in patients with SLE (A),
1272 asthma (B), sepsis (C), RA (D), psoriasis (E) and IBD (F) compared with healthy controls.

1273 G-L Heatmap showing the mRNA abundance of m^6A-related genes in THP-1 cells (G) and human
1274 macrophages (H) stimulated with LPS, in lung tissues of mice with LPS-induced lung injury (I), in
1275 TNF-α-stimulated HMECs (J), in *Mycobacterium tuberculosis*-infected THP-1 cells (K) or in *S.*
1276 *typhimurium*-infected macrophages (L). The relative mRNA expression of *WTAP* is shown below.

1277 Data are presented as the mean ± s.d. in A-L with individual measurements overlaid as dots,
1278 statistical analysis was performed using Mann–Whitney U test in A-F or two-tailed Student's *t*-test
1279 in G-L.

1280

1281 **Figure EV2. WTAP is an NF-κB p65-stimulated gene.**

1282 A, B Luciferase activity analyses in 293T cells transfected with a luciferase reporter for the *WTAP*
1283 promoter, together with increasing doses of Flag-tagged C/EBPβ (A) or IRF3 (B).

1284 C Luciferase activity analyses in 293T cells transfected with a luciferase reporter for mouse *Wtap*
1285 promoter, together with increasing doses of Flag-tagged NF-κB p65.

1286 D, E qRT-PCR (D) or immunoblots (E) showing the expression of WTAP in THP-1 cells treated
1287 with PG490, followed by stimulation with Pam3CSK4 at the indicated time points.

1288 F Immunoblots showing the efficiency of p65 knockout in THP-1 cells.

1289 G, H qRT-PCR (G) or immunoblots (H) showing the expression of WTAP in WT and $RELA^{-/-}$
1290 THP-1 cells that were stimulated with HKST or HKLM at the indicated time points.

1291 I DNA pull-down assays showing the effect of C/EBPβ binding with *WTAP* promoter probes.

1292 Data are presented as the mean ± s.d. in A-D and G with individual measurements overlaid as dots,
1293 statistical analysis was performed using a two-tailed Student's *t*-test. Data are representative of
1294 three independent biological experiments in A-C, E, F, H and I.

1295

1296 **Figure EV3. WTAP KO cells express shorter but dysfunctional isoforms of WTAP.**

1297 A Schematic representation of the construction of *WTAP* KO THP-1 cells.

B Genotypes of sequenced cells. PCR products were cloned and sequenced.

C Open reading frame prediction**.**

D Immunoblots showing the expression of WTAP in WT and KO THP-1 cells.

E Schematic showing the *Wtap* conditional KO (cKO) strategy using the Cre-loxP system in mouse myeloid cells.

F Genotypes of sequenced cells. PCR products were cloned and sequenced.

G Open reading frame prediction**.**

H Immunogen information for different brands of WTAP antibodies.

I Immunoblots showing the expression of WTAP in WT and KO BMDMs.

J Immunoblots showing the subcellular localization of wild-type and alternative WTAP proteins in WT, $WTAP^{\Delta 1\text{-}20}$ and $WTAP^{\Delta 1\text{-}77}$ THP-1 cells.

K LC–MS/MS detection the m^6A abundance in mRNA extracted from *WTAP* KO 293T cells transfected with PEGFP-N1, GFP-tagged WTAP, GFP-tagged $WTAP^{\Delta 1\text{-}20}$ or GFP-tagged $WTAP^{\Delta 1\text{-}77}$.

L LC–MS/MS detection the m^6A abundance in mRNA extracted from WT, $WTAP^{\Delta 1\text{-}20}$ and $WTAP^{\Delta 1\text{-}77}$ THP-1 cells.

M LC–MS/MS detection the m^6A abundance in mRNA extracted from WT and $Wtap^{\Delta 1\text{-}77}$ BMDMs.

Data are representative of three independent biological experiments in D, I and G. Data are presented as the mean ± s.d. in K-M, with individual measurements overlaid as dots, statistical analysis was performed using a two-tailed Student's *t*-test.

Figure EV4. *Wtap* deficiency in myeloid cells did not affect the development or maturation of major immune cell populations.

A The gating strategy for sorting out various immune cells.

B FACS analyses of major immune cell populations in spleens from $Wtap^{fl/fl}$ mice and *LyzM*-Cre^{+} $Wtap^{\Delta 1\text{-}77}$ mice. n = 3 mice per group.

C Percentage of macrophages, neutrophils, DC and NK cells from (B). n = 3 mice per group.

1326 Data are representative of three independent biological experiments in B. Data are presented as the
1327 mean ± s.d. in C, with individual measurements overlaid as dots, statistical analysis was performed
1328 using a two-tailed Student's *t*-test.
1329
1330 **Figure EV5. WTAP positively regulates the expression of proinflammatory cytokines.**
1331 A KEGG analyses of up-regulated DEGs in *WTAP*$^{\Delta 1\text{-}77}$ THP-1 cells during LPS-induced
1332 inflammatory stress compared with WT cells.
1333 B qRT–PCR showing the mRNA abundance of *IL6*, *CCL2*, *CCL8* and *CXCL8* in WT and *WTAP*$^{-/-}$
1334 THP-1 cells that were stimulated with Pam3CSK4, HKST or HKLM at 6 hr.
1335 C qRT–PCR and Immunoblots showing the ectopic expression of GFP-tagged WTAP in HeLa
1336 cells.
1337 D qRT–PCR showing the mRNA abundance of *IL6* in HeLa cells transfected with GFP-tagged
1338 WTAP, followed by stimulation with TNF-α or HKST at different time points.
1339 Data are presented as the mean ± s.d. in B-D, with individual measurements overlaid as dots,
1340 statistical analysis was performed using a two-tailed Student's *t*-test. Data are representative of
1341 three independent biological experiments in C.
1342
1343 **Figure EV6. WTAP aggravates LPS-induced sepsis in mice.**
1344 A, B qRT–PCR showing the mRNA abundance of *Il1a*, *Il1b* and *Tnfa* in the lung (A) or colon (B)
1345 tissues from *Wtap*$^{fl/fl}$ and *LyzM-cre*$^{+}$ *Wtap*$^{\Delta 1\text{-}77}$ mice that were intraperitoneally injected with LPS
1346 (10 mg kg^{-1}) for 12 hr. n = 10 mice per group.
1347 C, D qRT–PCR showing the mRNA abundance of *Ccl2* (C) and *Ccl8* (D) in the lung tissues from
1348 *Wtap*$^{fl/fl}$ and *LyzM-cre*$^{+}$ *Wtap*$^{\Delta 1\text{-}77}$ mice that were intraperitoneally injected with *P. aeruginosa* or *L.*
1349 *monocytogenes* for 16 hr. n = 8 mice per group.
1350 E-G qRT–PCR showing the mRNA abundance of *Il6* (E), *Ccl2* (F) and *Ccl8* (G) in the colon
1351 tissues from *Wtap*$^{fl/fl}$ and *LyzM-cre*$^{+}$ *Wtap*$^{fl/fl}$ mice that were intraperitoneally injected with *P.*
1352 *Aeruginosa* or *L. Monocytogenes* for 16 hr. n = 8 mice per group.
1353 Data are presented as the mean ± s.d. in A-G, with individual measurements overlaid as dots,
1354 statistical analysis was performed using a two-tailed Student's *t*-test.

1355

1356 **Figure EV7. WTAP deficiency significantly reduces the m^{6}A modification abundance of**
1357 **inflammatory genes.**

1358 A LC–MS/MS detection the m^{6}A abundance in mRNA extracted from 293T cells transfected with
1359 empty vector or GFP-tagged WTAP.

1360 B LC–MS/MS detection the m^{6}A abundance in mRNA extracted from WTAP KO and WT 293T
1361 cells.

1362 C Sequence motif was identified within m^{6}A peaks by HOMER analyses of WT and *WTAP*$^{\Delta 1\text{-}77}$
1363 THP-1 cells with or without LPS treatment.

1364 D Pie charts depicting the proportion of m^{6}A peak distribution in the 5' UTR, CDS, and 3' UTR
1365 regions across mRNA transcriptome.

1366 E, F Metagene profiles of m^{6}A peak distribution across the 5' UTR, CDS, and 3' UTR in WT and
1367 *WTAP*$^{\Delta 1\text{-}77}$ THP-1 cells (E) or *Wtap*$^{\Delta 1\text{-}77}$ BMDMs (F) with or without LPS treatment.

1368 G, H EGG enrichment analysis of the transcripts with decreased m^{6}A marks in *WTAP*$^{\Delta 1\text{-}77}$ THP-1
1369 cells (G) or *Wtap*$^{\Delta 1\text{-}77}$ BMDMs (H) after treatment with LPS.

1370 I qRT–PCR showing the expression of *TNFA*, *IL1B* and *LTA* in THP-1 cells treated with SC144,
1371 followed by stimulation with LPS at the indicated time points.

1372 J qRT–PCR showing the expression of *TNFA*, *IL1B* and *LTA* in WT and *WTAP*$^{\Delta 1\text{-}77}$ THP-1 cells
1373 that were stimulated with LPS at 3 and 6 hr.

1374 K, L ELISAs were performed to measure IL-1β (K) and TNF-α (L) secretion in supernatants of
1375 WT and *WTAP*$^{\Delta 1\text{-}77}$ THP-1 cells that were stimulated with HKST or HKLM at 3 and 6 hr.

1376 Data are presented as the mean ± s.d. in A, B and I-L, with individual measurements overlaid as
1377 dots, statistical analysis was performed using a two-tailed Student's *t*-test.

1378

1379 **Figure EV8. WTAP deficiency decreased the m^{6}A modification of many inflammatory genes.**

1380 **A-I** Integrative Genomics Viewer (IGV) browser tracks showing that m^{6}A peaks were enriched in
1381 the 3' UTR or CDS regions of *IL6ST* (**A**), *IL15RA* (**B**), *IL18R1* (**C**), *TYK2* (**D**), *JAK2* (**E**), *RIPK2*
1382 (**F**), *IL1A* (**G**), *IL12B* (**H**), and *CXCL11* (**I**) transcripts.

1383 **J-L** IGV browser tracks showing that m^6A peaks were enriched in the 3' UTR or CDS regions of
1384 *Il6st* (**J**), *Jak2* (**K**), and *Ripk2* (**L**) transcripts.
1385
1386 **Figure EV9. WTAP promotes the protein output of proinflammatory genes through m^6A**
1387 **modification.**
1388 A Immunoblots showing the expression of critical adaptors in the IL-6/STAT3 signaling pathway
1389 in BMDMs from *Wtap*$^{fl/fl}$ or *LyzM*-Cre$^+$ *Wtap*$^{\Delta 1\text{-}77}$ mice.
1390 B, C Immunoblots showing the expression of WTAP and IL6ST in in the lung (B) or colon (C)
1391 tissues from wild-type mice that had been intraperitoneally injected with LPS or PBS for 12 hr.
1392 D Relative luciferase activities of reporter vectors bearing *IL6ST*-3' UTR with wild-type m^6A sites
1393 after co-transfection with empty vector (EV) or Flag-tagged WTAP into *WTAP* KO 293T cells.
1394 E qRT–PCR showing the mRNA abundance of *IL6ST* in WT and *WTAP*$^{\Delta 1\text{-}77}$ THP-1 cells or
1395 BMDMs.
1396 F qRT–PCR showing the mRNA abundance of *IL6ST* in WT and *WTAP*$^{\Delta 1\text{-}77}$ THP-1 cells treated
1397 with Act D at the indicated time points.
1398 G Schematic representation of the polysome profiling.
1399 H qRT–PCR showing the proportion of *GAPDH* mRNA in polysome fractions from WT and
1400 *WTAP*$^{-/-}$ THP-1 cells treated with LPS for 6 hr.
1401 I Immunoblots showing the expression of IL6ST in WT and *YTHDF1*$^{-/-}$ or *YTHDF3*$^{-/-}$ THP-1 cells.
1402 J Schematic representation of the biotin-labeled probes of *IL6ST* transcripts.
1403 K RNA pull-down analyses showing the interaction between different *IL6ST* RNA probes and the
1404 YTHDF1 or YTHDF3 protein.
1405 L YTHDF1 or YTHDF3 were immunoprecipitated, and RNA immunoprecipitation (RIP)-qPCR
1406 was performed to assess the association of *IL6ST* with YTHDF1 or YTHDF3 in WT and *WTAP*$^{\Delta 1\text{-}}$
1407 ^{77} THP-1 cells.
1408 M, N qRT–PCR showing the proportion of *IL6ST* mRNA in polysome fractions from WT and
1409 *YTHDF1*$^{-/-}$ (M) or *YTHDF3*$^{-/-}$ (N) THP-1 cells.

1410 O qRT–PCR analyses showing the mRNA abundance of IL18Rα or IL15Rα in WT and *Wtap*$^{\Delta 1\text{-}77}$

1411 BMDMs stimulated with LPS at the indicated time points.

1412 P qRT–PCR showing the mRNA abundance of *IL15RA* in WT and *WTAP*$^{\Delta 1\text{-}77}$ THP-1 cells treated

1413 with Act D at the indicated time points.

1414 Q Relative luciferase activities in 293T cells after transfection with reporter vectors bearing *IL1A*-,

1415 *IL12B*- or *CXCL11*-3' UTR with WT or Mut m^{6}A sites. Renilla luciferase activity was measured

1416 and normalized to firefly luciferase activity.

1417 R Relative luciferase activities in WT and *WTAP* KO 293T cells after transfection with reporter

1418 vectors bearing the *IL1A*-, *IL12B*- or *CXCL11*-3' UTR with WT m^{6}A sites.

1419 S Relative luciferase activities of reporter vectors bearing *IL1A*-, *IL12B*- or *CXCL11*-3' UTR with

1420 wild-type m^{6}A sites after co-transfection with empty vector (EV) or Flag-tagged WTAP into

1421 *WTAP* KO 293T cells.

1422 Data are representative of three independent biological experiments in A-C, I and K. Data are

1423 presented as the mean ± s.d. in D-F, H and L-S, with individual measurements overlaid as dots,

1424 statistical analysis was performed using a two-tailed Student's *t*-test.

1425

1426 **Figure EV10. WTAP is deeply involved in the regulation of inflammatory response.**

1427 A Venn diagrams showing transcripts with decreased m^{6}A abundance in *WTAP*$^{\Delta 1\text{-}77}$ THP-1 cells

1428 compared with WT cells stimulated with or without LPS.

1429 B KEGG enrichment analysis of the 1816 transcripts with decreased m^{6}A abundance only at

1430 resting state.

1431 C KEGG enrichment analysis of the 770 transcripts with decreased m^{6}A abundance only after

1432 treatment with LPS for 4 h.

1433

1434 **Figure EV11. The phase separation of WTAP leads to METTL3 recruitment to modify**

1435 **inflammatory transcripts efficiently.**

1436 A Bacterial purified GFP-WTAP proteins were analyzed by SDS-PAGE and detected by

1437 coomassie blue staining.

1438 B Images of GFP-WTAP droplets formation at room temperature with indicated NaCl

1439 concentrations (5 μM GFP-WTAP).

1440 C EqDiameter (the diameter of a circle with the same area as the measured object) frequency
1441 distribution of GFP-WTAP liquid droplets formed at the indicated timepoints (350 mM NaCl, 5
1442 μM GFP-WTAP).

1443 D Time-lapse micrographs of the fusion at room temperature of GFP-WTAP (5 μM) liquid
1444 droplets formed at the indicated times.

1445 E GFP-WTAP were treated with 5% Hex and then subjected to droplet formation assay *in vitro*
1446 (350 mM NaCl, 5 μM GFP-WTAP).

1447 F Immunoblots showing of the expression of GFP-tagged WTAP.

1448 G qRT–PCR showing the mRNA abundance of *WTAP* in HeLa cells stimulated with TNF-α at the
1449 indicated time points.

1450 H Prediction of the unfolded intrinsically disordered regions (IDRs) of WTAP using the PONDR
1451 tool, and a series of truncated WTAP labeled with GFP are as shown.

1452 I, J Immunoblots (I) and representative confocal images (J) of 293T expressing truncated WTAP
1453 labeled with GFP.

1454 K Bacterial purified mCherry-METTL3 proteins were analyzed by SDS-PAGE and detected by
1455 coomassie blue staining.

1456 L Fluorescence of mCherry-METTL3 (10 μM) and GFP-WTAP (10 μM) mixed at room
1457 temperature with 350 mM NaCl. Quantitative line profile of colocalization along a white arrow of
1458 the image on the left.

1459 M Coimmunoprecipitation and immunoblot analyses of extracts of 293T cells transfected with
1460 various combinations of plasmids encoding GFP-tagged WTAP and mCherry-tagged METTL3.

1461 N, O METTL3 was immunoprecipitated (N) and RIP-qPCR was performed to assess the
1462 association of *IL15RA* or *IL18R1* transcripts with METTL3 (O).

1463 P m^6A dot quantification of m^6A abundance in mRNA extracted from *WTAP* KO 293T cells
1464 transfected with indicated plasmids.

1465 Data are representative of three independent biological experiments in A-F, I-N and P. Data are
1466 presented as the mean ± s.d. in G and O, with individual measurements overlaid as dots, statistical
1467 analysis was performed using a two-tailed Student's *t*-test. Indicated scale bars are shown in B, D,
1468 E, J and L.

1469

1470 **Figure EV12. The expression of WTAP and IL6ST is increased in patients with**
1471 **inflammatory diseases.**

1472 A The mRNA abundance of *IL6ST* in patients with SLE, asthma, RA, psoriasis and IBD compared
1473 with those in healthy controls.

1474 B, C The mRNA abundance of *WTAP* and *IL6ST* in patients with IBD compared with healthy
1475 controls.

1476 D Spearman correlations between m^6A regulators and IBD core cytokines in IBDMDB patients.

1477 E, F Spearman correlations between the expression of WTAP and the global m^6A abundance in
1478 RA (E) patients, or in ovalbumin (OVA)-induced acute allergic asthma mice (F).

1479 G, H m^6A dot blot quantification of m^6A abundance in mRNA extracted from skin tissues in IMQ-
1480 induced psoriasis (G) or colon tissues in DSS-induced colitis (H) of mice.

1481 Data are presented as the mean ± s.d. in A-C, with individual measurements overlaid as dots,
1482 statistical analysis was performed using Mann–Whitney U test. Data are representative of three
1483 independent biological experiments in G and H.

1484

1485 **Figure EV13. Reducing the level of m^6A modification can reverse the high inflammatory**
1486 **state.**

1487 A m^6A dot blot quantification of m^6A levels in mRNA extracted from BMDMs that treated with
1488 DMSO or STM2457, followed by stimulation with HKST for 6 hr. UN, unstimulated.

1489 B Heatmap showing the mRNA expression of proinflammatory genes in BMDMs treated with
1490 DMSO or STM2457, followed by stimulation with HKST for 6 hr. The number represents three
1491 independent experiments.

1492 C, D m^6A dot blot quantification of m^6A levels in mRNA extracted from colon (C) or lung (D)
1493 tissues in LPS-induced sepsis of mice, followed by four consecutive days of intraperitoneal
1494 injections of DMSO or STM2457. n = 3 mice per group.

1495 E, F qRT–PCR showing the mRNA abundance of *Il1b*, *Tnfa*, *Il16*, *Ccl2* and *Ccl8* in the colon (E)
1496 or lung (F) tissues from mice treated as above. n = 6 mice per group.

1497 G H&E assays showing the lung injury of LPS-induced sepsis of mice, followed by four
1498 consecutive days of intraperitoneal injections of DMSO or STM2457. Scale bars, 50 μm. n = 3

1499 mice per group.

1500 H m^6A dot blot quantification of m^6A levels in mRNA extracted from THP-1 cells that treated

1501 with DMSO or PG490, followed by stimulation with LPS at the indicated time points.

1502 Data are representative of three independent biological experiments in A, C, D and H. Data are

1503 presented as the mean ± s.d. in B, E and F, with individual measurements overlaid as dots,

1504 statistical analysis was performed using a two-tailed Student's *t*-test. Indicated scale bars are

1505 shown in I.

1506

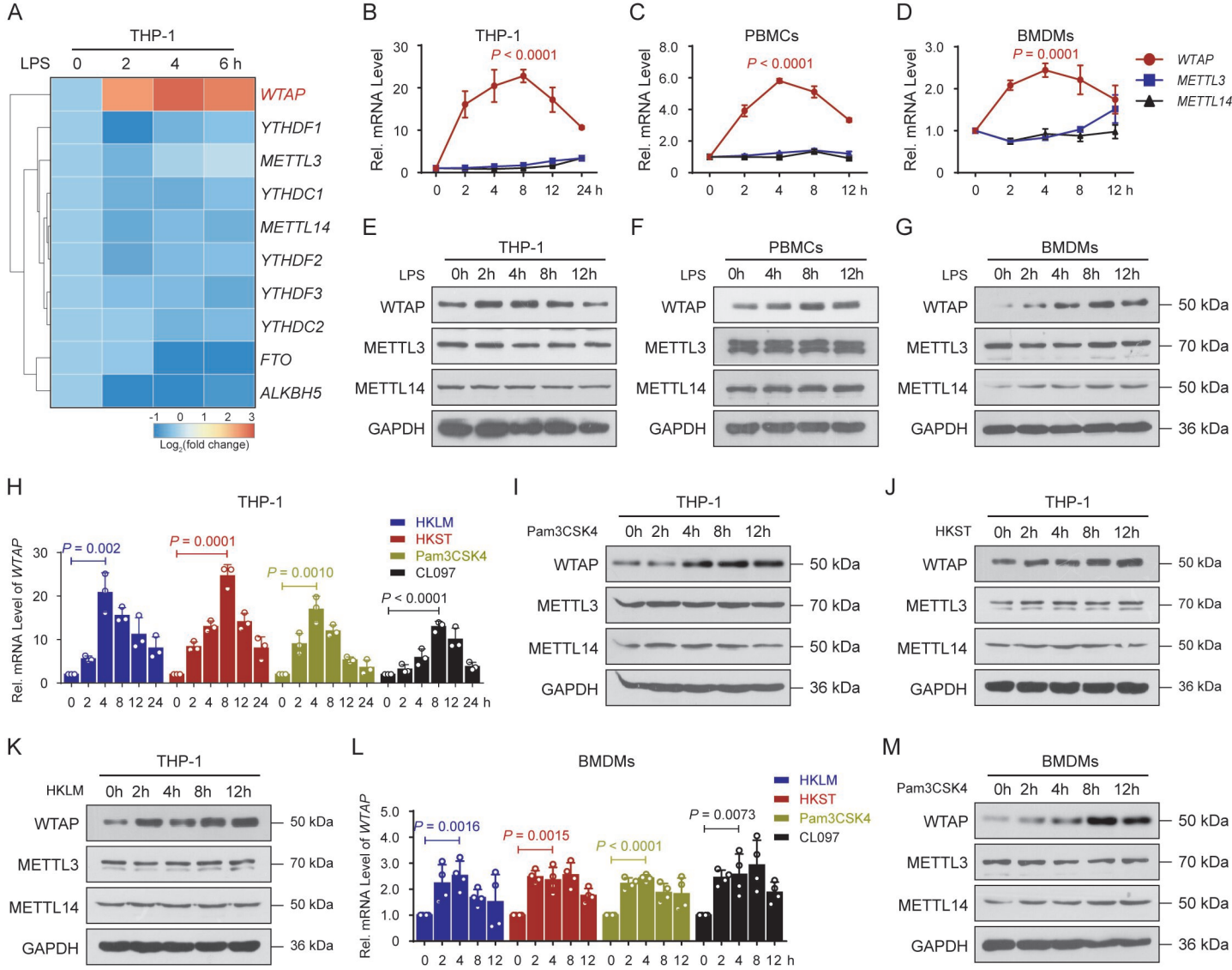
A
THP-1
LPS 0 2 4 6 h
WTAP
YTHDF1
METTL3
YTHDC1
METTL14
YTHDF2
YTHDF3
YTHDC2
FTO
ALKBH5
-1 0 1 2 3
Log2(fold change)
B
THP-1
P < 0.0001
Rel. mRNA Level
0 2 4 8 12 24 h
C
PBMCs
P < 0.0001
Rel. mRNA Level
0 2 4 8 12 h
D
BMDMs
P = 0.0001
Rel. mRNA Level
0 2 4 8 12 h
WTAP
METTL3
METTL14
E
THP-1
LPS 0h 2h 4h 8h 12h
WTAP
METTL3
METTL14
GAPDH
F
PBMCs
LPS 0h 4h 8h 12h
WTAP
METTL3
METTL14
GAPDH
G
BMDMs
LPS 0h 2h 4h 8h 12h
WTAP 50 kDa
METTL3 70 kDa
METTL14 50 kDa
GAPDH 36 kDa
H
THP-1
Rel. mRNA Level of WTAP
P = 0.002
P = 0.0001
P = 0.0010
P < 0.0001
HKLM
HKST
Pam3CSK4
CL097
0 2 4 8 12 24 h
I
THP-1
Pam3CSK4 0h 2h 4h 8h 12h
WTAP 50 kDa
METTL3 70 kDa
METTL14 50 kDa
GAPDH 36 kDa
J
THP-1
HKST 0h 2h 4h 8h 12h
WTAP 50 kDa
METTL3 70 kDa
METTL14 50 kDa
GAPDH 36 kDa
K
THP-1
HKLM 0h 2h 4h 8h 12h
WTAP 50 kDa
METTL3 70 kDa
METTL14 50 kDa
GAPDH 36 kDa
L
BMDMs
Rel. mRNA Level of WTAP
P = 0.0016
P = 0.0015
P < 0.0001
P = 0.0073
HKLM
HKST
Pam3CSK4
CL097
0 2 4 8 12 h
M
BMDMs
Pam3CSK4 0h 2h 4h 8h 12h
WTAP 50 kDa
METTL3 70 kDa
METTL14 50 kDa
GAPDH 36 kDa

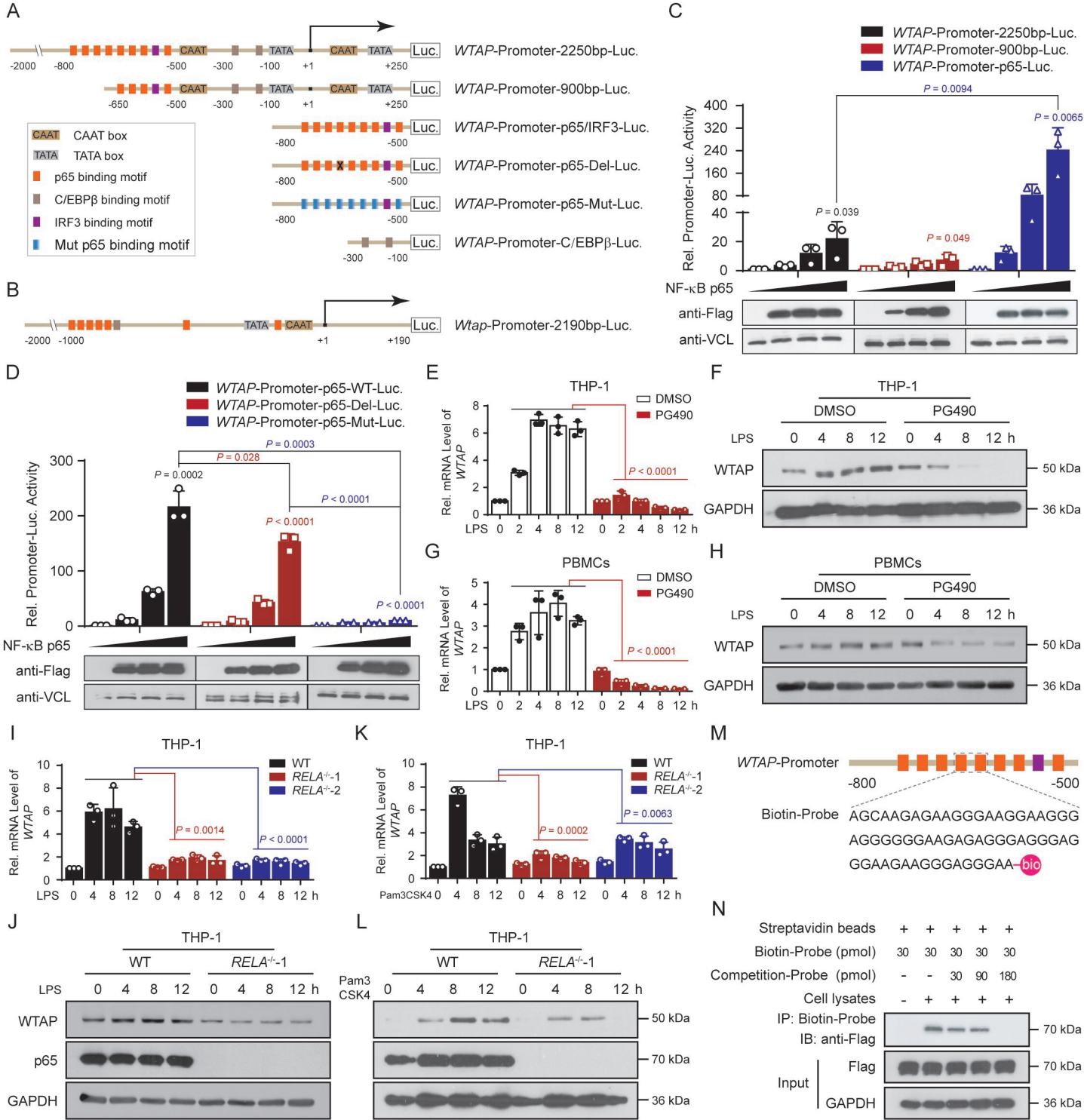
A
CAAT
TATA
Luc.
WTAP-Promoter-2250bp-Luc.
WTAP-Promoter-900bp-Luc.
WTAP-Promoter-p65/IRF3-Luc.
WTAP-Promoter-p65-Del-Luc.
WTAP-Promoter-p65-Mut-Luc.
WTAP-Promoter-C/EBPβ-Luc.
CAAT box
TATA box
p65 binding motif
C/EBPβ binding motif
IRF3 binding motif
Mut p65 binding motif
B
Wtap-Promoter-2190bp-Luc.
C
WTAP-Promoter-2250bp-Luc.
WTAP-Promoter-900bp-Luc.
WTAP-Promoter-p65-Luc.
Rel. Promoter-Luc. Activity
P = 0.0094
P = 0.0065
P = 0.039
P = 0.049
NF-κB p65
anti-Flag
anti-VCL
D
WTAP-Promoter-p65-WT-Luc.
WTAP-Promoter-p65-Del-Luc.
WTAP-Promoter-p65-Mut-Luc.
P = 0.0003
P = 0.028
P = 0.0002
P < 0.0001
E
THP-1
DMSO
PG490
Rel. mRNA Level of WTAP
F
THP-1
DMSO
PG490
LPS
WTAP
GAPDH
50 kDa
36 kDa
G
PBMCs
H
I
THP-1
WT
RELA-/--1
RELA-/--2
P = 0.0014
K
P = 0.0002
P = 0.0063
Pam3CSK4
M
WTAP-Promoter
Biotin-Probe
AGCAAGAGAAGGGAAGGAAGGG
AGGGGGGAAGAGAGGGAGGGAG
GGAAGAAGGGAGGGAA
bio
J
L
p65
N
Streptavidin beads
Biotin-Probe (pmol)
Competition-Probe (pmol)
Cell lysates
IP: Biotin-Probe
IB: anti-Flag
Input
Flag
70 kDa

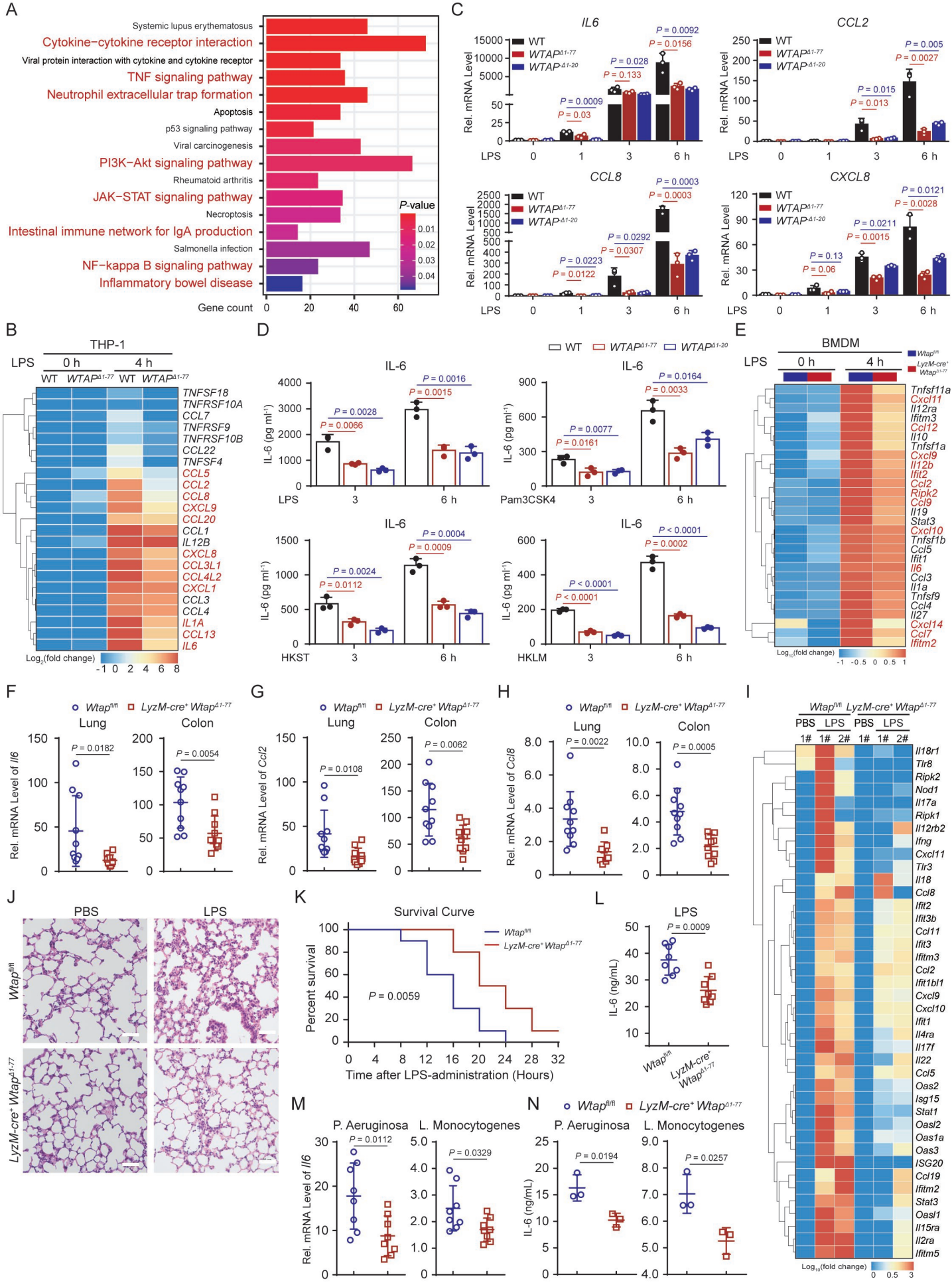
A
Systemic lupus erythematosus
Cytokine−cytokine receptor interaction
Viral protein interaction with cytokine and cytokine receptor
TNF signaling pathway
Neutrophil extracellular trap formation
Apoptosis
p53 signaling pathway
Viral carcinogenesis
PI3K−Akt signaling pathway
Rheumatoid arthritis
JAK−STAT signaling pathway
Necroptosis
Intestinal immune network for IgA production
Salmonella infection
NF−kappa B signaling pathway
Inflammatory bowel disease
P-value
Gene count
B
THP-1
LPS
0 h
4 h
WT
WTAP Δ1-77
TNFSF18
TNFRSF10A
CCL7
TNFRSF9
TNFRSF10B
CCL22
TNFSF4
CCL5
CCL2
CCL8
CXCL9
CCL20
CCL1
IL12B
CXCL8
CCL3L1
CCL4L2
CXCL1
CCL3
CCL4
IL1A
CCL13
IL6
Log2(fold change)
C
IL6
CCL2
CCL8
CXCL8
WT
WTAP Δ1-77
WTAP Δ1-20
Rel. mRNA Level
LPS
D
IL-6
IL-6 (pg ml-1)
LPS
Pam3CSK4
HKST
HKLM
E
BMDM
Wtapfl/fl
LyzM-cre+ Wtap Δ1-77
Log10(fold change)
F
Wtapfl/fl
LyzM-cre+ Wtap Δ1-77
Lung
Colon
Rel. mRNA Level of Il6
G
Rel. mRNA Level of Ccl2
H
Rel. mRNA Level of Ccl8
I
PBS
LPS
Il18r1
Tlr8
Ripk2
Nod1
Il17a
Ripk1
Il12rb2
Ifng
Cxcl11
Tlr3
Il18
Ccl8
Ifit2
Ifit3b
Ccl11
Ifit3
Ifitm3
Ccl2
Ifit1bl1
Cxcl9
Cxcl10
Ifit1
Il4ra
Il17f
Il22
Ccl5
Oas2
Isg15
Stat1
Oasl2
Oas1a
Oas3
ISG20
Ccl19
Ifitm2
Stat3
Oasl1
Il15ra
Il2ra
Ifitm5
Log10(fold change)
J
PBS
LPS
Wtapfl/fl
LyzM-cre+ Wtap Δ1-77
K
Survival Curve
Percent survival
Time after LPS-administration (Hours)
L
LPS
IL-6 (ng/mL)
M
P. Aeruginosa
L. Monocytogenes
Rel. mRNA Level of Il6
N
P. Aeruginosa
L. Monocytogenes
IL-6 (ng/mL)

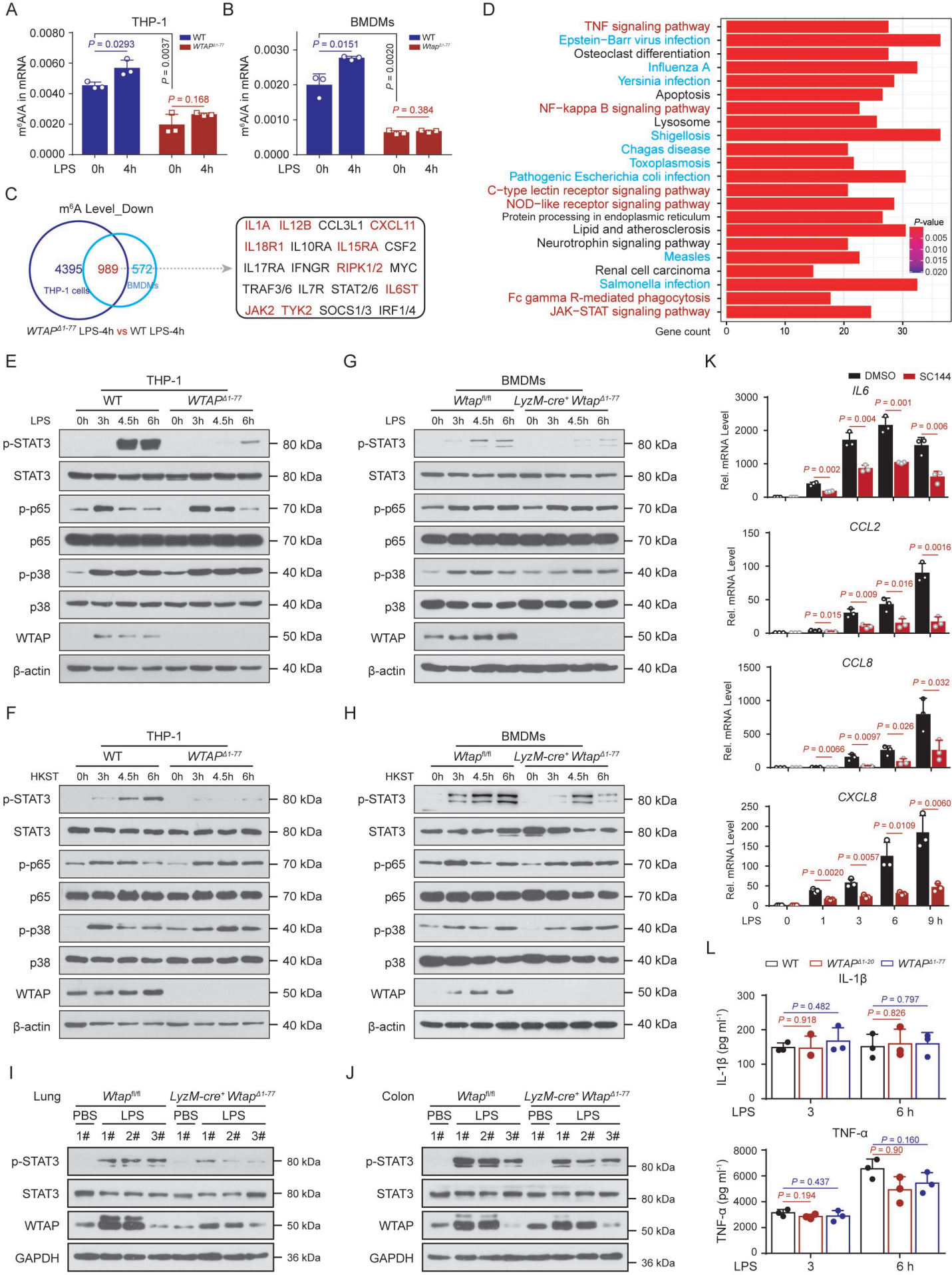
A
THP-1
m6A/A in mRNA
WT
WTAPΔ1-77
P = 0.0293
P = 0.0037
P = 0.168
LPS 0h 4h 0h 4h
B
BMDMs
P = 0.0151
P = 0.0020
P = 0.384
C
m6A Level_Down
4395
989
572
THP-1 cells
BMDMs
WTAPΔ1-77 LPS-4h vs WT LPS-4h
IL1A IL12B CCL3L1 CXCL11
IL18R1 IL10RA IL15RA CSF2
IL17RA IFNGR RIPK1/2 MYC
TRAF3/6 IL7R STAT2/6 IL6ST
JAK2 TYK2 SOCS1/3 IRF1/4
D
TNF signaling pathway
Epstein−Barr virus infection
Osteoclast differentiation
Influenza A
Yersinia infection
Apoptosis
NF−kappa B signaling pathway
Lysosome
Shigellosis
Chagas disease
Toxoplasmosis
Pathogenic Escherichia coli infection
C−type lectin receptor signaling pathway
NOD−like receptor signaling pathway
Protein processing in endoplasmic reticulum
Lipid and atherosclerosis
Neurotrophin signaling pathway
Measles
Renal cell carcinoma
Salmonella infection
Fc gamma R-mediated phagocytosis
JAK−STAT signaling pathway
Gene count
P-value
E
THP-1
WT
WTAPΔ1-77
LPS 0h 3h 4.5h 6h 0h 3h 4.5h 6h
p-STAT3
STAT3
p-p65
p65
p-p38
p38
WTAP
β-actin
80 kDa
70 kDa
40 kDa
50 kDa
F
HKST
G
BMDMs
Wtapfl/fl
LyzM-cre+ WtapΔ1-77
H
I
Lung
PBS LPS PBS LPS
1# 1# 2# 3# 1# 1# 2# 3#
GAPDH
36 kDa
J
Colon
K
DMSO
SC144
IL6
CCL2
CCL8
CXCL8
Rel. mRNA Level
LPS 0 1 3 6 9 h
L
WT
WTAPΔ1-20
WTAPΔ1-77
IL-1β
IL-1β (pg ml-1)
TNF-α
TNF-α (pg ml-1)
LPS 3 6 h

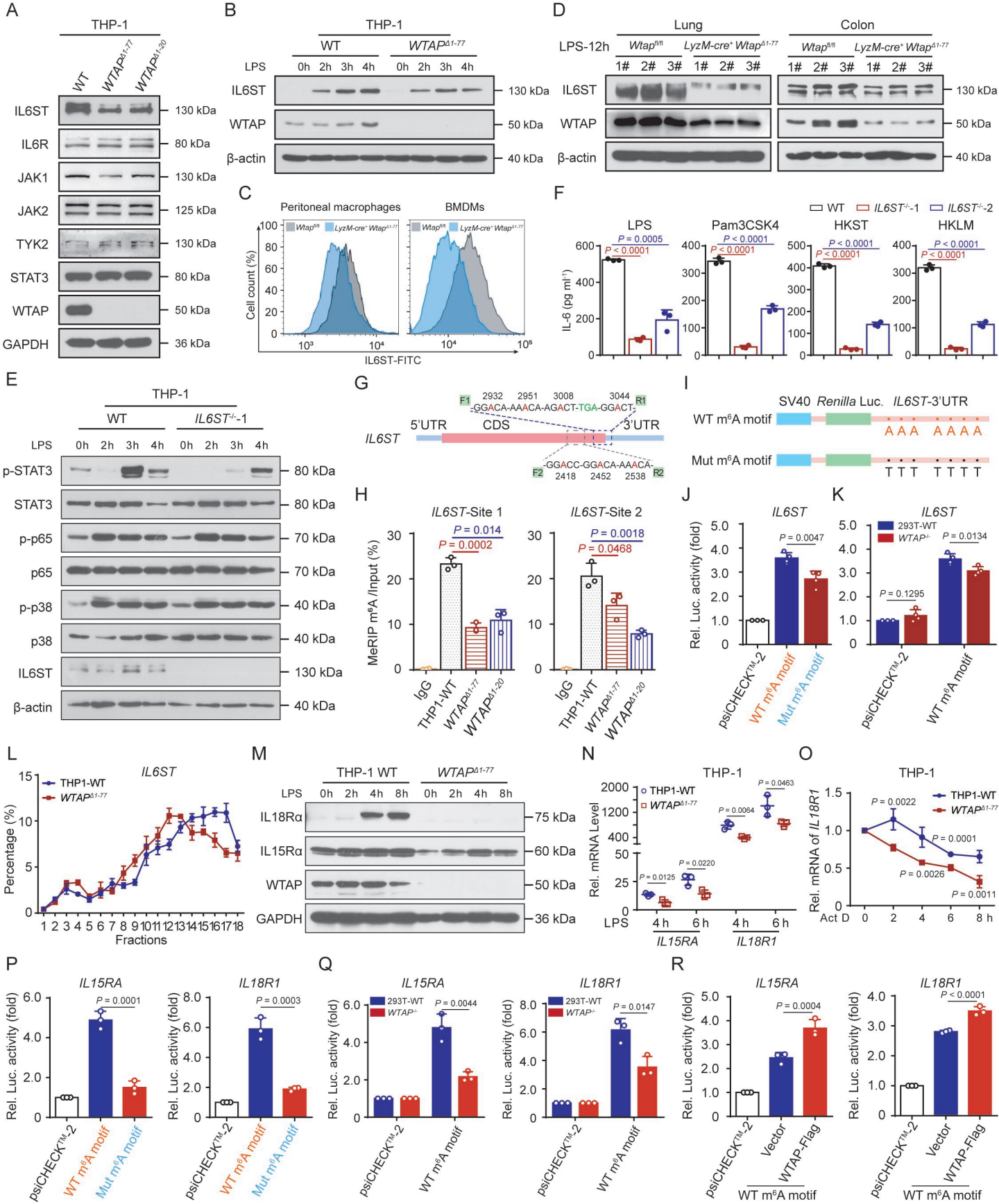
A
THP-1
WT
WTAPΔ1-77
WTAPΔ1-20
IL6ST
IL6R
JAK1
JAK2
TYK2
STAT3
WTAP
GAPDH
130 kDa
80 kDa
130 kDa
125 kDa
130 kDa
80 kDa
50 kDa
36 kDa
B
THP-1
WT
WTAPΔ1-77
LPS
0h 2h 3h 4h 0h 2h 3h 4h
IL6ST
WTAP
β-actin
130 kDa
50 kDa
40 kDa
C
Peritoneal macrophages
BMDMs
Wtapfl/fl
LyzM-cre+ WtapΔ1-77
Cell count (%)
IL6ST-FITC
D
Lung
Colon
LPS-12h
Wtapfl/fl
LyzM-cre+ WtapΔ1-77
1# 2# 3# 1# 2# 3#
IL6ST
WTAP
β-actin
130 kDa
50 kDa
40 kDa
E
THP-1
WT
IL6ST-/--1
LPS
0h 2h 3h 4h 0h 2h 3h 4h
p-STAT3
STAT3
p-p65
p65
p-p38
p38
IL6ST
β-actin
80 kDa
80 kDa
70 kDa
70 kDa
40 kDa
40 kDa
130 kDa
40 kDa
F
WT
IL6ST-/--1
IL6ST-/--2
LPS
Pam3CSK4
HKST
HKLM
IL-6 (pg ml-1)
P = 0.0005
P < 0.0001
P < 0.0001
P < 0.0001
P < 0.0001
P < 0.0001
P < 0.0001
P < 0.0001
G
F1
2932 2951 3008 3044
R1
-GGACA-AAACA-AGACT-TGA-GGACT-
5'UTR
CDS
3'UTR
IL6ST
-GGACC-GGACA-AAACA-
F2
2418 2452 2538
R2
H
IL6ST-Site 1
IL6ST-Site 2
MeRIP m6A /Input (%)
P = 0.014
P = 0.0002
P = 0.0018
P = 0.0468
IgG
THP1-WT
WTAPΔ1-77
WTAPΔ1-20
I
SV40
Renilla Luc.
IL6ST-3'UTR
WT m6A motif
Mut m6A motif
A A A
A A A A
T T T
T T T T
J
IL6ST
Rel. Luc. activity (fold)
P = 0.0047
psiCHECK™-2
WT m6A motif
Mut m6A motif
K
IL6ST
293T-WT
WTAP-/-
P = 0.0134
P = 0.1295
psiCHECK™-2
WT m6A motif
L
IL6ST
THP1-WT
WTAPΔ1-77
Percentage (%)
Fractions
M
THP-1 WT
WTAPΔ1-77
LPS
0h 2h 4h 8h 0h 2h 4h 8h
IL18Rα
IL15Rα
WTAP
GAPDH
75 kDa
60 kDa
50 kDa
36 kDa
N
THP-1
THP1-WT
WTAPΔ1-77
Rel. mRNA Level
P = 0.0125
P = 0.0220
P = 0.0064
P = 0.0463
LPS
4 h
6 h
IL15RA
IL18R1
O
THP-1
THP1-WT
WTAPΔ1-77
Rel. mRNA of IL18R1
P = 0.0022
P = 0.0001
P = 0.0026
P = 0.0011
Act D
0 2 4 6 8 h
P
IL15RA
IL18R1
Rel. Luc. activity (fold)
P = 0.0001
P = 0.0003
psiCHECK™-2
WT m6A motif
Mut m6A motif
Q
IL15RA
IL18R1
293T-WT
WTAP-/-
P = 0.0044
P = 0.0147
psiCHECK™-2
WT m6A motif
R
IL15RA
IL18R1
Rel. Luc. activity (fold)
P = 0.0004
P < 0.0001
psiCHECK™-2
Vector
WTAP-Flag
WT m6A motif

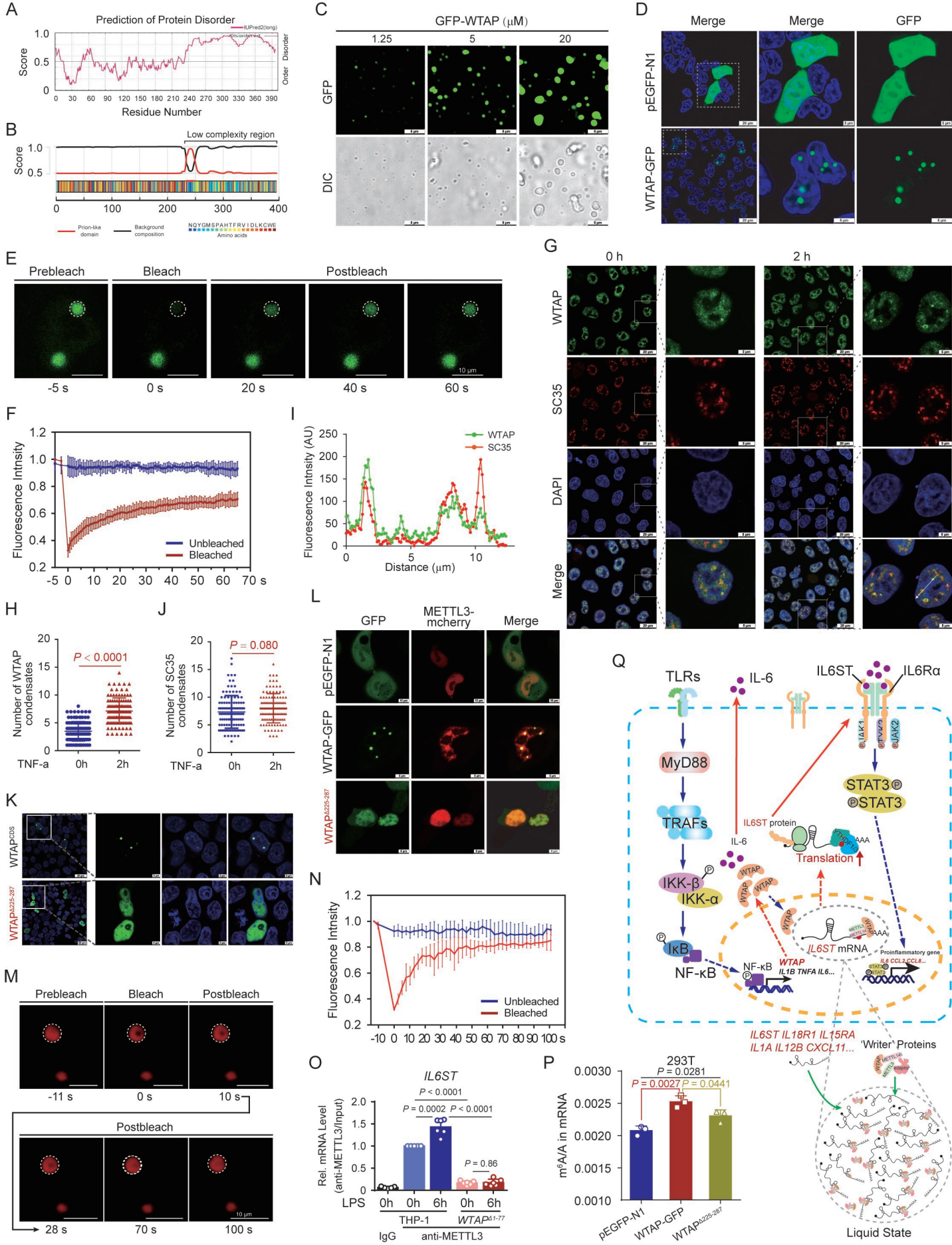
A
Prediction of Protein Disorder
IUPred2(long)
disordered
Score
Disorder
Order
Residue Number
B
Low complexity region
Score
Prion-like domain
Background composition
Amino acids
C
GFP-WTAP (μM)
1.25
5
20
GFP
DIC
D
Merge
Merge
GFP
pEGFP-N1
WTAP-GFP
E
Prebleach
Bleach
Postbleach
-5 s
0 s
20 s
40 s
60 s
10 μm
F
Fluorescence Intnsity
Unbleached
Bleached
G
0 h
2 h
WTAP
SC35
DAPI
Merge
I
Fluorescence Intnsity (AU)
WTAP
SC35
Distance (μm)
H
Number of WTAP condensates
P < 0.0001
TNF-a
0h
2h
J
Number of SC35 condensates
P = 0.080
TNF-a
0h
2h
K
WTAP^CDS
WTAP^Δ225-287
L
GFP
METTL3-mcherry
Merge
pEGFP-N1
WTAP-GFP
WTAP^Δ225-287
M
Prebleach
Bleach
Postbleach
-11 s
0 s
10 s
Postbleach
28 s
70 s
100 s
10 μm
N
Fluorescence Intnsity
Unbleached
Bleached
O
IL6ST
P < 0.0001
P = 0.0002
P < 0.0001
P = 0.86
Rel. mRNA Level (anti-METTL3/Input)
LPS
0h
0h
6h
0h
6h
THP-1
WTAP^Δ1-77
IgG
anti-METTL3
P
293T
P = 0.0281
P = 0.0027
P = 0.0441
m^6A/A in mRNA
pEGFP-N1
WTAP-GFP
WTAP^Δ225-287
Q
TLRs
IL-6
IL6ST
IL6Rα
MyD88
TRAFs
IKK-β
IKK-α
IκB
NF-κB
IL6ST protein
Translation
IL6ST mRNA
WTAP
IL1B TNFA IL6...
Proinflammatory gene
IL6 CCL2 CCL8...
STAT3
IL6ST IL18R1 IL15RA
IL1A IL12B CXCL11...
'Writer' Proteins
Liquid State

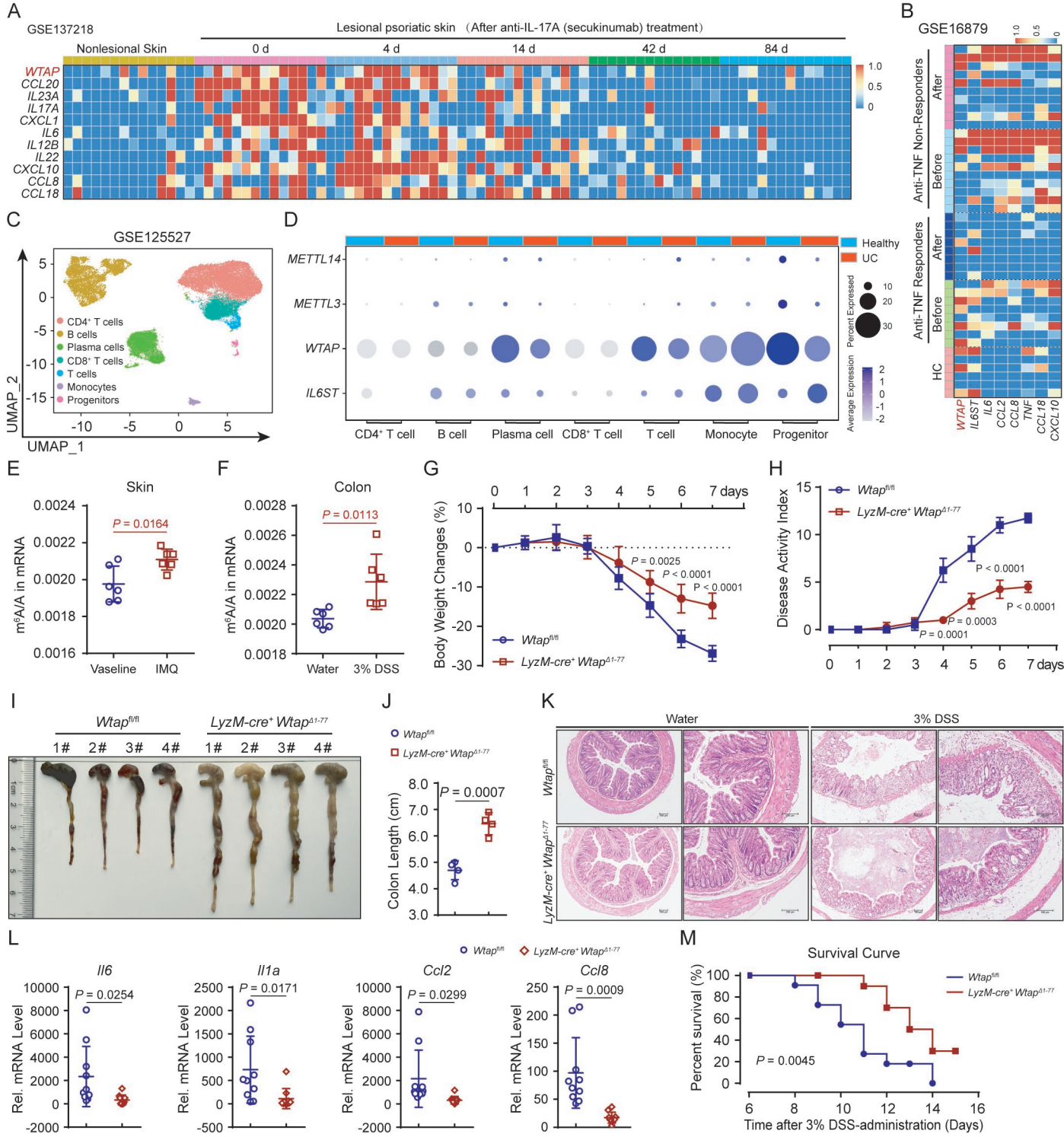
A
GSE137218
Lesional psoriatic skin （After anti-IL-17A (secukinumab) treatment）
Nonlesional Skin
0 d
4 d
14 d
42 d
84 d
WTAP
CCL20
IL23A
IL17A
CXCL1
IL6
IL12B
IL22
CXCL10
CCL8
CCL18
1.0
0.5
0
B
GSE16879
Anti-TNF Non-Responders
After
Before
Anti-TNF Responders
After
Before
HC
WTAP
IL6ST
IL6
CCL2
CCL8
TNF
CCL18
CXCL10
C
GSE125527
CD4⁺ T cells
B cells
Plasma cells
CD8⁺ T cells
T cells
Monocytes
Progenitors
UMAP_2
UMAP_1
D
METTL14
METTL3
WTAP
IL6ST
Healthy
UC
Percent Expressed
Average Expression
CD4⁺ T cell
B cell
Plasma cell
CD8⁺ T cell
T cell
Monocyte
Progenitor
E
Skin
m⁶A/A in mRNA
P = 0.0164
Vaseline
IMQ
F
Colon
m⁶A/A in mRNA
P = 0.0113
Water
3% DSS
G
Body Weight Changes (%)
7 days
P = 0.0025
P < 0.0001
P < 0.0001
Wtap^fl/fl
LyzM-cre⁺ Wtap^Δ1-77
H
Disease Activity Index
Wtap^fl/fl
LyzM-cre⁺ Wtap^Δ1-77
P < 0.0001
P < 0.0001
P = 0.0003
P = 0.0001
7 days
I
Wtap^fl/fl
LyzM-cre⁺ Wtap^Δ1-77
1#
2#
3#
4#
J
Wtap^fl/fl
LyzM-cre⁺ Wtap^Δ1-77
Colon Length (cm)
P = 0.0007
K
Water
3% DSS
Wtap^fl/fl
LyzM-cre⁺ Wtap^Δ1-77
L
Wtap^fl/fl
LyzM-cre⁺ Wtap^Δ1-77
Il6
P = 0.0254
Il1a
P = 0.0171
Ccl2
P = 0.0299
Ccl8
P = 0.0009
Rel. mRNA Level
M
Survival Curve
Percent survival (%)
Wtap^fl/fl
LyzM-cre⁺ Wtap^Δ1-77
P = 0.0045
Time after 3% DSS-administration (Days)

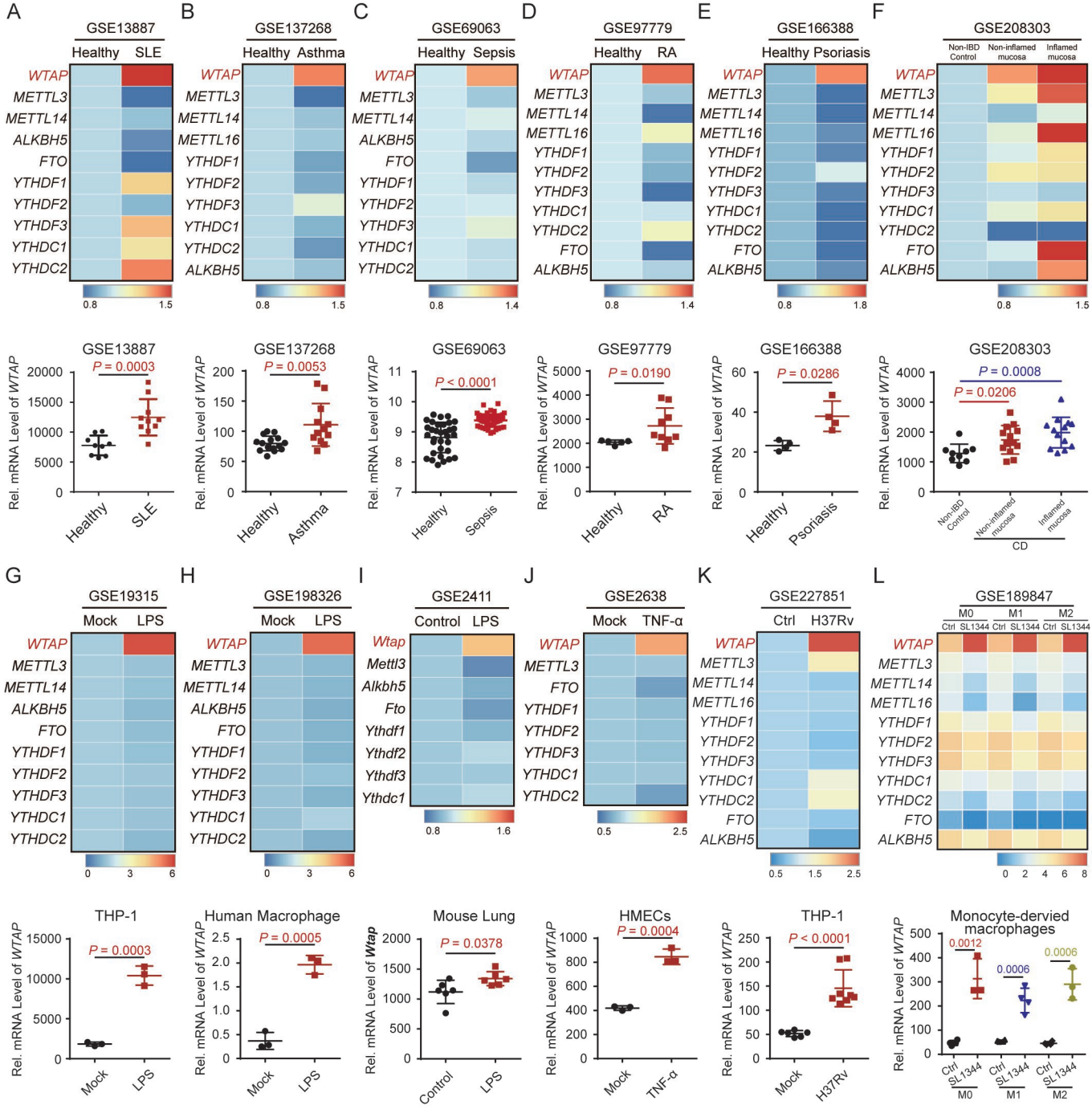
A
GSE13887
Healthy SLE
B
GSE137268
Healthy Asthma
C
GSE69063
Healthy Sepsis
D
GSE97779
Healthy RA
E
GSE166388
Healthy Psoriasis
F
GSE208303
Non-IBD Control
Non-inflamed mucosa
Inflamed mucosa
WTAP
METTL3
METTL14
ALKBH5
FTO
METTL16
YTHDF1
YTHDF2
YTHDF3
YTHDC1
YTHDC2
Rel. mRNA Level of WTAP
P = 0.0003
P = 0.0053
P < 0.0001
P = 0.0190
P = 0.0286
P = 0.0008
P = 0.0206
Healthy
SLE
Asthma
Sepsis
RA
Psoriasis
CD
G
GSE19315
Mock LPS
H
GSE198326
Mock LPS
I
GSE2411
Control LPS
Wtap
Mettl3
Alkbh5
Fto
Ythdf1
Ythdf2
Ythdf3
Ythdc1
J
GSE2638
Mock TNF-α
K
GSE227851
Ctrl H37Rv
L
GSE189847
M0 M1 M2
Ctrl SL1344
THP-1
Human Macrophage
Mouse Lung
HMECs
Monocyte-dervied macrophages
P = 0.0005
P = 0.0378
P = 0.0004
P < 0.0001
0.0012
0.0006
0.0006
Mock
LPS
Control
TNF-α
H37Rv

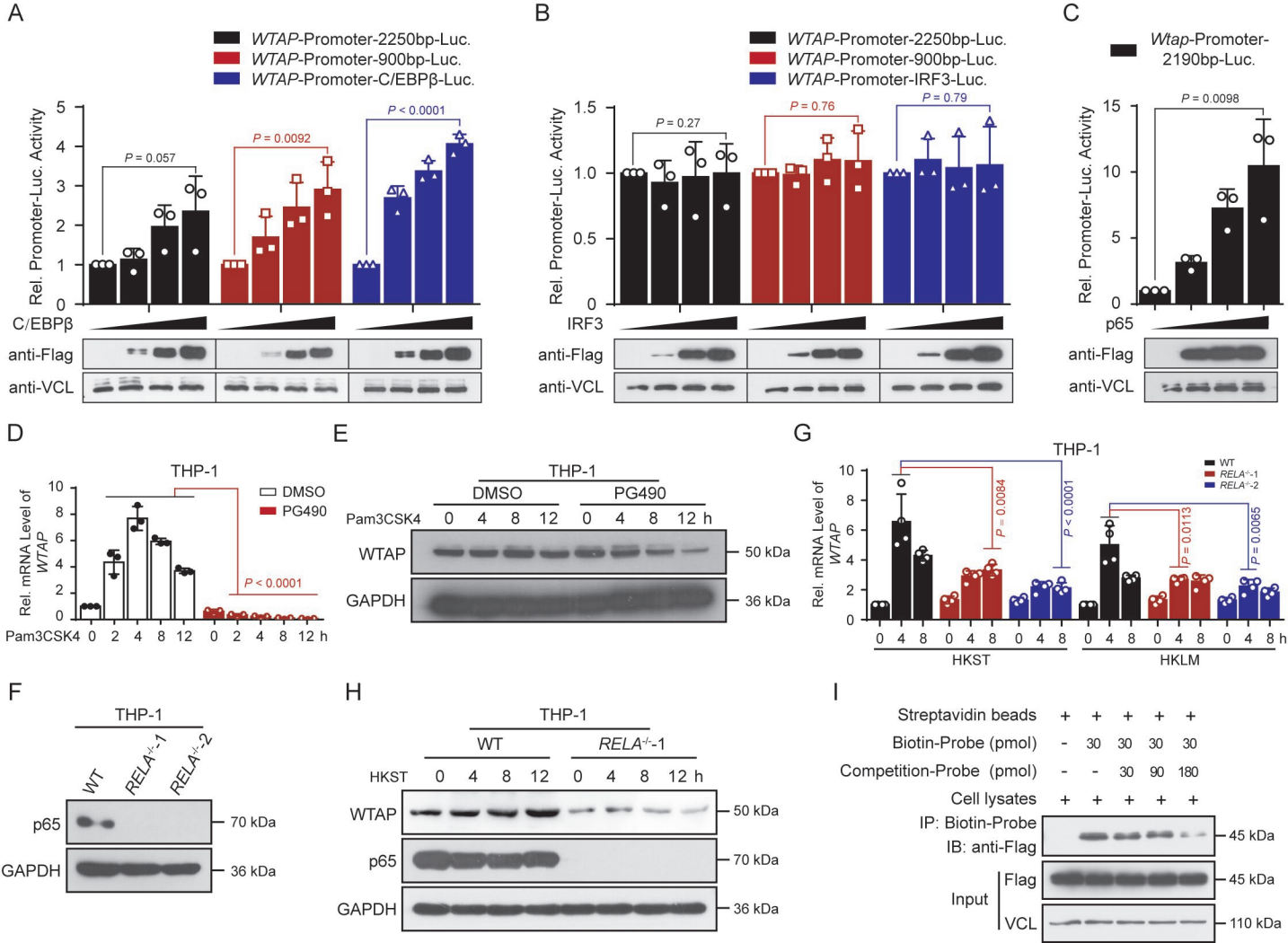
A
WTAP-Promoter-2250bp-Luc.
WTAP-Promoter-900bp-Luc.
WTAP-Promoter-C/EBPβ-Luc.
Rel. Promoter-Luc. Activity
P = 0.057
P = 0.0092
P < 0.0001
C/EBPβ
anti-Flag
anti-VCL
B
WTAP-Promoter-2250bp-Luc.
WTAP-Promoter-900bp-Luc.
WTAP-Promoter-IRF3-Luc.
Rel. Promoter-Luc. Activity
P = 0.27
P = 0.76
P = 0.79
IRF3
anti-Flag
anti-VCL
C
Wtap-Promoter-2190bp-Luc.
Rel. Promoter-Luc. Activity
P = 0.0098
p65
anti-Flag
anti-VCL
D
THP-1
DMSO
PG490
Rel. mRNA Level of WTAP
P < 0.0001
Pam3CSK4 0 2 4 8 12 0 2 4 8 12 h
E
THP-1
DMSO
PG490
Pam3CSK4 0 4 8 12 0 4 8 12 h
WTAP
GAPDH
50 kDa
36 kDa
G
THP-1
WT
RELA-/--1
RELA-/--2
Rel. mRNA Level of WTAP
P = 0.0084
P < 0.0001
P = 0.0113
P = 0.0065
0 4 8 0 4 8 0 4 8 0 4 8 0 4 8 0 4 8 h
HKST
HKLM
F
THP-1
WT
RELA-/--1
RELA-/--2
p65
GAPDH
70 kDa
36 kDa
H
THP-1
WT
RELA-/--1
HKST 0 4 8 12 0 4 8 12 h
WTAP
p65
GAPDH
50 kDa
70 kDa
36 kDa
I
Streptavidin beads + + + + +
Biotin-Probe (pmol) - 30 30 30 30
Competition-Probe (pmol) - - 30 90 180
Cell lysates + + + + +
IP: Biotin-Probe
IB: anti-Flag
Input
Flag
VCL
45 kDa
45 kDa
110 kDa

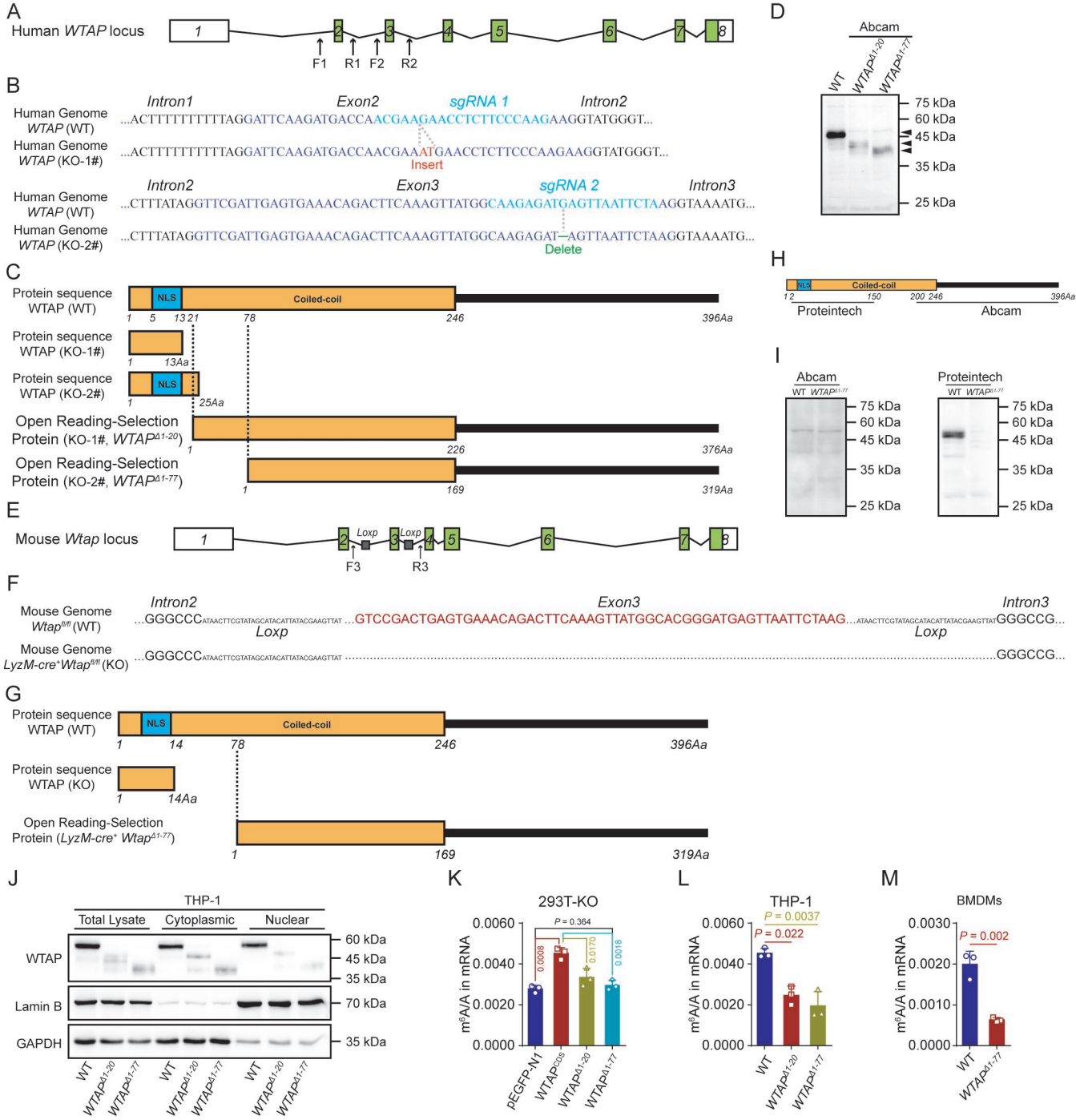
A
Human WTAP locus
1
2
3
4
5
6
7
8
F1
R1
F2
R2
B
Intron1
Exon2
sgRNA 1
Intron2
Human Genome WTAP (WT)
...ACTTTTTTTTTTAGGATTCAAGATGACCAACGAAGAACCTCTTCCCAAGAAGGTATGGGT...
Human Genome WTAP (KO-1#)
...ACTTTTTTTTTTAGGATTCAAGATGACCAACGAAATGAACCTCTTCCCAAGAAGGTATGGGT...
Insert
Intron2
Exon3
sgRNA 2
Intron3
Human Genome WTAP (WT)
...CTTTATAGGTTCGATTGAGTGAAACAGACTTCAAAGTTATGGCAAGAGATGAGTTAATTCTAAGGTAAAATG...
Human Genome WTAP (KO-2#)
...CTTTATAGGTTCGATTGAGTGAAACAGACTTCAAAGTTATGGCAAGAGAT—AGTTAATTCTAAGGTAAAATG...
Delete
C
Protein sequence WTAP (WT)
NLS
Coiled-coil
1
5
13
21
78
246
396Aa
Protein sequence WTAP (KO-1#)
1
13Aa
Protein sequence WTAP (KO-2#)
NLS
1
25Aa
Open Reading-Selection Protein (KO-1#, WTAPΔ1-20)
1
226
376Aa
Open Reading-Selection Protein (KO-2#, WTAPΔ1-77)
1
169
319Aa
D
Abcam
WT
WTAPΔ1-20
WTAPΔ1-77
75 kDa
60 kDa
45 kDa
35 kDa
25 kDa
E
Mouse Wtap locus
1
2
Loxp
3
Loxp
4
5
6
7
8
F3
R3
F
Intron2
Exon3
Intron3
Mouse Genome Wtapfl/fl (WT)
...GGGCCCATAACTTCGTATAGCATACATTATACGAAGTTAT...GTCCGACTGAGTGAAACAGACTTCAAAGTTATGGCACGGGATGAGTTAATTCTAAG...ATAACTTCGTATAGCATACATTATACGAAGTTATGGGCCG...
Loxp
Loxp
Mouse Genome LyzM-cre+Wtapfl/fl (KO)
...GGGCCCATAACTTCGTATAGCATACATTATACGAAGTTAT.....GGGCCG...
G
Protein sequence WTAP (WT)
NLS
Coiled-coil
1
14
78
246
396Aa
Protein sequence WTAP (KO)
1
14Aa
Open Reading-Selection Protein (LyzM-cre+ WtapΔ1-77)
1
169
319Aa
H
NLS
Coiled-coil
1 2
150
200 246
396Aa
Proteintech
Abcam
I
Abcam
WT
WTAPΔ1-77
Proteintech
WT
WTAPΔ1-77
75 kDa
60 kDa
45 kDa
35 kDa
25 kDa
J
THP-1
Total Lysate
Cytoplasmic
Nuclear
WTAP
Lamin B
GAPDH
60 kDa
45 kDa
35 kDa
70 kDa
35 kDa
WT
WTAPΔ1-20
WTAPΔ1-77
K
293T-KO
m6A/A in mRNA
0.0060
0.0040
0.0020
0.0000
P = 0.364
0.0008
0.0170
0.0018
pEGFP-N1
WTAPCDS
WTAPΔ1-20
WTAPΔ1-77
L
THP-1
m6A/A in mRNA
0.0060
0.0040
0.0020
0.0000
P = 0.0037
P = 0.022
WT
WTAPΔ1-20
WTAPΔ1-77
M
BMDMs
m6A/A in mRNA
0.0030
0.0020
0.0010
0.0000
P = 0.002
WT
WTAPΔ1-77

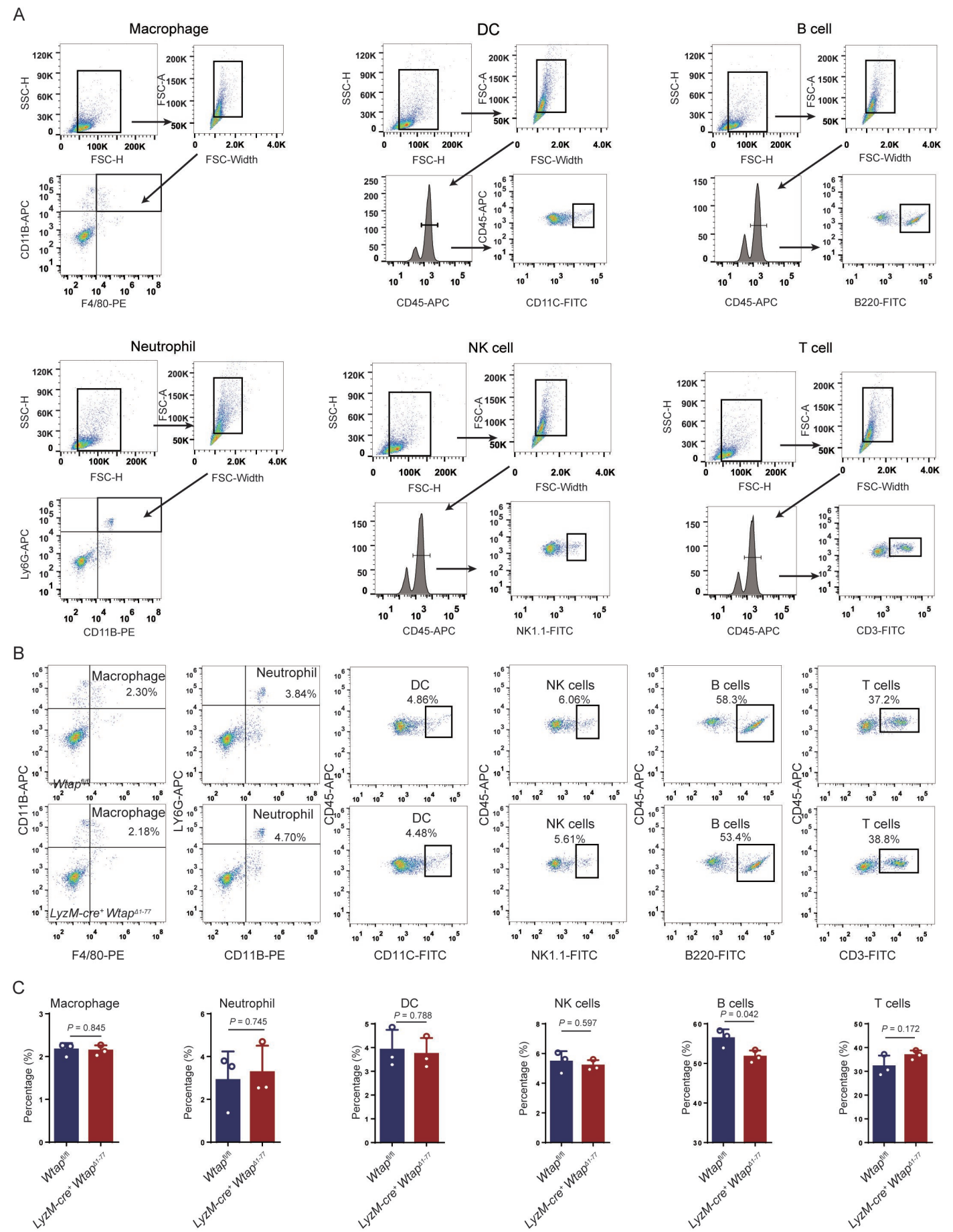
A
Macrophage
DC
B cell
Neutrophil
NK cell
T cell
SSC-H
FSC-H
FSC-A
FSC-Width
CD11B-APC
F4/80-PE
CD45-APC
CD11C-FITC
B220-FITC
Ly6G-APC
CD11B-PE
NK1.1-FITC
CD3-FITC
B
Macrophage 2.30%
Neutrophil 3.84%
DC 4.86%
NK cells 6.06%
B cells 58.3%
T cells 37.2%
Wtap fl/fl
Macrophage 2.18%
Neutrophil 4.70%
DC 4.48%
NK cells 5.61%
B cells 53.4%
T cells 38.8%
LyzM-cre+ Wtap Δ1-77
LY6G-APC
C
Macrophage
Neutrophil
DC
NK cells
B cells
T cells
P = 0.845
P = 0.745
P = 0.788
P = 0.597
P = 0.042
P = 0.172
Percentage (%)
Wtap fl/fl
LyzM-cre+ Wtap Δ1-77

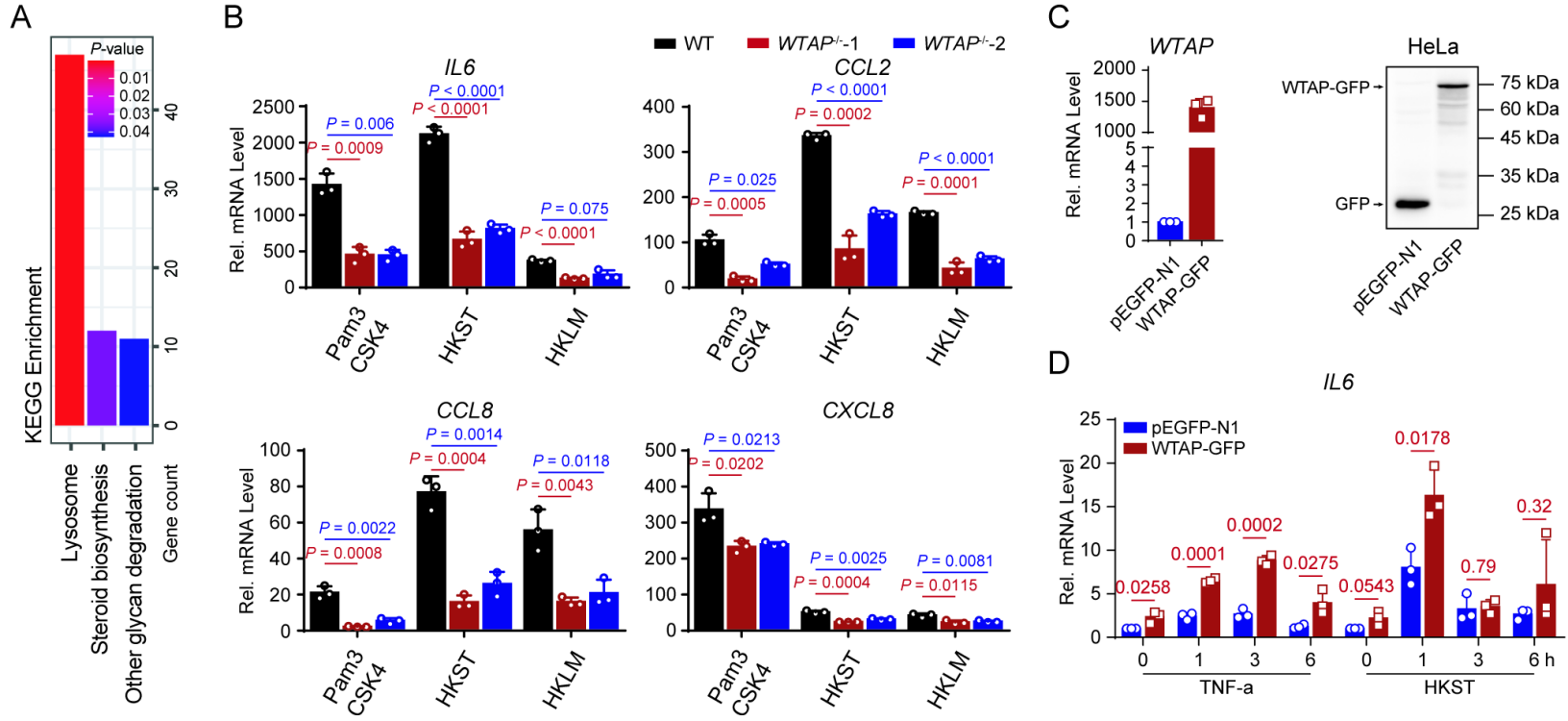
A
P-value
0.01
0.02
0.03
0.04
KEGG Enrichment
Lysosome
Steroid biosynthesis
Other glycan degradation
Gene count
B
WT
WTAP-/--1
WTAP-/--2
IL6
CCL2
CCL8
CXCL8
Rel. mRNA Level
Pam3 CSK4
HKST
HKLM
C
WTAP
HeLa
WTAP-GFP
GFP
75 kDa
60 kDa
45 kDa
35 kDa
25 kDa
pEGFP-N1
WTAP-GFP
D
IL6
pEGFP-N1
WTAP-GFP
TNF-a
HKST

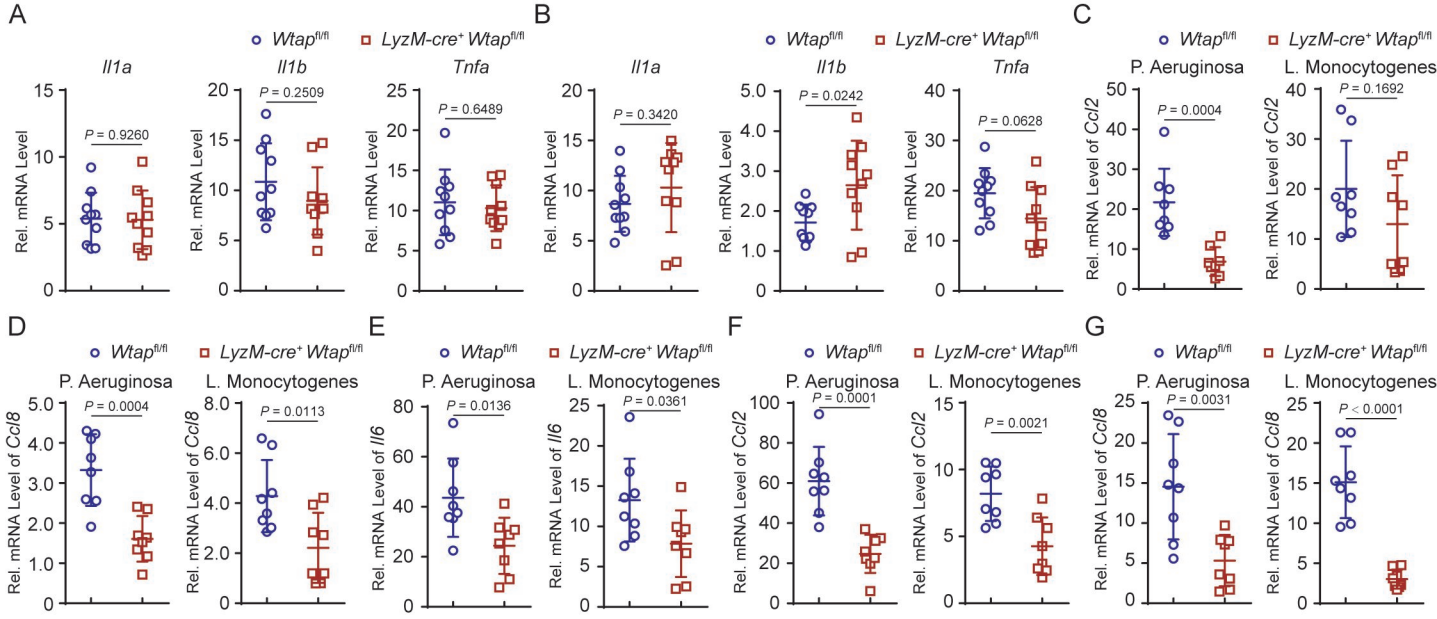
A
Wtap fl/fl
LyzM-cre+ Wtap fl/fl
Il1a
Il1b
Tnfa
Rel. mRNA Level
P = 0.9260
P = 0.2509
P = 0.6489
B
Il1a
Il1b
Tnfa
P = 0.3420
P = 0.0242
P = 0.0628
C
P. Aeruginosa
L. Monocytogenes
Rel. mRNA Level of Ccl2
P = 0.0004
P = 0.1692
D
P. Aeruginosa
L. Monocytogenes
Rel. mRNA Level of Ccl8
P = 0.0004
P = 0.0113
E
P. Aeruginosa
L. Monocytogenes
Rel. mRNA Level of Il6
P = 0.0136
P = 0.0361
F
P. Aeruginosa
L. Monocytogenes
Rel. mRNA Level of Ccl2
P = 0.0001
P = 0.0021
G
P. Aeruginosa
L. Monocytogenes
Rel. mRNA Level of Ccl8
P = 0.0031
P < 0.0001

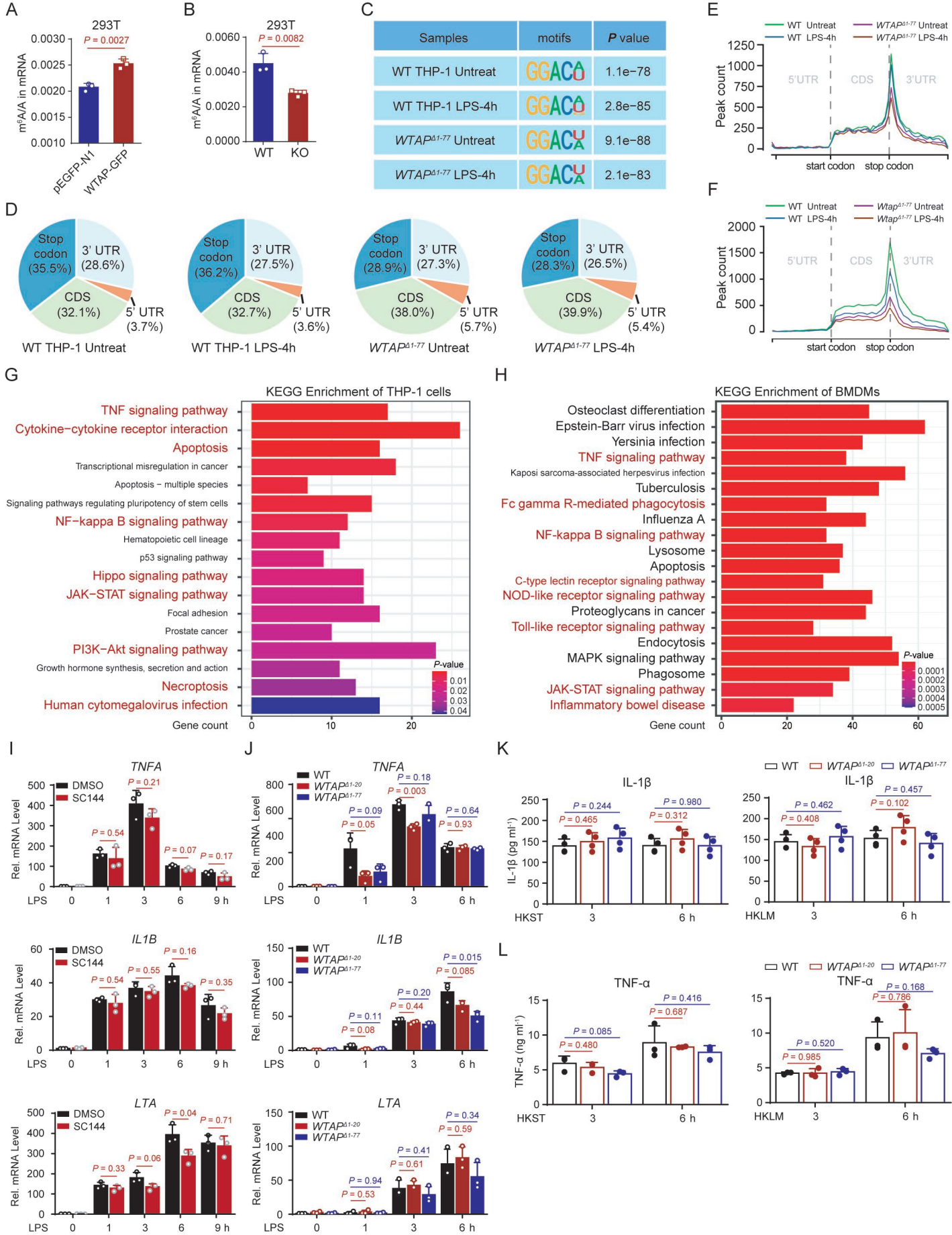
A
293T
P = 0.0027
m6A/A in mRNA
pEGFP-N1
WTAP-GFP
B
293T
P = 0.0082
m6A/A in mRNA
WT
KO
C
Samples
motifs
P value
WT THP-1 Untreat
1.1e−78
WT THP-1 LPS-4h
2.8e−85
WTAPΔ1-77 Untreat
9.1e−88
WTAPΔ1-77 LPS-4h
2.1e−83
D
Stop codon (35.5%)
3' UTR (28.6%)
CDS (32.1%)
5' UTR (3.7%)
WT THP-1 Untreat
Stop codon (36.2%)
3' UTR (27.5%)
CDS (32.7%)
5' UTR (3.6%)
WT THP-1 LPS-4h
Stop codon (28.9%)
3' UTR (27.3%)
CDS (38.0%)
5' UTR (5.7%)
WTAPΔ1-77 Untreat
Stop codon (28.3%)
3' UTR (26.5%)
CDS (39.9%)
5' UTR (5.4%)
WTAPΔ1-77 LPS-4h
E
WT Untreat
WT LPS-4h
WTAPΔ1-77 Untreat
WTAPΔ1-77 LPS-4h
Peak count
5'UTR
CDS
3'UTR
start codon
stop codon
F
WT Untreat
WT LPS-4h
Wtap Δ1-77 Untreat
Wtap Δ1-77 LPS-4h
Peak count
5'UTR
CDS
3'UTR
start codon
stop codon
G
KEGG Enrichment of THP-1 cells
TNF signaling pathway
Cytokine−cytokine receptor interaction
Apoptosis
Transcriptional misregulation in cancer
Apoptosis − multiple species
Signaling pathways regulating pluripotency of stem cells
NF−kappa B signaling pathway
Hematopoietic cell lineage
p53 signaling pathway
Hippo signaling pathway
JAK−STAT signaling pathway
Focal adhesion
Prostate cancer
PI3K−Akt signaling pathway
Growth hormone synthesis, secretion and action
Necroptosis
Human cytomegalovirus infection
P-value
Gene count
H
KEGG Enrichment of BMDMs
Osteoclast differentiation
Epstein-Barr virus infection
Yersinia infection
TNF signaling pathway
Kaposi sarcoma-associated herpesvirus infection
Tuberculosis
Fc gamma R-mediated phagocytosis
Influenza A
NF-kappa B signaling pathway
Lysosome
Apoptosis
C-type lectin receptor signaling pathway
NOD-like receptor signaling pathway
Proteoglycans in cancer
Toll-like receptor signaling pathway
Endocytosis
MAPK signaling pathway
Phagosome
JAK-STAT signaling pathway
Inflammatory bowel disease
P-value
Gene count
I
TNFA
DMSO
SC144
Rel. mRNA Level
LPS
IL1B
LTA
J
WT
WTAPΔ1-20
WTAPΔ1-77
TNFA
IL1B
LTA
K
WT
WTAPΔ1-20
WTAPΔ1-77
IL-1β
IL-1β (pg ml⁻¹)
HKST
HKLM
L
TNF-α
TNF-α (ng ml⁻¹)
HKST
HKLM

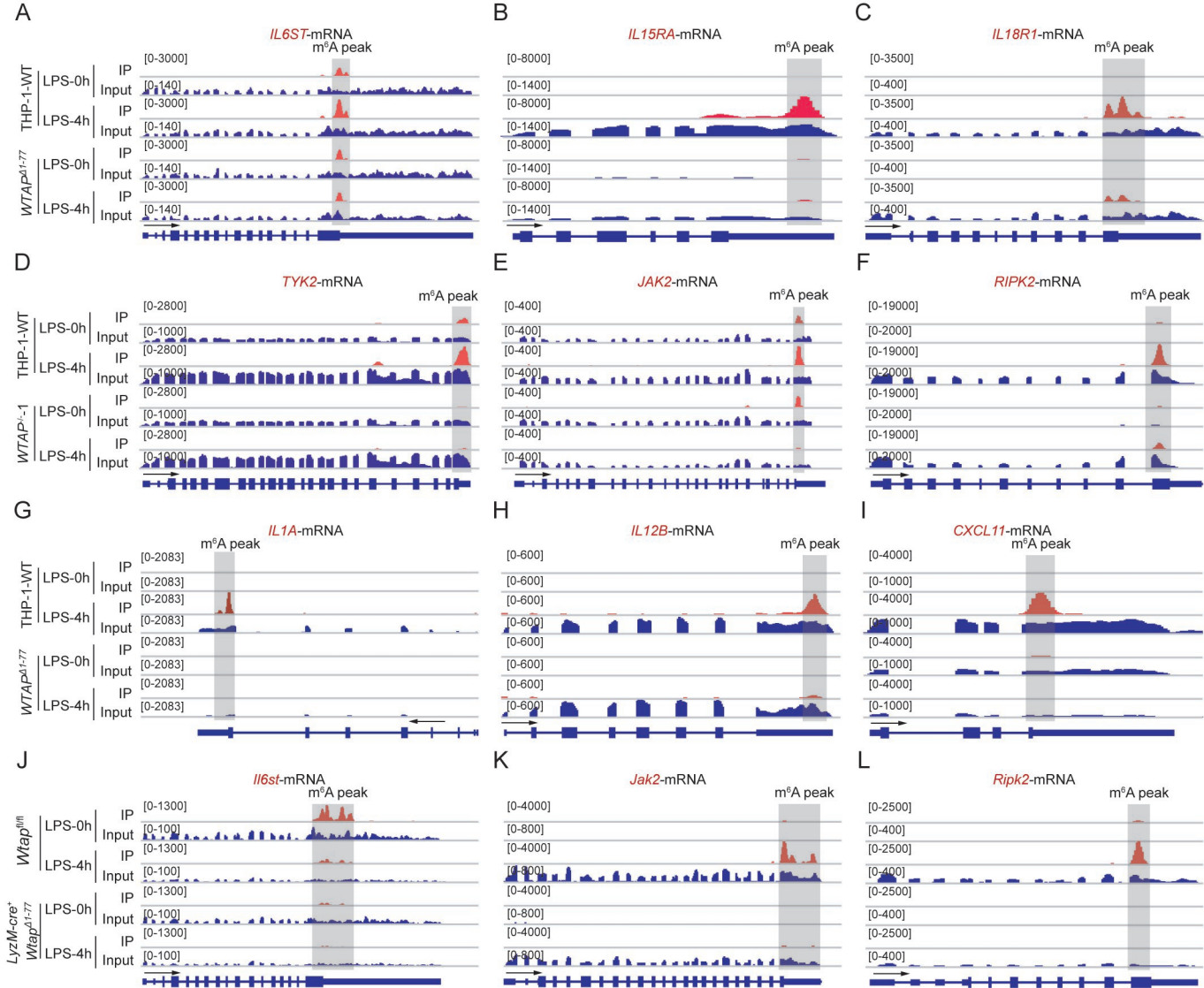
A
IL6ST-mRNA
m6A peak
THP-1-WT
LPS-0h
LPS-4h
WTAPΔ1-77
IP
Input
[0-3000]
[0-140]
B
IL15RA-mRNA
m6A peak
[0-8000]
[0-1400]
C
IL18R1-mRNA
m6A peak
[0-3500]
[0-400]
D
TYK2-mRNA
m6A peak
[0-2800]
[0-1000]
WTAP-/--1
E
JAK2-mRNA
m6A peak
[0-400]
F
RIPK2-mRNA
m6A peak
[0-19000]
[0-2000]
G
IL1A-mRNA
m6A peak
[0-2083]
H
IL12B-mRNA
m6A peak
[0-600]
I
CXCL11-mRNA
m6A peak
[0-4000]
[0-1000]
J
Il6st-mRNA
m6A peak
Wtapfl/fl
LyzM-cre+ Wtap Δ1-77
[0-1300]
[0-100]
K
Jak2-mRNA
m6A peak
[0-4000]
[0-800]
L
Ripk2-mRNA
m6A peak
[0-2500]
[0-400]

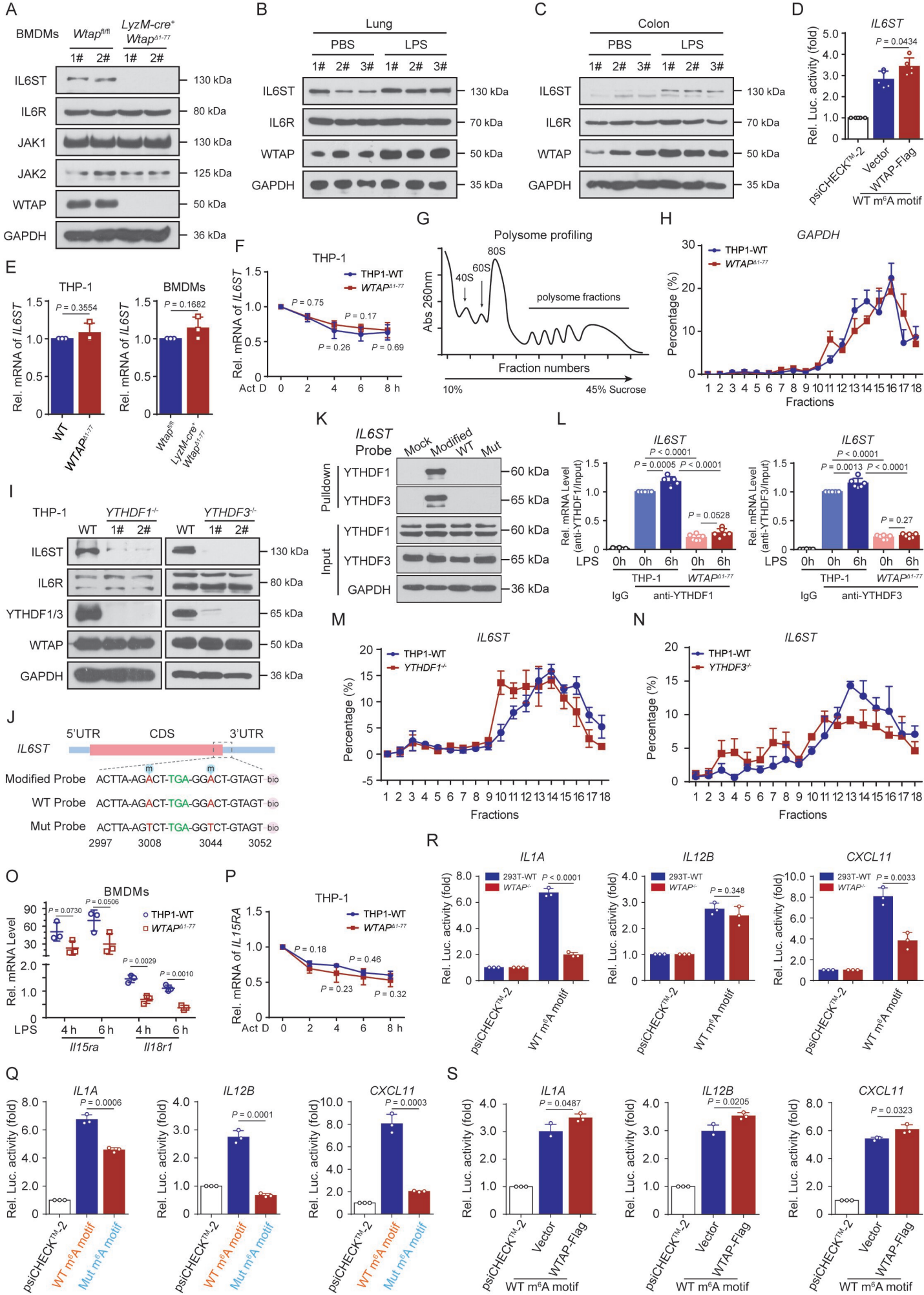
A
BMDMs
Wtap fl/fl
LyzM-cre+ Wtap Δ1-77
1# 2# 1# 2#
IL6ST
IL6R
JAK1
JAK2
WTAP
GAPDH
130 kDa
80 kDa
130 kDa
125 kDa
50 kDa
36 kDa
B
Lung
PBS
LPS
1# 2# 3# 1# 2# 3#
IL6ST
IL6R
WTAP
GAPDH
130 kDa
70 kDa
50 kDa
35 kDa
C
Colon
PBS
LPS
1# 2# 3# 1# 2# 3#
IL6ST
IL6R
WTAP
GAPDH
130 kDa
70 kDa
50 kDa
35 kDa
D
IL6ST
P = 0.0434
Rel. Luc. activity (fold)
psiCHECK™-2
Vector
WTAP-Flag
WT m6A motif
E
THP-1
BMDMs
P = 0.3554
P = 0.1682
Rel. mRNA of IL6ST
WT
WTAP Δ1-77
Wtap fl/fl
LyzM-cre+ Wtap Δ1-77
F
THP-1
THP1-WT
WTAP Δ1-77
P = 0.75
P = 0.17
P = 0.26
P = 0.69
Rel. mRNA of IL6ST
Act D
G
Polysome profiling
40S
60S
80S
Abs 260nm
polysome fractions
Fraction numbers
10%
45% Sucrose
H
GAPDH
THP1-WT
WTAP Δ1-77
Percentage (%)
Fractions
I
THP-1
YTHDF1-/-
YTHDF3-/-
WT 1# 2# WT 1# 2#
IL6ST
IL6R
YTHDF1/3
WTAP
GAPDH
130 kDa
80 kDa
65 kDa
50 kDa
36 kDa
J
5'UTR
CDS
3'UTR
IL6ST
m
m
Modified Probe ACTTA-AGACT-TGA-GGACT-GTAGT bio
WT Probe ACTTA-AGACT-TGA-GGACT-GTAGT bio
Mut Probe ACTTA-AGTCT-TGA-GGTCT-GTAGT bio
2997 3008 3044 3052
K
IL6ST
Probe
Mock
Modified
WT
Mut
Pulldown
YTHDF1
YTHDF3
Input
YTHDF1
YTHDF3
GAPDH
60 kDa
65 kDa
60 kDa
65 kDa
36 kDa
L
IL6ST
P < 0.0001
P = 0.0005
P < 0.0001
P = 0.0528
Rel. mRNA Level (anti-YTHDF1/Input)
LPS
0h 0h 6h 0h 6h
THP-1
WTAP Δ1-77
IgG
anti-YTHDF1
IL6ST
P < 0.0001
P = 0.0013
P < 0.0001
P = 0.27
Rel. mRNA Level (anti-YTHDF3/Input)
anti-YTHDF3
M
IL6ST
THP1-WT
YTHDF1-/-
Percentage (%)
Fractions
N
IL6ST
THP1-WT
YTHDF3-/-
Percentage (%)
Fractions
O
BMDMs
THP1-WT
WTAP Δ1-77
P = 0.0730
P = 0.0506
P = 0.0029
P = 0.0010
Rel. mRNA Level
LPS
4 h 6 h 4 h 6 h
Il15ra
Il18r1
P
THP-1
THP1-WT
WTAP Δ1-77
P = 0.18
P = 0.46
P = 0.23
P = 0.32
Rel. mRNA of IL15RA
Act D
R
IL1A
IL12B
CXCL11
293T-WT
WTAP-/-
P < 0.0001
P = 0.348
P = 0.0033
Rel. Luc. activity (fold)
psiCHECK™-2
WT m6A motif
Q
IL1A
P = 0.0006
IL12B
P = 0.0001
CXCL11
P = 0.0003
Rel. Luc. activity (fold)
psiCHECK™-2
WT m6A motif
Mut m6A motif
S
IL1A
P = 0.0487
IL12B
P = 0.0205
CXCL11
P = 0.0323
Rel. Luc. activity (fold)
psiCHECK™-2
Vector
WTAP-Flag
WT m6A motif

A

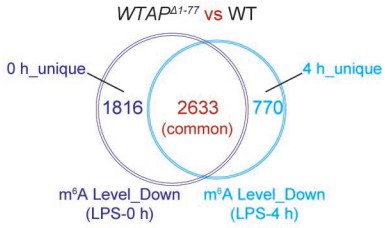
WTAP$^{\Delta 1-77}$ vs WT
0 h_unique
4 h_unique
1816
2633
(common)
770
m^{6}A Level_Down
(LPS-0 h)
m^{6}A Level_Down
(LPS-4 h)

B

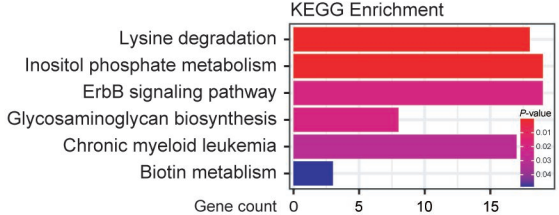
KEGG Enrichment
Lysine degradation
Inositol phosphate metabolism
ErbB signaling pathway
Glycosaminoglycan biosynthesis
Chronic myeloid leukemia
Biotin metablism
P-value
0.01
0.02
0.03
0.04
Gene count
0
5
10
15

C

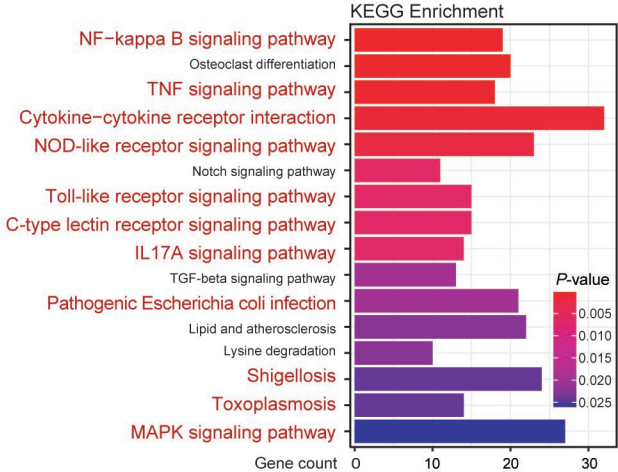
KEGG Enrichment
NF−kappa B signaling pathway
Osteoclast differentiation
TNF signaling pathway
Cytokine−cytokine receptor interaction
NOD-like receptor signaling pathway
Notch signaling pathway
Toll-like receptor signaling pathway
C-type lectin receptor signaling pathway
IL17A signaling pathway
TGF-beta signaling pathway
Pathogenic Escherichia coli infection
Lipid and atherosclerosis
Lysine degradation
Shigellosis
Toxoplasmosis
MAPK signaling pathway
P-value
0.005
0.010
0.015
0.020
0.025
Gene count
0
10
20
30

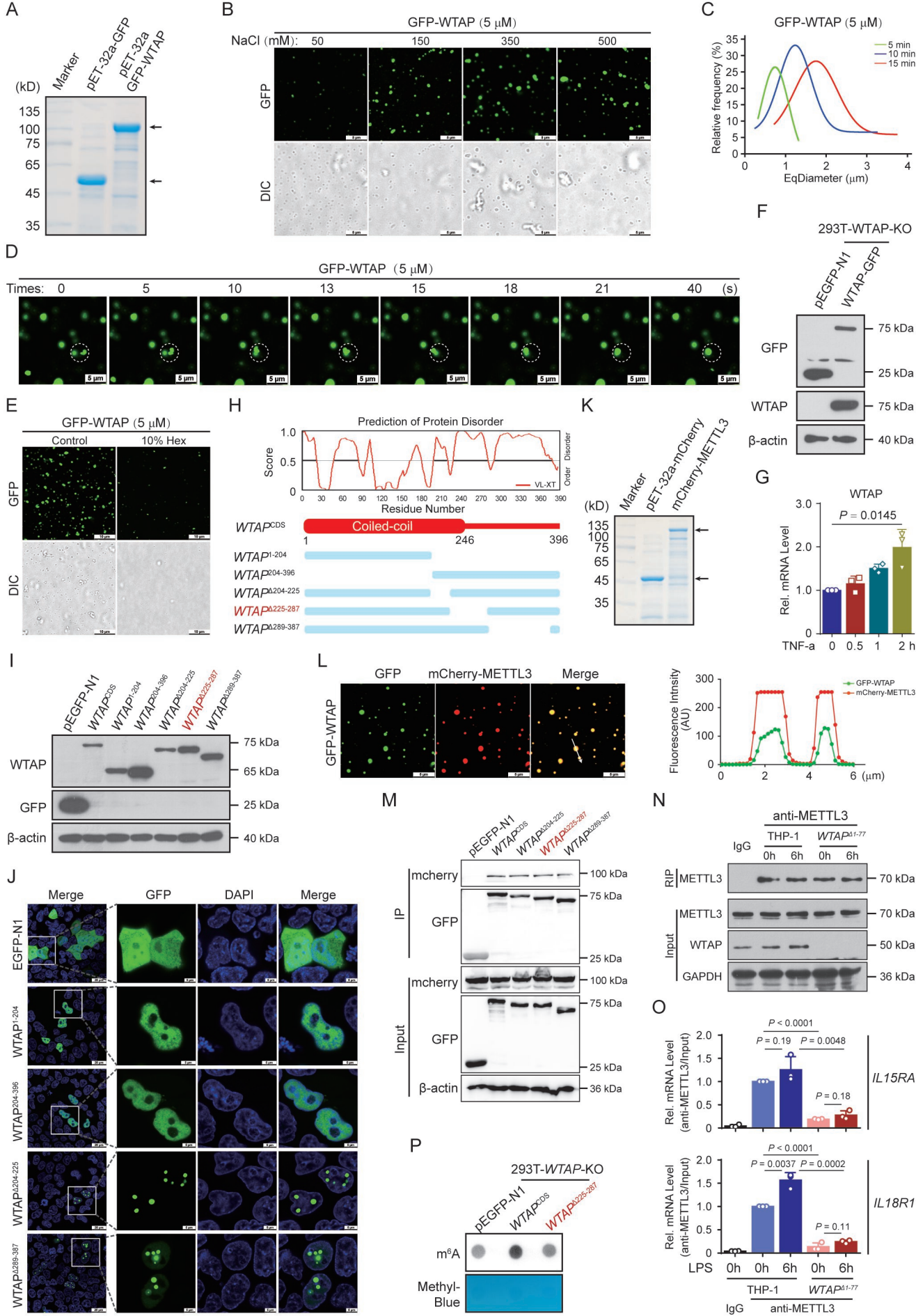
A
Marker
pET-32a-GFP
pET-32a
GFP-WTAP
(kD)
135
100
75
65
45
35
B
GFP-WTAP (5 μM)
NaCl (mM): 50 150 350 500
GFP
DIC
C
GFP-WTAP (5 μM)
5 min
10 min
15 min
Relative frequency (%)
EqDiameter (μm)
D
GFP-WTAP (5 μM)
Times: 0 5 10 13 15 18 21 40 (s)
5 μm
E
GFP-WTAP (5 μM)
Control
10% Hex
GFP
DIC
F
293T-WTAP-KO
pEGFP-N1
WTAP-GFP
GFP
WTAP
β-actin
75 kDa
25 kDa
75 kDa
40 kDa
G
WTAP
P = 0.0145
Rel. mRNA Level
TNF-a 0 0.5 1 2 h
H
Prediction of Protein Disorder
Score
Order
Disorder
VL-XT
Residue Number
WTAP^CDS
Coiled-coil
1
246
396
WTAP^1-204
WTAP^204-396
WTAP^Δ204-225
WTAP^Δ225-287
WTAP^Δ289-387
I
pEGFP-N1
WTAP^CDS
WTAP^1-204
WTAP^204-396
WTAP^Δ204-225
WTAP^Δ225-287
WTAP^Δ289-387
WTAP
GFP
β-actin
75 kDa
65 kDa
25 kDa
40 kDa
J
Merge
GFP
DAPI
Merge
EGFP-N1
WTAP^1-204
WTAP^204-396
WTAP^Δ204-225
WTAP^Δ289-387
K
Marker
pET-32a-mCherry
mCherry-METTL3
(kD)
135
100
75
65
45
35
L
GFP
mCherry-METTL3
Merge
GFP-WTAP
Fluorescence Intnsity (AU)
GFP-WTAP
mCherry-METTL3
(μm)
M
pEGFP-N1
WTAP^CDS
WTAP^Δ204-225
WTAP^Δ225-287
WTAP^Δ289-387
IP
mcherry
GFP
Input
mcherry
GFP
β-actin
100 kDa
75 kDa
25 kDa
100 kDa
75 kDa
25 kDa
36 kDa
N
anti-METTL3
IgG
THP-1
WTAP^Δ1-77
0h 6h 0h 6h
RIP
METTL3
Input
METTL3
WTAP
GAPDH
70 kDa
70 kDa
50 kDa
36 kDa
O
P < 0.0001
P = 0.19
P = 0.0048
P = 0.18
IL15RA
Rel. mRNA Level (anti-METTL3/Input)
P < 0.0001
P = 0.0037
P = 0.0002
P = 0.11
IL18R1
LPS 0h 0h 6h 0h 6h
THP-1
WTAP^Δ1-77
IgG
anti-METTL3
P
293T-WTAP-KO
pEGFP-N1
WTAP^CDS
WTAP^Δ225-287
m6A
Methyl-Blue

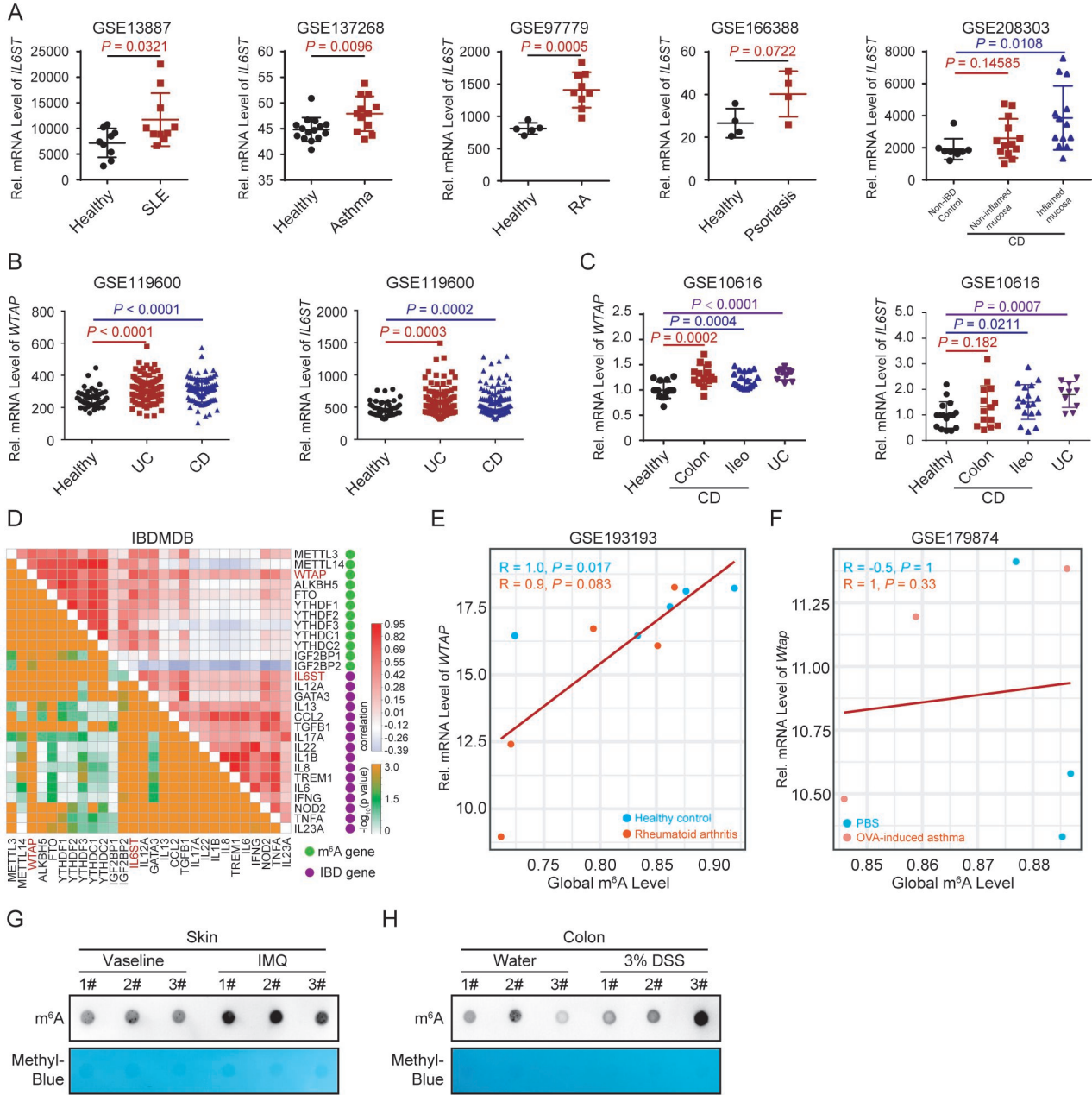
A
GSE13887
P = 0.0321
Rel. mRNA Level of IL6ST
Healthy
SLE
GSE137268
P = 0.0096
Healthy
Asthma
GSE97779
P = 0.0005
Healthy
RA
GSE166388
P = 0.0722
Healthy
Psoriasis
GSE208303
P = 0.0108
P = 0.14585
Non-IBD Control
Non-inflamed mucosa
Inflamed mucosa
CD
B
GSE119600
P < 0.0001
P < 0.0001
Rel. mRNA Level of WTAP
Healthy
UC
CD
GSE119600
P = 0.0002
P = 0.0003
Rel. mRNA Level of IL6ST
C
GSE10616
P < 0.0001
P = 0.0004
P = 0.0002
Rel. mRNA Level of WTAP
Healthy
Colon
Ileo
UC
CD
GSE10616
P = 0.0007
P = 0.0211
P = 0.182
Rel. mRNA Level of IL6ST
D
IBDMDB
METTL3
METTL14
WTAP
ALKBH5
FTO
YTHDF1
YTHDF2
YTHDF3
YTHDC1
YTHDC2
IGF2BP1
IGF2BP2
IL6ST
IL12A
GATA3
IL13
CCL2
TGFB1
IL17A
IL22
IL1B
IL8
TREM1
IL6
IFNG
NOD2
TNFA
IL23A
correlation
-log10(p value)
m6A gene
IBD gene
E
GSE193193
R = 1.0, P = 0.017
R = 0.9, P = 0.083
Rel. mRNA Level of WTAP
Healthy control
Rheumatoid arthritis
Global m6A Level
F
GSE179874
R = -0.5, P = 1
R = 1, P = 0.33
Rel. mRNA Level of Wtap
PBS
OVA-induced asthma
Global m6A Level
G
Skin
Vaseline
IMQ
1#
2#
3#
m6A
Methyl-Blue
H
Colon
Water
3% DSS
1#
2#
3#
m6A
Methyl-Blue

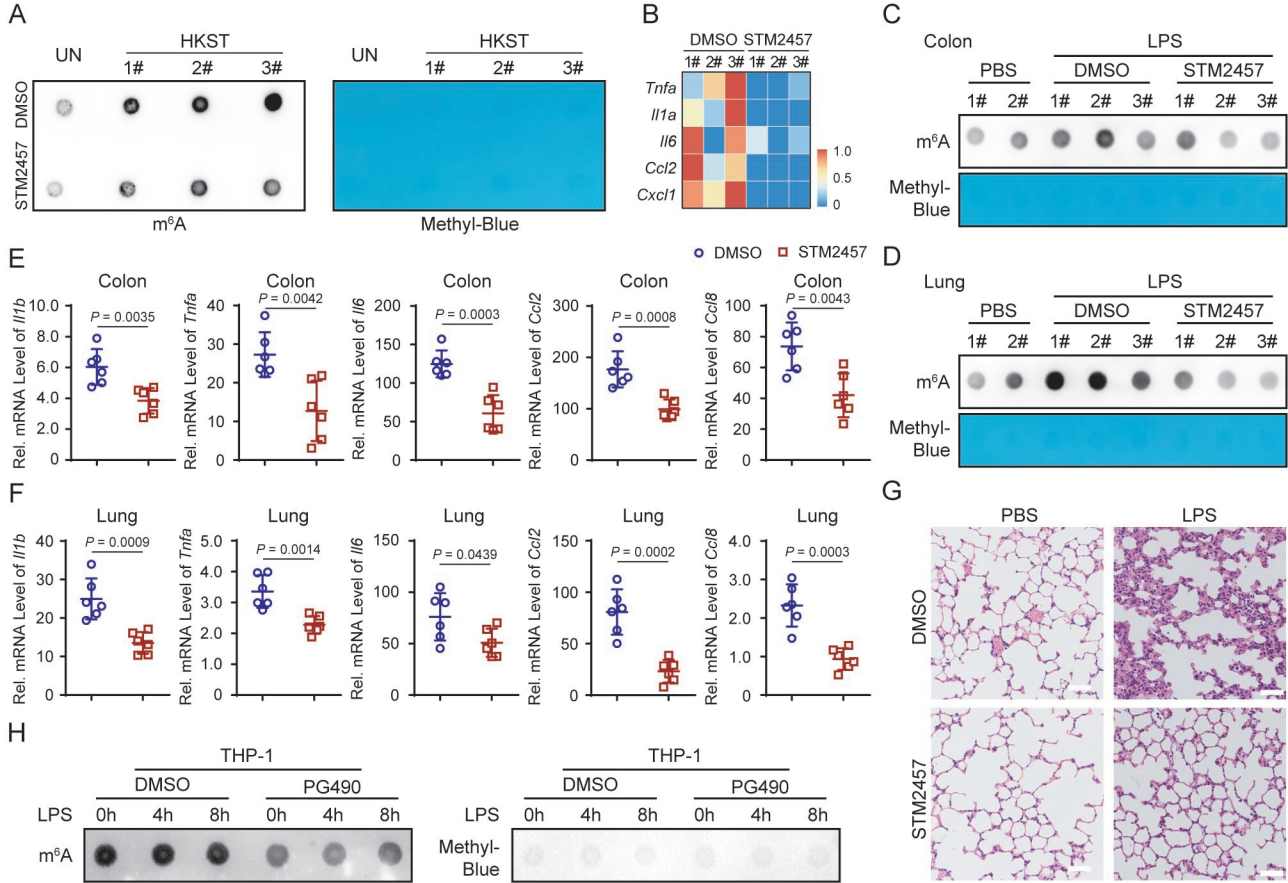
A
UN
HKST
1#
2#
3#
DMSO
STM2457
m6A
Methyl-Blue
B
DMSO STM2457
Tnfa
Il1a
Il6
Ccl2
Cxcl1
1.0
0.5
0
C
Colon
LPS
PBS
DMSO
STM2457
m6A
Methyl-Blue
D
Lung
E
DMSO
STM2457
Colon
Rel. mRNA Level of Il1b
Rel. mRNA Level of Tnfa
Rel. mRNA Level of Il6
Rel. mRNA Level of Ccl2
Rel. mRNA Level of Ccl8
P = 0.0035
P = 0.0042
P = 0.0003
P = 0.0008
P = 0.0043
F
Lung
P = 0.0009
P = 0.0014
P = 0.0439
P = 0.0002
P = 0.0003
G
PBS
LPS
DMSO
STM2457
H
THP-1
DMSO
PG490
LPS
0h
4h
8h
m6A
Methyl-Blue